The optimization of oil operation for a dry low NOx gas turbine combustor

Lloyd, Jonathan

Thesis for

Master of Science

at the Engineering School of the University of Durham

October 1999

The Optimization of Oil Operation for a Dry Low NOx Gas Turbine Combustor

Author: **Jonathan Lloyd**

Abstract

As the market for Gas Turbines becomes more aggressive, and the legislation for emissions more stringent, manufacturers are looking for better ways of becoming competitive. One competitive criteria is the ability to create robust low emission burners. While it is relatively easy to design a premixed burner for natural gas operation, the process involved in producing a reliable Low NOx burner for oil is considerably more complicated.

Within the bounds of the given burner geometry, this works surrounds the optimisation of the premix oil mixture in preparation for Gas Turbine combustion, in able to achieve a Dry Low NOx performance with values less than 25ppm.

The main development included the use of numerical methods involving CFD codes to vary different nozzle parameters and operating conditions.

The author defined the critical parameters for the nozzle design operating in such a burner, and suggested a new type of nozzle. This nozzle was designed and modelled, and proved to be the optimal solution providing the lowest emissions for a Dry oil burner available in the power generation business.

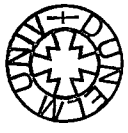

Foreward

The following thesis is a combination of commercial technical reports, conference papers, and purpose written text for the submission of an external Masters degree at Durham University, England.

The majority of the work has been completed by the author, or under the supervision of the author. Work not fully completed by the author is acknowledged to the corresponding people in the appropriate place.

The work contained in this report is the result of investigations spanning from Easter 1995 to Autumn 1997 undertaken at ABB Corporate Research Ltd., Switzerland on the development of the AEV (advanced EV) Low NOx burner.
As a consequence of the commercial application, the information contained in this report is confidential intellectual property of ABB, and should not be transferred to any party either orally or in any written form without the consent of the author. No facts in this report should be taken as official or state-of-the-art technology. I would like to take this opportunity to thank ABB for the permission to release the information, in order to make this submission for a Masters degree.

I would also like express my thanks to Dr. David Gregory-Smith of Durham University for the support and advice throughout the completion of this work.

The report can be split into three main parts.
The first part, including the introduction and theory addresses the motivation of this work, and the present technological background used in the development programme. It gives a detailed review on the theoretical considerations of oil atomisation, evaporation and combustion, simulation models, NOx production and other such aspects.
The second part represents the core of the development work, and contains the numerical simulation for oil operation of the AEV75 burner, including a stand-alone technical report, further results, limitation suggestions, and the final chosen design. The similar development of the oil injection system for the larger AEV100 burner is shown in Chapter 5. Discussion in the differing designs is also given.
The final section describes future and continuing work. Options for other scalings of the burner are discussed in Chapter 6. In Chapter 7 the practical development of specific nozzles is shown. This includes experimental results and design considerations. The conclusion contains the closing statements of the whole work.

The best preface that can be given to this thesis is to request that a glace is taken at the final result of the work: the newly released GTX100 ABB Gas Turbine (see Appendix C), and to compare the emission levels for Dry Oil Combustion with any competitor. This report is based on a significant part of that burner development.

Jonathan Lloyd
October 1999

Contents

Nomenclature

a	constant
A	area
b	constant
C_D	coefficient of drag
$C_{D\text{-}Corr}$	corrected coefficient of drag
C_i	concentration of fuel vapour
C_P	specific heat capacity
d	constant
D	droplet diameter
D_0	initial droplet diameter
$\overline{D}$	average droplet diameter
Di	diffusion coefficient
e	constant
E	activation energy
f	constant
F	force
g	gravitational acceleration
h	convective heat transfer coeff.
h_{fg}	latent heat of vaporisation
k	constant
k_m	mass transfer coefficient
l_t	liquid thickness
L	length
$\dot{m}$	mass flow rate
$\overline{m_i}$	average drop mass in cell
M	mass
M_D	% mass of spray with drop size less than D
M_i	constant
n	spread factor
N_i	molar flux
Nu	Nusselt number
Oh	Ohnesorge number
P	static pressure
ΔP	total pressure head difference
Pr	Prandlt number
Q	rate of heat transfer/flux
r	radius
R	universal gas constant
Re	Reynolds number
Sc	Schmidt number
SMD	Sauter Mean Diameter
t	time
T	temperature
u	axial velocity component
v	radial velocity component
w	tangential velocity component
We	Weber number
x	distance
X_M	mass transfer number
β	evaporation constant
θ_R	radiative temperature
ε	emissivity
Φ	fuel to air ratio
μ	dynamic viscosity
λ	excess air ratio (actual air: stoichiometric)
ρ	density
σ	surface tension
σ_B	Boltzmans constant
τ	self-ignition delay time
ζ	reciprocal of the loss coefficient

Subscripts:

	Characteristic of:
AIR	air
AMB	ambient pressure
BACKPRESSURE	oil back pressure
C	air core diameter
CRIT	critical pressure
D	drag
DROP	droplet
EXTERNAL-AERODYN	external aero influence
FLUID	fluid
GRAV	gravity
IN	inlet orifice
INERT	inertia
INTERNAL	internal aero influence
JET	jet
OIL	oil
OUT	outlet orifice
OUTFLOW	area used by fluid in outlet orifice
PRESS	pressure
SAT	saturated
SPRAY	spray
SURF	surface
SURFACE TENSION	surface tension
THERM	thermophoretic
TOTAL	total pressure
WATER	water
X-S	cross-section

1. Introduction and Background Information

International regulations and high competition has meant that the main emphasis in Gas Turbine combustor development in the past decade has been on lowering emissions. This came to a head in 1988, when scientists discovered a hole in the ozone layer above the Antarctic. Since then legislation and environmental groups have caused the direction of development of combustion systems for power stations and transport to concentrate on reducing such emissions in an effort to preserve the planet's fragile atmosphere before it is too late. Of these emissions, NOx, SO_2, and CO_2 are the most harmful.

The impact of emissions can be divided into three separate groups: local, regional, and global. Local impact concerns the health and welfare of the local population including smog, lung damage and poisonous fumes all leading to worsened health. Regional issues concern the impact of acid rain and ozone at low levels, while global impacts deal with the greenhouse effect and the stratospheric ozone depletion.

1.1 Emissions

1.1.1 NOx

NOx is the short form for all derivatives of Nitrogen Oxides in combustion emissions mainly consisting of Nitric Oxide (NO), Nitric Dioxide (NO_2) and Nitrous Oxide (N_2O). These are undesired emissions as they contribute to the imbalance of the earth's atmosphere, in particular by changing the equilibrium of the ozone (O_3) layer, and by causing irritating photochemical smog.

Along with SO_2, NOx is a known source of destructive acid rain, when NO reacts in the atmosphere to form NO_2 and then to HNO_3 (Nitric Acid). NO_x can also oxidise to form ozone at low levels and H_2O_2 (hydrogen peroxide).

These reactions can be summarised in the following way:

NO_2 + certain sun wavelengths -> $O(^3P)$ + NO

$O(^3P) + O_2$ -> O_3 (ozone)

This occurs in the stratosphere and troposphere.

This reaction can reverse, mainly occurring at night without sunlight

$$O_3 + NO \rightarrow NO_2 + O_2$$

But unfortunately an additional reaction can occur that eats up ozone and produces NO_3:

$$O_3 + NO_2 \rightarrow NO_3 + O_2$$

this continues

$$NO_2 + NO_3 \rightarrow N_2O_5$$

When N_2O_5 finally comes into contact with cloud droplets, a critical reaction takes place, producing acid rain:

$$N_2O_5 + H_2O \text{ (cloud)} \rightarrow 2H^+ + 2NO_3^- \text{ (nitric acid)}$$

N_2O (also considered as a NOx), together with methane, CO2 and CFCs, is one of the main contributors to the Greenhouse effect, by reflecting infrared-waves back to earth, that would otherwise be emitted back into space.

1.1.2 CO and CO_2

CO_2 is also a player in the greenhouse effect, contributing to about 50% of the greenhouse effect, due to inefficient combustion of fuels with old technology. However, its influence in increasing dangerous radiation is around 200 times less per molecule than that of N_2O.

As CO emissions lie at similar levels to NOx in a GT combustor along with the fact that CO emissions decrease with increasing flame temperature, CO_2 is only of consideration to the turbine designer at part load conditions. CO plays a more important role on local health impact, not only oxidising into CO_2, but also being poisonous to both plants and animal life.

1.1.3 Unburnt Hydrocarbons

Unburnt hydrocarbons induced into the atmosphere are another cause of the greenhouse effect. However these are a small worry to a combustor designer, due to the fact that any unburned hydrocarbons should not occur in an efficient burner design with a stable flame. If this is the case, the burner needs a major design change.

1.1.4 SO_2

Sulphur Dioxide is a cause of acid rain and a major environmental concern. Again it is of little concern to the gas turbine developer. The main fuels used, namely natural gas (methane) and light oils (No.2), have little sulphur content.

1.1.5 Present emission levels

In order to put objectives in perspective, international emission standards set in a collateral agreement between Gas Turbine producers have forced natural gas combustors to meet a hurdle of 25ppm in NOx emissions. In some US states, e.g. Texas, this level is being reduced even further to 9ppm. With oil combustion this number is somewhat relaxed to 42ppm, although it will soon become more stringent. Before the development of the AEV burner started, emission levels in operational ABB EV burners lay at 25ppm for natural gas. Operation with oil combustion was for many reasons undesired, not only for the fact that emission levels for NOx were in the hundreds of ppm. With the addition of water, it was possible to restrict these levels to around 70ppm.

As a result, the major hurdle for the Gas Turbine developer is the reduction of NOx emissions for oil operation.

1.2 Mixture Preparation

1.2.1 Natural Gas

Natural gas combustion is comparatively simple, due to the ease that total premixed combustion can be achieved. The mixing of two gases is much simpler than the mixing of a liquid and a gas. Good fuel distribution can be attained through the use of many injection points and the increase of turbulence as a means of higher dissipation levels.

1.2.2 Liquid Fuel

Oil combustion is a more difficult and complicated process. Fuel preparation at the flame front has to be achieved in a similar distance and under similar conditions to gas operation. If possible, the oil should appear shortly before the flame front in a fully premixed gaseous form, so that there is the possibility of complete combustion with low emissions. The problems of full droplet evaporation injected from a singular point (or certainly from a single nozzle) need to be overcome, and the mixing process should occur in both liquid and vapour phases, in order to obtain the optimum fuel distribution shortly before combustion. This process is hindered by the multi-component fuel which has a compound evaporation temperature and long carbon chains that are more difficult to fully combust.

1.2.3 Dry Oil - What does it mean?

In the past, it has been impossible to achieve low emissions by direct injection of oil into GT burners. There are several reasons for this. The short self-ignition time of oil, especially at high air pressures prevents the possibility of a long residence time in the burner and with it the lack of time for good mixing. This in turn means either droplets still exist at the flame front (catastrophic for emissions) or the distribution of oil vapour is poor causing local high flame temperatures and the production of thermal NOx (discussed later). As a result, water is added to the oil to create an emulsion. This aids emissions by firstly creating smaller droplets. Evaporation occurs faster and therefore no liquid oil is found at the flame front, and the risk of self-ignition is reduced. Secondly it means that the self-ignition time is increased due to the larger thermal capacity of the mixture. Finally the water vapour reduces the temperature of the flame, and therefore the NOx emissions (NOx emissions are related to the flame temperature). This is technically known as running 'wet oil'. Of course the disadvantage of this method is three-fold: first the turbine becomes less efficient, second is that an auxiliary system has to be constructed for the water supply, and third the stress on the critical hot gas components is larger resulting in shorter lifetimes. These issues increase costs. Also the availability of demineralized water is not possible at many plants in remote locations. This makes the concept and the resulting plant less economically viable.

Therefore it is the aim to run dry oil (without the addition of water) and to overcome the above problems.

1.3 An Introduction to the AEV Burner in its present form.

It is not within the span of this work to give an account on the aerodynamic and geometrical development of the AEV burner, but some words of introduction should be given to explain the present state of design, and the basic technical functions.

The AEV burner is an advanced generation of the commonly known EV burner that is presently used in many ABB turbines. Both burners use the same philosophy of creating a large swirling flowfield which then, upon a sudden geometric expansion, produces a vortex breakdown where the flame stabilises. The aim of the AEV is to reduce NOx emissions for natural gas to an even lower level than the EV, while being able to run with dry oil conditions also at a emissions level well below 100ppm. No burner presently on the market is able to achieve these levels for oil without the addition of water.

The AEV (advanced environmental burner) consists of three main components: the swirl generator, the transition piece, and the mixing tube. (see Figure 1).

(Notation explanation: e.g. AEV75 - the number represents the mixing tube diameter in millimetres and is a scaling of the burner.)

1.3.1 The swirl generator

The swirl generator is made up of four quarter cones with an internal angle of 18°, each offset from each other to allow for four inlet slots. The inlet air is forced through the slots and sets up a flowfield with a certain axial and tangential profile across the radius of the burner. These profiles are very sensitive to the inlet slots width, and cone peak region, and have a large influence on the final position of the vortex breakdown. High axial velocities prevent any flashback along the axis. In contrast to the EV burner, there is no precessing vortex, but a stable, relatively steady state vortex. Along the side of the inlet slots are the gas injection holes, positioned in order that the best premixed conditions can be obtained by the point of combustion. This includes mixing the gas and air, so that it is as homogenous as possible by the burner exit.

Oil is injected in liquid form through a nozzle at the head (peak) of the swirl generator. The oil nozzle design itself, is the task of this work, and shall be discussed later. For reasons of simple servicing, the nozzle is retractable in the form of a long lance.

In order to produce the large axial velocity along the burner axis and thereby holding the vortex breakdown in a stable position at the burner outlet, so-called head air is introduced around the nozzle. This air does not enter the main inlet slots, but instead enters the burner through four slots in the burner head, flowing into a small volume in between the nozzle and the nozzle chamber walls, and entering the swirl generator around the nozzle head.

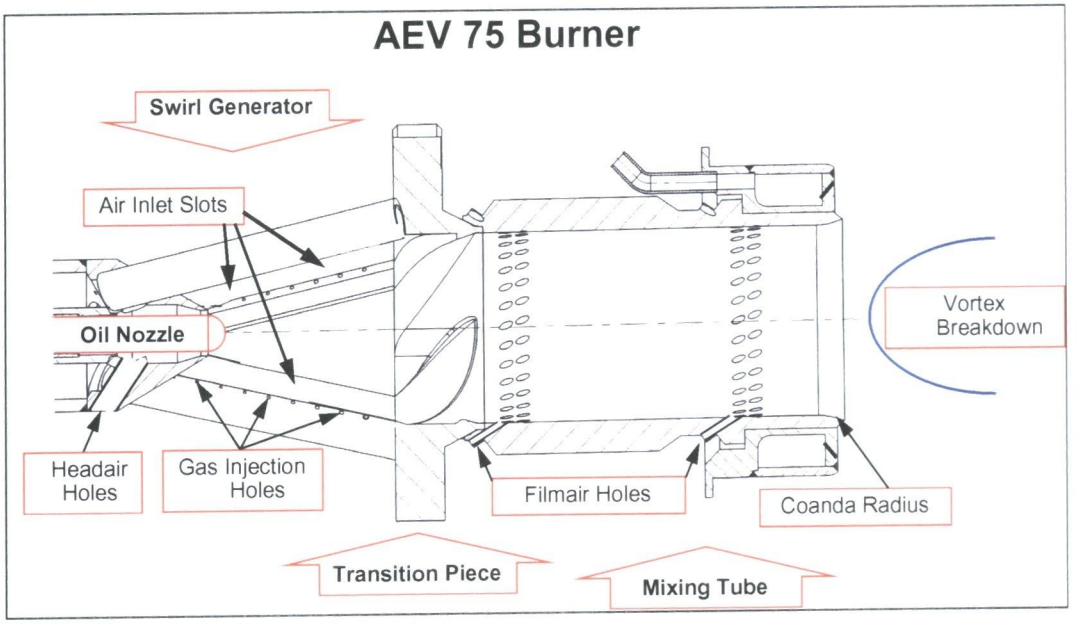

Figure 1

1.3.2 The transition piece

The transition piece, which is geometrically complicated, simply transfers the flowfield formed in the swirl generator to the cylindrical mixing tube, and in doing so attempts to retain the same swirl number and cross-sectional area, creating recirculation zones. Recirculation zones cause high pressure-loss, and more critically create long residence times that could lead to self-ignition.

1.3.3 The mixing tube

In its simplest form, the mixing tube is a cylinder that connects to the transition piece, and finishes by a sudden expansion into the combustion chamber. In this length, the homogeneity of the mixture should be improved, as the fuel and the air mix through turbulence and dissipation. However, contained within the mixing tube are some features that are vital to the successful operation of the burner.

The first are the so-called film-air holes. The holes, laid out to coincide with internal burner flow, allow air to be injected in the near-wall regions of the mixing tube, and have two main functions. The first is to increase the velocities in the boundary layer. As the boundary layer grows, velocities next to the wall become considerably lower towards the end of the mixing tube, and as a result cause the flashback limit to be considerably reduced. (Flashback is the point when the flame speed is higher than the opposing flowfield velocity, where upon the flame works its way upstream. This can cause large pulsations, undesired in turbines, or even worse, can melt the burner walls due to the local high flame temperatures.) By increasing the velocities in the boundary layer, the flashback limit is improved. The second function of the film-air holes is to weaken the mixture in the near-wall region. By injecting pure air into the boundary layer, it becomes considerably weaker and more difficult to combust, and therefore the chance of self-ignition or flashback is reduced.

The other vital feature of the mixing tube is the Coanda radius applied to the exit edge. The Coanda effect is the adhesion of flow to a convex surface under certain conditions. These conditions can be described by the Reynolds number of the flow along with the radius of the convex surface. With the correct choice of geometry, this principle can be applied to the exit of the mixing tube, by rounding the sharp edge. This then guides the near-wall flow in a desired direction and gives more stability to the vortex breakdown.

1.3.4 The vortex breakdown

The vortex breakdown is used to refer to an abrupt and drastic change of structure in a swirling flow, particularly in the leading edge vortex formed above a sweptback lifting surface. (Benjamin - Ref 4) The abrupt expansion of the stream surfaces near the axis leave a low pressure zone in the centre. As a result, some air is forced back towards the axis, and even a little upstream, where upon it recirculates. This is known as the

recirculation zone. Due to the area ratios of the burner to the combustion chamber, velocities decrease, and at the point where the turbulent flame speed is equivalent to the flowfield velocity, (somewhere in the breakdown region), the flame stabilises.

1.3.5 Development of the Burner Geometry

The burner geometry has been developed iteratively in three stages, often with a return to the initial stage.

Firstly the geometry was laid out from results of scaled water tests, where with the help of Laser Doppler Anenometry and Light Induced Fluorescence, accurate measurements could be made of the whole flowfield. Using these methods, the vortex breakdown position and behaviour was optimised.

Later the operation of combustion with natural gas was included, which considered the optimisation of the gas injection holes in order to achieve the most homogeneous mixture, and lowest emission levels. This of course included part load operation, piloting, start-up, lean blow-out limits, and pulsation tests. With this geometry, work could start on the design of a good oil combustion system, with the final aim for dry oil operation with acceptable NOx emissions and reliability. If this could be achieved, a dual fuel, Dry Low NOx burner could be produced.

However, all these processes are interconnected, and the design optimisation of one stage, must be completed with the consideration of the other two. The remainder of the report considers only the third option (the oil combustion development), which started with the optimised burner geometry for gas operation. However, naturally the geometry has altered with time due to the continuous improvement of all three stages.

1.4 Present Nozzles used in ABB Burners

As this is the initial stage of development for oil operation in the AEV burner, no nozzle presently exists. In previous EV burners plain jet nozzles have generally been used (see Chapter 2.2.1). They have the advantage of long penetration depths, and reduce the chance of droplets hitting the side walls of the relatively narrow angled swirl generator. The disadvantage is the relatively large droplets produced, and the inability to achieve a homogeneous mixture before the flame front.

For the AEV burner a pressure swirl nozzle was initially considered. This produces a hollow cone spray and gives small droplets that evaporate quickly. Larger angled sprays can be tolerated as the cone angle of the AEV burner is considerably bigger than the previous EV burner, and there is less chance of drops hitting the swirl generator. Early vaporised oil has a longer time to achieve full mixing with the air before the burner exit.

This was the base point for the start of this development work.

2. Theory

The chapter is split into five main sections describing the theory that applies to the droplet history within a combustion system: *atomisation, penetration, evaporation, mixing & combustion.* Each section explains theories developed and used for the design of such a process. Many of these theories are implemented within the numerical methods applied for the predictions in the core work. These are also described.
Finally a word is written about the consequences that the theory and practice have on the design of the burner.

2.1 Atomisation

2.1.1 Disintegration Theory

The physics of atomisation is complicated and still not fully understood especially at high Reynolds numbers. However, in order for atomisation to occur easily, liquid should contain instabilities at the surface. These instabilities can be created through high turbulence in the liquid, or the interaction with air. High surface instabilities are found in liquids in the form of thin jets or thin sheets, known as lamels or films. It is the task of the nozzle geometry to create these forms, and to supply the liquid with the required energy for instabilities to occur. These two most common forms differ in their disintegration process, and are discussed below. However, some basic theory is the same for them both. Disintegration of the liquid is started by oscillations at the liquid surface. These oscillations grow in amplitude until the forces holding the liquid together at the surface are overpowered. One can describe the equilibrium point of these forces in the following way:

$$P_{\text{internal}} = P_{external-aerodyn.} + P_{surface-tension} \qquad \text{Eq. 1}$$

Weber (Ref 8, Faeth) also considered the external forces due to aerodynamic effects, and related the two opposing forces (surface tension and aerodynamic drag) to give a dimensionless number describing the likelihood of initial break-up. This is known as Weber's number :

$$We = \frac{\rho_{AIR}(u_{DROP} - u_{AIR})^2 D_{DROP}}{\sigma} \qquad \text{Eq. 2}$$

where D can be the diameter of the jet or drop (if considering secondary break-up). The critical Weber number (the initial condition of break-up) can be calculated to be

$$We_{CRIT} = \frac{8}{C_D} \qquad \text{Eq. 3}$$

where C_D is the coefficient of drag as discussed later. Pilch and Erdman (Ref. 24) take considerable detail to discuss the critical Weber's numbers for different breakup regimes. It follows that the higher the Weber number, the higher the chance of break-up and good atomisation. In terms of nozzle design for oil injection in a gas turbine, the parameters that can be optimised are the film thickness and the relative velocity. Relative velocity in a pressure nozzle is proportional to the square-root of the back pressure supplied to the oil. i.e. the higher the back pressure, the smaller the droplets.

After the initial break-up of jets or films, so-called secondary break-up of larger droplets into smaller ones occur.

Large droplets can behave in different ways, depending on the aerodynamic conditions, either fluctuating in shape, or breaking up totally. The most commonly observed disintegration of a large drop is shown in Figure 2. Here the drop flattens due to the air pressure. It then forms a cup shape, which develops into a half-bubble with a thick rim. The bubble and the rim burst into small droplets.

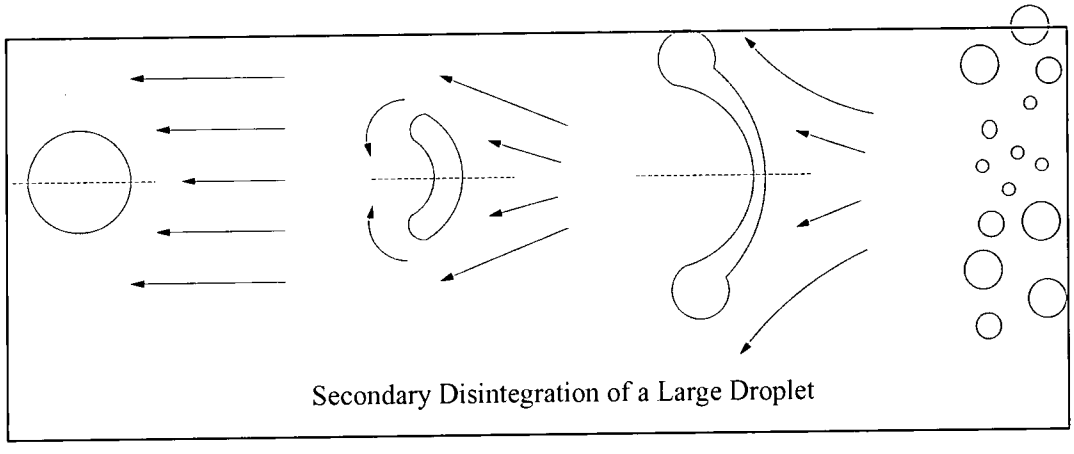

Secondary Disintegration of a Large Droplet

Figure 2

Another common cause of secondary break-up is collision. Two larger droplets that collide can break up into many smaller droplets (see Fig. 3),

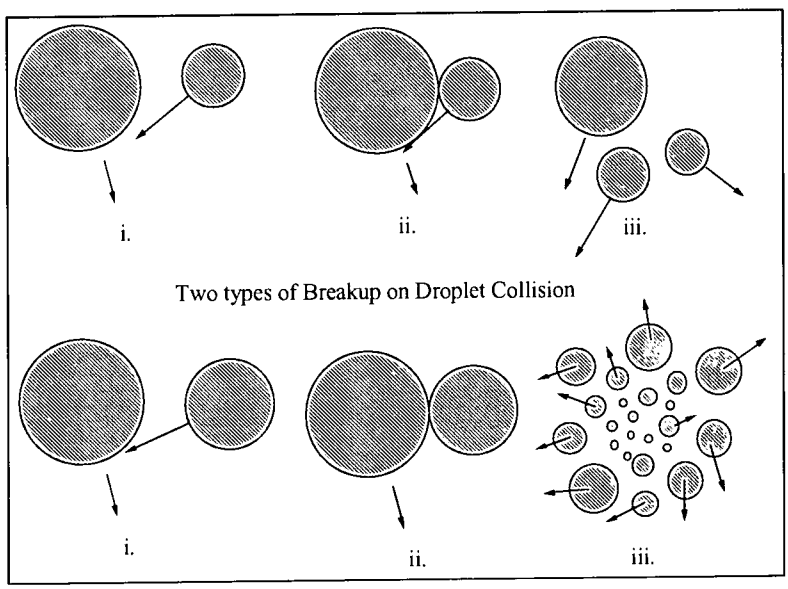

Figure 3

or join together (known as coalescence)(see Fig 4). The outcome is related to Weber's number, break-up generally occurring the higher the Weber number.

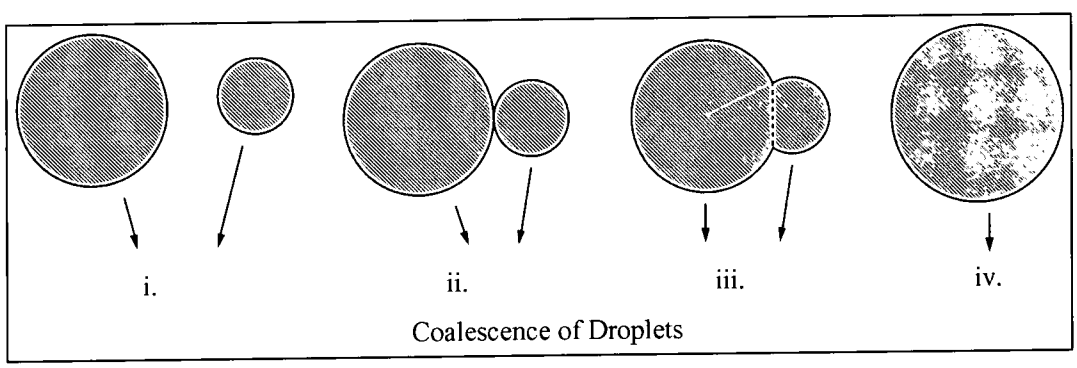

Figure 4

2.1.2 Liquid Jets

The disintegration of liquid jets can occur in different ways, depending upon the exit velocity of the liquid. It is generally accepted that there are three mechanisms that can take place, all using oscillations or perturbations as a means to atomisation. The first is the occurrence of axisymmetric waves that develop in the jet. (see Figure 5).

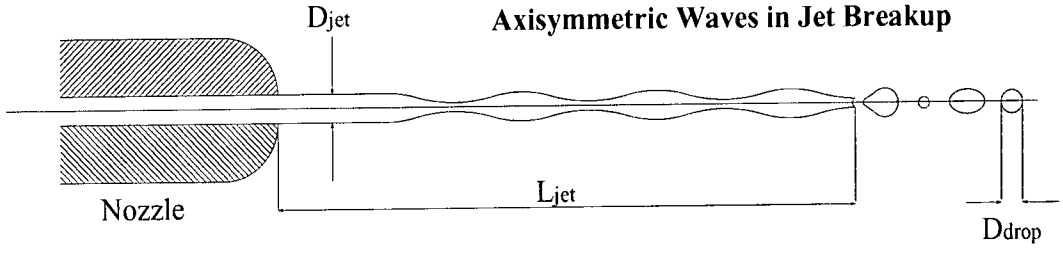

Figure 5

These rotationally symmetric waves in the radial direction can have an amplitude large enough to break through the whole jet diameter . It has been shown that certain wavelength oscillations are damped, while others are likely to become unstable, and grow rapidly leading to jet break-up. In Rayleigh's investigations (1876), he concluded that these unstable oscillations occur when the wavelength is greater than the perimeter of the jet. Weber continued this work for higher flowrates with the aerodynamic influence of air, to conclude that this critical wavelength reduced with a relative air velocity to around only twice the diameter (as compared to 3.14D from Rayleigh). An optimal wavelength for amplitude growth can also be described, and has been found to lie at 4.5 times the diameter. It can then be assumed that this length of jet is turned into a spherical droplet, and the correlation of the droplet size can be calculated (Ref 19, Lefebvre):

$$D_{drop}=1.9D_{jet} \qquad \text{Eq. 4}$$

As the velocity is increased, the oscillation in the jet changes from being axisymmetric to asymmetric, as seen in Figure 6.

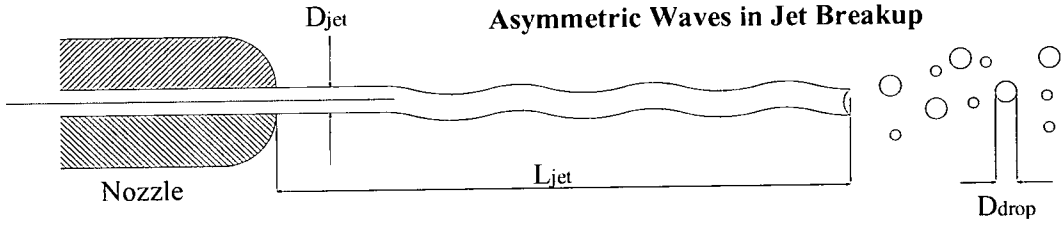

Figure 6

This change to an asymmetric form is due to the increased interaction with the surrounding air. It is for the same reason that jets in varying ambient pressures behave

differently, therefore changing droplet size. This phenomena should be accounted for when designing nozzles for gas turbines that run at relatively high operating pressures. Finally, as the jet velocity is increased even further, aerodynamic forces take priority, and atomisation takes place almost immediately (see Figure 7).

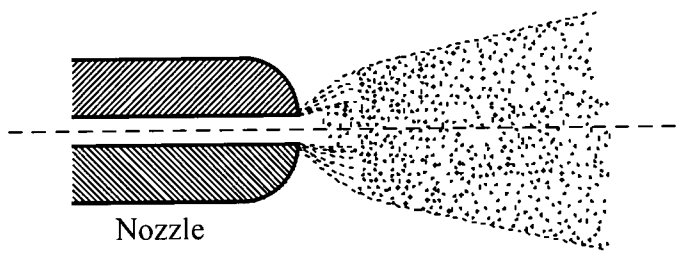

Immediate Atomisation at High Velocities

Figure 7

Ohnesorge's number, a relation of Reynolds number and Weber number, relates these three mechanisms:

$$Oh = \frac{\sqrt{We}}{\mathrm{Re}} \qquad \text{Eq. 5}$$

For a certain Oh number, a specific break-up regime can be assumed. (Ref. 25, Prandtl et al.)

Important parameters that need to be known in jet break-up are the position of break-up, or jet length, and the droplet size formed.

As the jet exits the nozzle, it can do so in either a laminar or a turbulent form depending on the Reynolds number at the orifice. Laminar jets are not so likely to disintegrate due to the lack of perturbations at the jet surface. However, laminar jets are subject to small internal disturbances, that can then cause sudden break-up.

Fully turbulent jets are likely to break-up earlier than laminar jets due to the large radial perturbations at the surface that cause immediate atomisation. The length of jet before break-up in this case is defined by Lefebvre (Ref 19) as

$$L_{jet} = D_{jet} 11.5 We^{0.31} \qquad \text{Eq. 6}$$

As often is the case, the emerging jets are neither fully laminar nor fully turbulent, but a mixture, having a turbulent centre core and a laminar coat. In this case the laminar

coat protects the surface from protruding turbulent perturbations, and as a result of the relatively high impulse, penetrates far into the flow field.

These three length dependencies can be summed up in figure 8.

It can be concluded that it is necessary to create a fully turbulent jet, if early atomisation with small droplets is required.

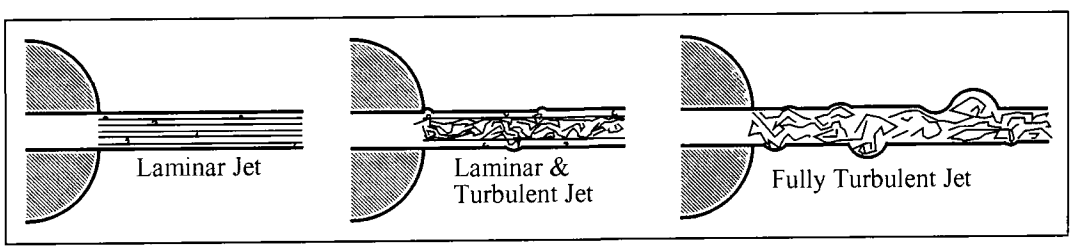

Figure 8

2.1.3 Liquid Sheets

The second type of break-up that occurs from nozzles is that of liquid sheets. There are two break-up mechanisms for sheets: wave and perforation disintegration.

At relatively low velocities, perforation occurs. After at certain distance from the nozzle exit, the film thickness becomes so thin, and the interaction of the surrounding air so high, that the holes and seams appear, which rapidly increase in size. Surface tension pulls the liquid together into ligaments, that then disintegrate into droplets in a similar way to axisymmetric jets.

With rising liquid velocities, the disintegration process changes to a wave break-up system. As the sheet becomes further away from the nozzle exit, axial waves appear. Opposing forces occur; surface tension forces attempting to retain the original form, while external aerodynamic effects (changes in static pressure behind the waves) cause instabilities and lead to an exponential rise in wave amplitude. Whichever effect is initially stronger prevails. The growth of the wave amplitude is found to be a function and wavelength to thickness ratio, and the Weber number. Eventually part of the sheet, normally half a wavelength long, tears away and contracts into a long ligament. This ligament disintegrates further in the usual way into droplets. The resulting average droplet size (SMD), can be related to the film thickness, and is found to be proportional (Ref. 19 – Lefebvre):

$$SMD \propto l_t^{0.4} \qquad \text{Eq. 7}$$

where l_t is the liquid thickness.

In sheet disintegration, the Weber number is the overriding factor in atomisation quality. However, also important is viscosity, and air characteristics such as density and turbulence.

2.2 Nozzles

Many different types of nozzles exist. However those generally used in industrial gas turbines contain no moving parts, and are efficient in their atomisation process: pressure atomisers. Pressure atomisers rely only on the back pressure of the oil to provide the energy needed for the atomisation. Other main group types include rotary atomisers and air assisted atomisers. Air assisted atomisers make use of some of the high pressure air exiting the turbine compressor to provide energy and drive the oil into atomisation. Although air assisted atomisers are used in some industrial turbines, pressure atomisers are preferred for their simplicity.

In order to obtain a good spray and atomisation, energy has to be transferred into liquid kinetic energy and local turbulence. It is local turbulence in the liquid, along with cavitation and reaction with the surrounding air field, that causes the disturbances needed for the disintegration of films or jets into droplets. This process is limited by the surface tension and viscosity that hold the liquid together.

Energy can be provided in three ways. The first, in the case of rotary and ultrasonic atomisers, is through the energy in the nozzle head itself. Rotating or pulsating parts allow the liquid to increase in energy, that finally leads to evaporation.

In air-assist atomisers, it is the surrounding high velocity air that provides the energy. Kinetic energy of the air is impinged on the liquid to provide better turbulence characteristics and finer atomisation, and allow the high shear layer caused by relatively high velocity gradients between the two fluids, to assist in disintegration.

Finally energy transfer for the atomisation process can come directly from the liquid itself in the form of a back pressure. A high pressure drop across the nozzle converts static pressure into kinetic energy. It can be described by the formula:

$$\Delta P = \zeta \tfrac{1}{2} \rho u^2 \qquad \text{Eq. 8}$$

where $1/\zeta$ is the pressure loss coefficient. This type of nozzle, known as a pressure atomiser, is the most efficient and is the most appropriate design for the AEV burner at present. This group can be subdivided into further types, which themselves produce different spray characteristics. Those types considered in this work are discussed in more detail below.

2.2.1 Plain Orifice / Plain Jet

This is, as the name describes, a simple circular orifice at the end of a distribution tube. This is the simplest form of pressure atomiser available. The nozzle produces a full round jet of liquid that breaks up at a relatively large distance from the nozzle exit. The internal nozzle losses are small, and the exit velocities therefore high with respect to other nozzles. The droplets produced are large and result from the fragmentation of the solid jet as described in the section on liquid break-up.

2.2.2 Simplex Pressure Swirl Atomisers

The fluid is injected tangentially into a cylindrical chamber shortly before the nozzle outlet, where a highly swirling flow is created. At the circular nozzle exit a circular thin film of fluid is ejected in the radial direction where upon it follows atomisation regimes consistent to those found in film break-up. Due to the low pressure in the centre of the vortex flow, air is found to creep up the core, well into the swirl chamber of the nozzle. The higher swirling flow field causes a reduction in film layer thickness at the outlet orifice, creating droplets smaller in size. This can be achieved by changing certain dimensions of the nozzle design.

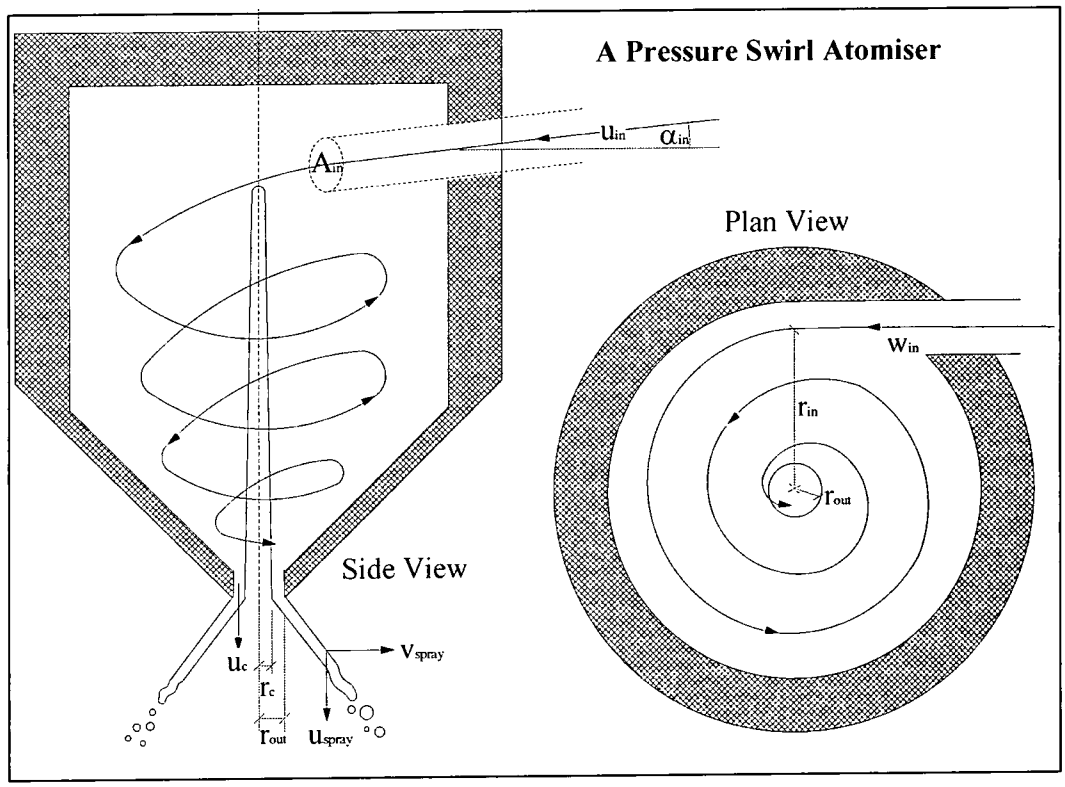

Figure 9

In order to design a swirl atomiser to the requirements of film thickness, spray angle and injection velocity it is necessary to correlate the dimensions of the nozzle to the characteristics of the spray. The dimensions governing the spray characteristics are the following (see Figure 9)

- outlet orifice diameter
- swirl chamber inlet orifice diameter, approach angle, and radial position
- mass flow rate and oil back pressure

Assuming Euler type flow, certain conditions can be observed in the nozzle and equations derived:

Mass continuity

$$\dot{m} = \rho\pi\left(r_{OUT}^2 - r_C^2\right)u_C \qquad \text{Eq. 9}$$

$$\dot{m} = \rho\pi r_{IN}^2 w_{IN} \qquad \text{Eq. 10}$$

Continuity of Angular Momentum

$$\dot{m} r_{IN} w_{IN} = \dot{m} r_c w_C \qquad \text{Eq. 11}$$

Bernoulli's equation

$$\Delta P_{BACKPRESSURE} = \tfrac{1}{2}\rho(u_C^2 + w_C^2) \qquad \text{Eq. 12}$$

This assumes that the applied pressure is stored in the fluid as kinetic energy.

In the Euler flowfield, with the assumption of no losses

$$P_{TOTAL} = const. = P + \tfrac{1}{2}\rho u^2 + \tfrac{1}{2}\rho w^2 \qquad \text{Eq. 13}$$

For a free (potential) vortex

$$\frac{dP}{dr} = \rho\frac{w^2}{r} \quad \text{and u is constant across the radius.} \qquad \text{Eq.14}$$

However at the free surface where the air meets the fluid, the pressure must be equal to the ambient pressure of the air, and therefore

$$P = P_{AMB} + \tfrac{1}{2}\rho w_C^2\left(\frac{r^2 - r_C^2}{r^2}\right) \qquad \text{Eq. 15}$$

At outlet :

$$u_C^2 + w_C^2 = u_{SPRAY}^2 + v_{SPRAY}^2 \qquad \text{Eq. 16}$$

Utilising these equations, the film thickness (r_{OUT}-r_C), along with the velocities and the exit spray angle can be calculated. From these characteristics, a droplet size can be empirically determined. However there is no unique solution, and inaccuracies incurred due to simplifications and assumptions need to be accounted for.

2.2.3 Turbulence Enhanced Jets

This type of nozzle can *not* be found in any text book. It is a commercial design that has recently been found to be both effective and simple. As previously mentioned, the turbulence level in the exiting orifice is an influencing factor in the atomisation quality. With this knowledge, the design aims to increase the turbulence level before the exit orifice by introducing it in the pre-plenum through two or four small holes (see Figure 10). These inlets produce high velocity jets in the pre-plenum that create chaotic swirling turbulent flow patterns. By positioning the inlet holes correctly with respect to the outlet orifice, the turbulence level in the exiting liquid can be optimised, therefore producing earlier atomisation and smaller droplets. Work by Steinbach and Hoferer (Ref. 8) shows the optimisation of this design.

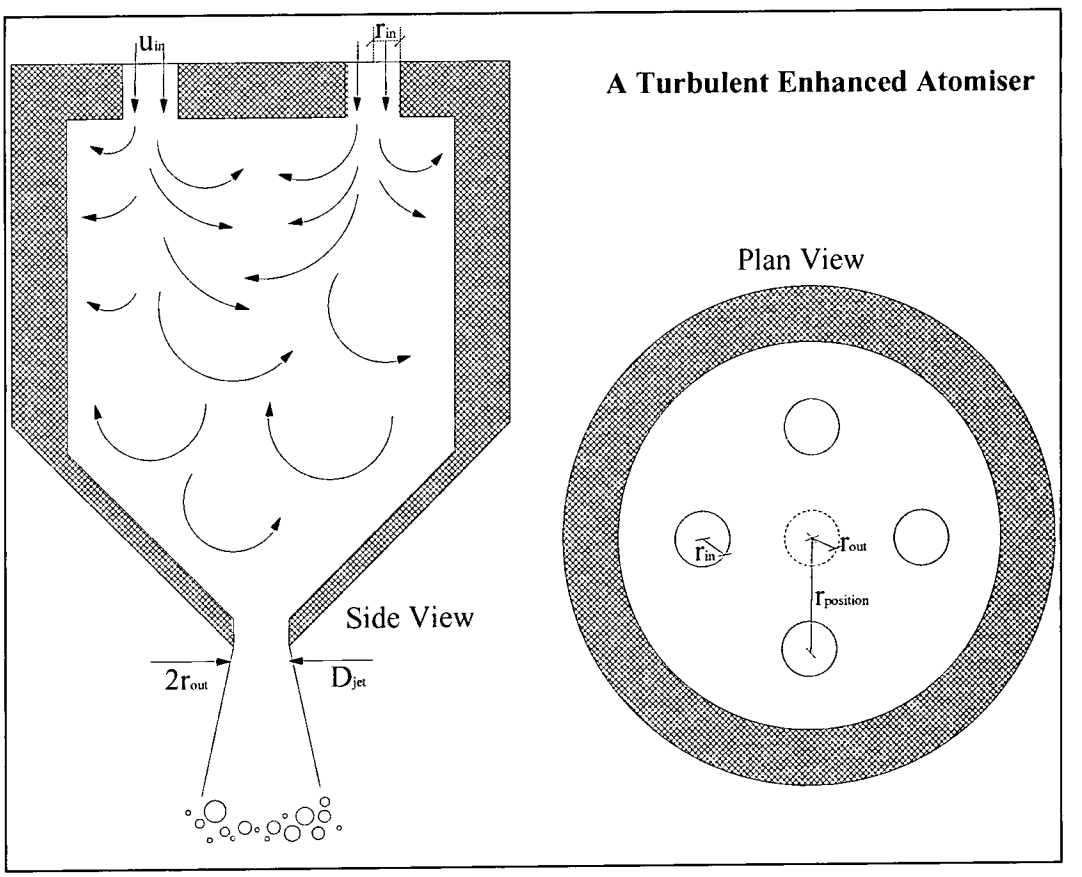

Figure 10

As of yet there are no empirical correlations relating the nozzle geometry to the loss coefficient and droplet size. The loss coefficient can easily be found for a practical nozzle. From this point, other similar nozzles can be designed by scaling.

2.3 *Initial Conditions and Spray Size Definitions*

There are many different ways of describing spray characteristics, but most commonly drop size distributions are important. It is unusual in practice that a nozzle produces constant singular droplet sizes. Most nozzles produce a droplet size range, along with some repeatable distribution, characterised by the break-up regime and near nozzle region flow conditions. The definition of average drop size is the decision of the user, depending on the relevance of the drop parameter, be it surface area, volume, or mass flow rate of the spray. Distribution definition is even more complicated, as almost no model can describe some of the complicated distributions found in certain sprays, often produced by ligament break-up, coalescence and satellite formation.

The most common diameter definition is known as the Sauter Mean Diameter. This is a mean based on the volume to area ratio of the droplets, and gives a realistic value for use in drag calculations and mass transfer. It can be defined as followed:

$$SMD = D_{32} = \frac{\sum N_i D_i^3}{\sum N_i D_i^2} \qquad \text{Eq. 17}$$

Also common is the surface based average:

$$D_{20} = \sqrt{\left(\frac{\sum N_i D_i^2}{\sum N_i}\right)} \qquad \text{Eq. 18}$$

and the volume based average:

$$D_{30} = \sqrt[3]{\left(\frac{\sum N_i D^3}{\sum N_i}\right)} \qquad \text{Eq. 19}$$

Either the median drop size or the mean average drop size is not representative of the spray, as the majority of the mass lies above these values.

In defining the distribution, it is common to use two other representative droplet diameters:

$D_{0.1}$ and $D_{0.9}$ correspond to the diameter below which 10% and 90% of the volume flow of the whole spray exist.

As mechanisms of atomisation are not fully understood, and vary from nozzle to nozzle, it is impossible to create a model describing every spray distribution. There are two frequently used distribution curves aimed at providing a satisfactory fit to data regularly acquired. The first is the pure mathematical function known as Gaussian log-law. More often used is the empirical formula by Rosin and Rammler. This can be described in the following way:

$$M_D = 1 - e^{-\left(\frac{D}{\overline{D}}\right)^n} \qquad \text{Eq. 20}$$

where M_D is the percentage of the spray mass with a droplet size less than D. $\overline{D}$ is the average drop size, while the spread of the distribution is described by n. For the boundary conditions for simulations, data was taken from PDPA measurements, and the values for the average drop size and spread number fitted to correlate a Rosin-Rammler type distribution.

Sprays can also be characterised by their angle, the spread of the angle, and volume flux across a radial plane.

Unfortunately at present, there is not enough theory, along with available software, to present a reliable model of the liquid break-up at the exit of a nozzle into the burner. This is certainly a desire for the future, but for these computations other approximations and methods need to be used.

As there is no break-up or coalescence model in the code used, it is necessary to prescribe the droplets, both in size and quantity, directly at the nozzle exit. For the computations, a mixture of empirical, theoretical and experimental data was used (see Appendix D). As Faeth (Ref. 9) confirms, the problem of adequately specifying nozzle spray exit conditions constitutes the major impediment to the proper use of flow model of sprays.

Initially, a nozzle similar to that expected to be used in the gas turbine was constructed in the form of hardware. Using water as the liquid, and with the correct back pressure in the nozzle, the spray was evaluated using a PDPA (Particle Doppler Phase Anemometry) system. Here 3 laser beams are directed to a measurement volume which are refracted as they pass through droplets. The scattered light intensity is collected by a fibre optic transceiver which can be evaluated through signal analysers. This gives information on the size and quantitative frequency of the droplets from which an SMD value and a corresponding spread value can be calculated. However, these values are for water at atmospheric conditions, and need to be converted into values for oil at the operating pressure of the machine. Using empirical correlations, the author (of this thesis) derived a combination of formula to convert the SMD of water at atmospheric conditions to oil at high pressure. The conversion is as follows:

$$SMD_{\text{oil at 15bar}} = SMD_{\text{water at 1bar}} * f(\text{surface tension}) * f(\text{viscosity}) * f(\text{air pressure}) \qquad \text{Eq. 21}$$

I.) $SMD_{\text{water at 1bar}}$ is taken from measured results from lab tests with the PDPA system.

II.) $$f(Surface\ Tension) = \left(\frac{SurfaceTension_{OIL}}{SurfaceTension_{WATER}} \right)^{a} \qquad \text{Eq. 22}$$

where $a = M_0 + M_1\mu$ (taken from Dorfner et al. - Ref.7)

and surface tension$_{oil}$ = $M_2 + M_3.T_{oil}$ (°C) or taken from tables.

III.) $f(Viscosity) = \left(\frac{Viscosity_{OIL}}{Viscosity_{WATER}} \right)^b$ Eq. 23

where b = constant = 0.25 (taken from Dorfner et al.- Ref.7).

Viscosity$_{oil}$ = $\mu_{OIL} = {}^{\nu_{OIL}}/_{\rho_{OIL}}$ where $\nu_{OIL} = M_4 + \left(T_{OIL}^{KELVIN}\right)^{M_5}$

or taken from tables.

IV.) f(*Air Pressure*) is as follows:

for 1 to 3 bar SMD α $P_A^{0.27}$

for > 3 bar SMD α $P_A^{-0.25}$ (taken from Lefebvre - Ref. 19)

So for machine conditions above 3 bar:

$$f(Air\ Pressure) = \left(\frac{3}{P_{A1}} \right)^{0.27} \left(\frac{P_{A2}}{3} \right)^{-0.25}$$ Eq. 24

If P_{A1} is test rig air pressure (i.e - atmospheric pressure) then $P_{A1} = 1$

and P_{A2} is operating pressure from machine, then

$f(Air\ Pressure) = 1.77 \cdot P_{A2}^{-0.25}$ (applies for atmospheric test rig and machine operating pressure > 3 bar)

Therefore

$$SMD_{oil\ at\ 15bar} = SMD_{water\ at\ 1bar} * \left(\frac{\sigma_{OIL}}{\sigma_{WATER}} \right)^{M_0 + M_1 \mu_{OIL}} * \left(\frac{\mu_{OIL}}{\mu_{WATER}} \right)^{0.25} * 1.77 \cdot P_{A2}^{-0.25}$$ Eq. 25

This provides the SMD at initial conditions. Also required is the droplet exit velocity. This can be calculated in two ways. The first is by knowing the loss coefficient , ζ, of the nozzle. This can be calculated from experimental results. The mass flow rate can be measured, and knowing the density and area of the outlet flow, velocity can be calculated through:

$$u = {}^{\dot{m}}/_{\rho A_{outflow}}$$ Eq. 26

The outlet flow area can be complicated to calculate, as it is a function of the film thickness of the exiting liquid. This is in turn a function of the swirl nozzle geometry as mentioned previously, and should be determined with as high an accuracy as possible. Knowing the experimental back pressure in the nozzle, ζ can be calculated by assuming any additional pressure remaining at the nozzle exit is converted into kinetic energy:

$$\zeta = \Delta P / \tfrac{1}{2}\rho u^2 \qquad \text{Eq. 27}$$

This formula can then be used in the reversed form to calculate the velocity for any desired pressure.

The second possible way to calculate the initial velocity, is by measuring the velocity of the droplets at a specific point after injection, and using an inverse iterative process to calculate the reverse path of the droplet back to the point of injection by applying the Drag Law assumptions for deceleration. It is impossible to measure droplet velocities at the exit point of the nozzle using the PDPA system, as the spray intensity is too high, and individual droplets can not be determined. As Faeth (Ref 8) rightly claims, it is only possible to measure the droplet size some distance away from the nozzle, and then average spray characteristics must suffice. Also break-up does not in practice occur at the nozzle exit itself, but somewhat downstream, as discussed in the Droplet Break-up Section 2.1. A program was then written, that uses the formula describing the deceleration due to drag (as described in Section 2.5 – Forces on Droplets), to calculate the initial velocity of the droplets.

In areas where the droplets did not induce substantial entrainment of the air (i.e. as in the core of the hollow cone spray), good agreement was found between the two methods. In inner areas, the spray causes entrainment of the air, which means that assumptions for $v_{DROP} - v_{AIR}$ are no longer valid, because v_{AIR} cannot be correctly calculated. An average droplet in a spray will penetrate further than a single isolated droplet injected with the same conditions.

2.4 Droplet Trajectory Theory

2.4.1 CFD Techniques

It is not within the scope of this thesis to discuss the continuous gaseous phase numerical theory. This work has been completed with a commercial Navier-Stokes solver (see Ref. 5). However, this section describes the theory for the second phase trajectories (i.e. droplets), most of which is implemented in the CFD code.

2.4.2 Euler-Euler Methods

For two phase modelling in numerical codes two possible techniques are commonly used: Lagrangian and Euler methods. The way the liquid phase is treated is quite different in each case. Within the Euler-Euler method the phases and species are calculated on a volume-fraction based method, where conservation equations are continuous in both time and space. Each of the two phases can have x number of species within that state. Equations are solved through a common pressure term, and other equations of momentum and mass exchange are implicitly calculated. Turbulence interaction between the phases is also possible. This model is mainly used when the volume fraction of the second phase is of the same order of magnitude as the first phase. Disadvantages include the long CPU times, large memory usage, slow convergence, and more importantly the inability to allow phase change. In the case of evaporating droplets, this ability is critical for the correct vapour prediction.

2.4.3 Lagrangian Methods

Lagrangian methods use a converged continuous phase solution and model the secondary phase (droplets) by integrating the forces on the particle over discrete time steps. By coupling the two phases, the mass and heat exchange can also be calculated. Using time averaged Navier-Stokes equations and a k-ε turbulence model, the air-field is calculated in the normal way without the influence of oil droplets. After convergence the oil droplets are injected from a specific cartesian coordinate defined by their initial velocity, average size, size spread, temperature and mass flow rate. The forces acting on them are calculated using values corresponding to that particular coordinate in the air-flowfield. The effects of turbulence from the air-field can also be accounted for. Heat exchange is calculated, and a new droplet temperature calculated. These values are used to calculate the new position and size of the droplet after a single time step,

using a simple integration over time (u.dt = dx). The process repeats itself until the droplet reaches one of the domain boundaries, hence terminating.

With such a method the direct trajectory of every particle can be observed.

However this approach should only be used when the volume fraction of the dispersed phase is small, as there is no consideration of droplet-droplet collision or interaction. No effect on the local gaseous phase pressure field is considered due to the small specific volume ratio. This is valid in the case of oil droplet in the AEV burner with the exception of cells very close to the nozzle.

2.4.4 Coupling in the Lagrangian reference frame

By coupling both phases, the interaction and effect of the particles on the continuous flowfield can also be accounted for. When the solver calculates the heat and momentum exchange *to* the droplet in the trajectory calculations, exchange values can be stored for every cell/co-ordinate and used as inputs for a new continuous phase solution. After each complete droplet/spray trajectory calculation, the continuous phase can be recalculated with the source values, and a new 'droplet influenced' air-flowfield solved. When the solution is converged, another similar droplet trajectory calculation can be made on the 'new' air-flowfield. This method can be repeated until a stable coupled solution is found.

It is not possible to calculate the effect of the droplet turbulence on the air-field, as there is no turbulence term stored for the droplet.

2.5 Forces on Drops

In reality, the trajectory of the particle is governed by forces exerted on the droplet which change its velocity. Newton's Second Law of Motion provides the basic principle equation describing the trajectory motion:

$$F = m\,du/dt \qquad \text{Eq. 28}$$

F, the force acting upon the droplet, consists of a number of components, the most influential being drag force. Other forces of importance are gravitation, inertia, thermopheretic and large static pressure gradients. Some forces are negligible in certain circumstances, while others play a large role. For each computation, one needs to

assess the conditions, and prescribe those forces necessary for an accurate prediction. The above forces are discussed in more detail below.

2.5.1 Drag Force

The most influential force on a particle's acceleration is the drag force. Stokes Law states that

$$F_D = 3\pi\mu_{AIR}u_{DROP}D_{DROP} \qquad \text{Eq. 29}$$

However this is only true for very low droplet Reynolds numbers (<1) (Ref. 29 – Loo) where the inertial forces are so small that they can be neglected. (see Figure11 from Ref. 12). Within the investigation for Gas Turbine burners, droplet Reynolds numbers lie in the range 10 to 1000. Therefore the drag force must be described in another way. This can be described as a function of the kinetic energy the particle exchanges with the air. The force equation

$$F_D = \dot{m}\frac{du}{dt} = A_{X-S}\cdot C_D\cdot(\tfrac{1}{2}\rho_{AIR}(u_{DROP}-u_{AIR})^2) \qquad \text{Eq. 30}$$

contains the projected area and a co-efficient of drag. Replacing F_D by equation 29 in the above equation, C_D for the Stokes equation becomes

$$C_D = \frac{24}{\mathrm{Re}} \qquad \text{Eq. 31}$$

This drag co-efficient is a function of Reynolds number, where

$$\mathrm{Re} = \frac{\rho_{AIR}(u_{DROP}-u_{AIR})D_{DROP}}{\mu_{AIR}} \qquad \text{Eq. 32}$$

However for the whole Re value range, the standard coefficient of drag was later experimentally derived. Alexander and Morsi solved this empirically and describe the corresponding co-efficient in the following way:

$$C_D = d/\mathrm{Re}^2 + e/\mathrm{Re} + f \qquad \text{Eq. 33}$$

However to retain accuracy, the constants of the quadratic equation must be changed every order of magnitude. These can be found in reference 14. For Reynolds number values used in this work, which generally start in the range 100-1000, d=2778, e=98.3 and f=0.3644.

The dependency of C_D value on Reynolds number is determined by the position of the separation of the boundary layer behind the droplet. As the layer turns from laminar to

turbulent (at Re=3x10^5), a sudden drop in C_D value can be seen as the separation of the boundary appears further downstream on the droplet surface.

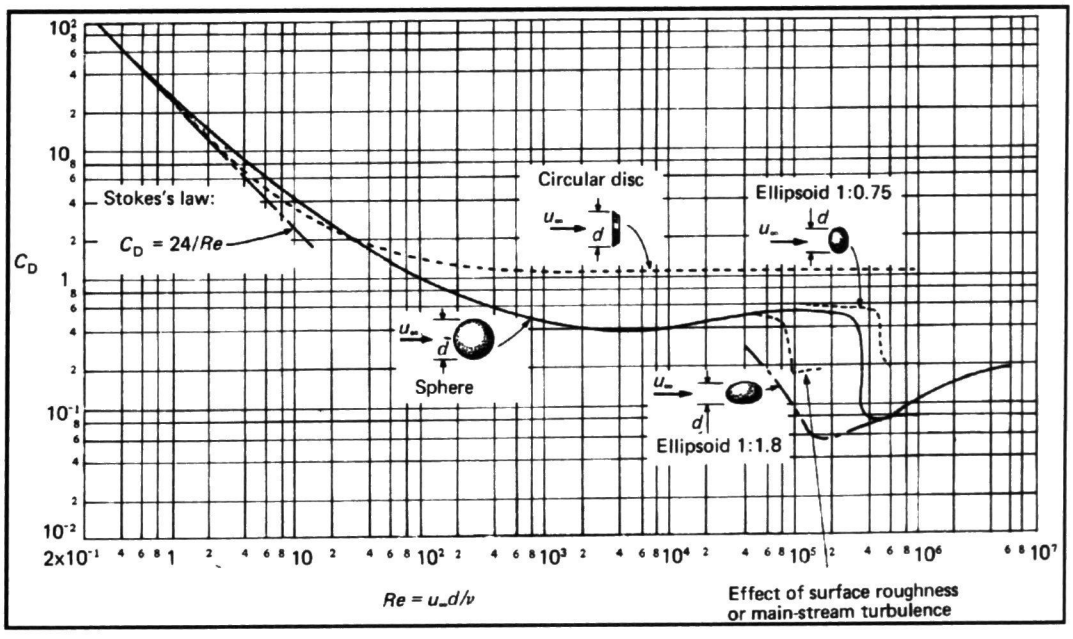

Figure 11

Implementing Eq. 30 into Eq. 28,

and knowing $$A_{X-S} = \pi \frac{D_{DROP}^2}{4} \qquad \text{Eq. 34}$$

and the droplet mass $$M = \pi \frac{\rho_{DROP} D_{DROP}^3}{6} \qquad \text{Eq. 35}$$

simplification reduces the acceleration due to drag to the formula

$$du/dt = \frac{3}{4} \frac{C_D \rho_{AIR} (u_{DROP} - u_{AIR})^2}{\rho_{DROP} D} \qquad \text{Eq. 36}$$

Knowing droplet velocities from the PDPA test rig, this formula can be used to calculate initial droplet velocities.

2.5.1.1 Modifications to the drag model

The drag coefficient of evaporating droplets is complex. Due to the fact that the droplet has an evaporation function at some or the majority of time during its trajectory, certain factors affect its drag performance. The effect of the heat and mass transfer by conduction, convection or diffusion between the droplet surface and the external medium, known as the Stefan flow, results in the thickening of the boundary layer. As vaporisation of the droplet takes places, air-vapour exchange at the droplet surface

causes this change in the boundary layer effect. Alongside this, the temperature distribution in the near-surface region is lowered, due to the lower vapour temperature. This principle cause is known as the blowing effect.

These alter skin friction and drag losses. The drag form model can be crudely corrected by the simple formula derived by Renksizbulut & Yeun

$$C_{D-Corr} = \frac{C_D}{1 + X_M} \qquad \text{Eq. 37}$$

(Ref 1, Abramzon et al.)

where X_M is the mass transfer number describing the vapour mass diffusion rate of the droplet in terms of concentration gradient. The mass transfer number can also be described in different ways, the most common being the Spalding number (Ref. 1, Arbamzon et al., Ref. 5, Chin et al; Ref. 8, Faeth):

$$X_M = \frac{C_{i,surf}}{1 - C_{i,surf}} \qquad \text{Eq. 38}$$

($C_{i,surf}$ = mass fraction concentration of fuel vapour at the droplet surface)

More complicated ways of accounting for the blowing effect can be found, often resulting in a totally new drag formula.

A simplified expression for evaporating droplets is proposed by Putnam where

$$C_D \frac{\mathrm{Re}}{24} = 1 + \frac{\mathrm{Re}^{2/3}}{6} \qquad \text{Eq. 39.}$$

This is often taken as the standard drag curve for evaporating droplets. (Ref. 1, Abramzon et al.)

A method has been derived by Sparrow and Gregg known as the '1/3 rule', which takes

$$T = T_{SURF} + \tfrac{1}{3}(T_{AIR} - T_{SURF}) \qquad \text{Eq. 40}$$

and

$$C = C_{SURF} + \tfrac{1}{3}(C_{AIR} - C_{SURF}) \qquad \text{Eq. 41}$$

These values can then be used to calculate the gas viscosity for the Reynolds number, which can then be applied to the standard drag curve. (Ref 8, Faeth; Ref 5, Chin & Lefevre; Ref. 17, Kreutzer, Ref. 28, Sirignano)

In the following computations, blowing effects have been omitted, firstly due to the coarseness of the simple correction, and secondly to the complexity of the implementation of a more accurate model.

As discussed later, experimental results have shown that the basic drag model shows very good agreement with droplet trajectories of swirl atomisizers.

2.5.2 Gravitational force

Gravitation can cause considerable trajectory changes when density ratio between the continuous fluid and the droplets is high, and the velocity to droplet residence time is low. This gravitational force is also known as buoyancy.

$$F_{GRAV} = g\frac{\pi D^3}{6}(\rho_{DROP} - \rho_{AIR}) \qquad \text{Eq. 42}$$

2.5.3 Inertial Force

The droplet is subject to an extra force in order to accelerate the surrounding fluid. This is most important when the droplet density is lower than the fluid density (i.e. bubble regimes), although can have minor effects in other situations, especially when there is a large relative acceleration. It can be described by the following:

$$F_{INERT} = \frac{\rho_{AIR}\pi D^3}{12}\left(\frac{d(u_{AIR} - u_{DROP})}{dt}\right) \qquad \text{Eq. 43}$$

(Ref. 8, Faeth)

The inertial effects are also the cause of droplet breakup.

2.5.4 Pressure Gradient

Static Pressure Gradients found in the fluid field, (mainly built up from the acceleration of fluid as described above) can provide an additional force. These are, however normally negligible. These forces can act in a positive or negative direction. Integration around the droplet surface (Ref. 29, Loo) gives:

$$F_{PRESS} = \frac{\rho_{AIR}\pi D^3}{6}\left(\frac{du_{AIR}}{dt}\right) \qquad \text{Eq. 44}$$

2.5.5 Thermopheretic Force

When high temperature gradients are present locally, a thermo-term is needed for the force correction. In the case of a Gas turbine burner, it can be taken to be irrelevant, because the force only has considerable effect at low temperatures.

$$F_{THERM} = \frac{\rho_{AIR}\pi D^3}{6} D^T \frac{1}{T}\left(\frac{\delta T}{\delta x}\right) \qquad \text{Eq. 45}$$

2.5.6 Bassett's Force

The final force that has been omitted from the calculations, although should be considered as a program limitation, is the Bassett force. This accounts for deviations in the velocity from the steady state case (mean free path) by considering the boundary layer slip effect. It is equated to

$$\frac{3}{2} D_{DROP}^2 (\pi \rho_{AIR} \mu_{AIR})^{1/2} x \int \frac{d(u_{AIR} - u_{DROP})}{dt'} \cdot \frac{dt'}{\sqrt{t - t'}} \qquad \text{Eq. 46}$$

As the density difference is so large it can be ignored (Ref. 16 – Krämer). It can be important in laminar flows where Reynolds number is low.

Slip can also occur due to the fact that the liquid surface moves under shear causing internal circulation.

All the above equations apply to single droplets. In reality a cloud of droplets creates a different drag co-efficient to that of a single droplet. Steinmour (Ref. 29 – Loo) claimed a higher volume fraction than 2% gives significant droplet-droplet interaction. There are many corrections to the formula for C_D for a single droplet in a spray cloud. One of these is derive from Ergun and Orning as:

$$C_D = 200\left(\frac{1-\varepsilon}{\varepsilon^2}\right)\frac{\mu}{Du_\varepsilon \bar{\rho}_{OIL}} + \frac{7}{3\varepsilon} \qquad \text{Eq. 47}$$

where u_ε is the relative velocity of the cloud to droplet and ε is the void fraction.

2.6 Evaporation Models

The full evaporation process of a droplet, which includes the heat and mass exchange between the droplet surface and the surrounding air, is complicated. Many investigations have lead to summarizing experimental results by the so called d-squared law of constant evaporation (Ref. 5, Chin et al, Ref 8, Faeth, Ref. 18, Law; Ref. 28, Sirignano) . This describes the reduction of droplet size as:

$$D_0^2 - D^2 = \beta t \qquad \text{Eq. 48}$$

where D_0 is the initial droplet size, and β the evaporation constant. However, this law has many simplifications. These include:

- The neglect of forced and natural convection of vapour from the drop surface
- no droplet-droplet interaction or concentration/temperature gradient dependability. This is known as the 'dilute spray approximation' and is generally valid for phase regions where the length from the nozzle in comparison to the nozzle diameter is greater than 10. (Ref 8, Faeth)
- it is a diffusion controlled process
- the droplet is assumed spherical even though drag is likely to deform it into a elliptical form. All simple correlations implicitly treat drops as spherical (Ref. 9, Faeth)
- it is isobaric
- there is no account for the blowing effect
- the droplet has zero gradient temperature profile. In reality the temperature inside the drop is not uniform, but is cooler at the centre of the drop than at the surface. (see figure 13). Slip between the droplet and the surrounding gas leads to the formation of a boundary layer with increased convective heating. The friction at the droplet surface causes internal circulation, increasing 'diffusion' rates and tending closer to a zero temperature gradient droplet (in comparison to a stationary droplet). However, according to Sirignano (Ref. 28) these do not reduce temperature gradients to a negligible amount.

It should also be noted that droplet evaporation is actually unsteady due to the following reasons:

- droplet heating occurs - this is the primary heat sink in the initial part of the trajectory, not the need for heat of vaporisation. Therefore a slight swelling due to heating without evaporation occurs at the beginning of the droplets lifetime.(Ref 8 – Faeth)
- there is fuel-vapour accumulation in the gaseous phase causing lower concentration gradients. This is particularly the case in real sprays where the spacing between droplets is small. Not only this, but also the outward flow of fuel vapour impedes the rate of heat transfer to the droplet.
- there is forced and natural convection both inside the droplet and in the gaseous phase that is not accounted for in non-steady processes

- Oil is a multi-compound fuel, that has varying evaporation temperatures and therefore varying evaporation rates

Taking fewer assumptions, droplet evaporation can be divided up into three main stages: heating, evaporation, and boiling. Here are two main assumptions. Firstly is that the droplet is spherical. Form drag most likely reduces it to an ellipsoidal form, although to what extent depends on the Re number. The second assumption is that of total temperature uniformity throughout the droplet. This is unlikely to be the case with large droplets at the beginning of their trajectory. At the surface, the temperature will be somewhat higher than the centre of the droplet. As time continues, the gradients inside the droplet become smaller. Finally a point is reached where all the heat transferred to the droplet is used for vaporisation, as the droplet temperature stabilizes. This is known as the 'wet-bulb' temperature. Using the correct vaporisation temperature described below, one can account for these effects.

2.6.1 Heating

The first law, heating, applies so long as the temperature of the droplet is below the theoretical 'vaporisation' temperature. This contains terms for the heat of the droplet due to convection and radiation.

$$m_{DROP} C_P \frac{dT_{DROP}}{dt} = hA_{DROP}(T_{AIR} - T_{DROP}) + \varepsilon_{DROP} A_{DROP} \sigma_B (\theta_R^4 - T_{DROP}^4) \qquad \text{Eq. 49}$$

The first term on the right hand side of the equation relates to the convective heat transfer, by a simple temperature gradient. h, the convective heat transfer co-efficient is Reynolds number dependent, and can be calculated from the Ranz-Marshall correlation, where

$$h = {Nu \cdot k_{AIR}}/{D} \qquad \text{Eq. 50}$$

(Ref. 28, Loo; Ref 8, Faeth;)

(k-thermal conductivity of air)

and the Nusselt number

$$Nu = 2 + 0.6 \mathrm{Re}_{DROP}^{0.5} \mathrm{Pr}_{AIR}^{0.33} \qquad \text{Eq. 51}$$

(Ref 8, Faeth)

Other formulae for the Nusselt number can be found, for example, by Drake (Ref. 29, Loo), who claims the best fit empirical curve to experimental data is

$$Nu = 2 + 0.459\,\mathrm{Re}_{DROP}^{0.55}\,\mathrm{Pr}_{AIR}^{0.33} \qquad \text{Eq. 52}$$

where Prandtl number is defined as

$$\mathrm{Pr} = \frac{C_P \mu}{k} \qquad \text{Eq. 53}$$

The second term of equation 49 is the resulting radiation absorption as a function of Boltzman's theory, using the emissivity of oil, ε, the radiative area of the drop, A, Boltzman's constant, σ, and the difference of the temperatures to the fourth power. However according to Faeth (Ref. 9), radiation effects can be neglected as gaseous radiation bands are generally not coincident with absorption bands of most liquid fuels. In the heating stage, there is no mass transfer equation required.

2.6.2 Evaporation

When the vaporisation temperature is reached, a new formula is applied to describe the heat exchange. It is very similar to the heating law equation, with the simple addition of an extra mass flux term for the vaporising part.

$$m_{DROP} C_P \frac{dT_{DROP}}{dt} = hA_{DROP}(T_{AIR} - T_{DROP}) + \varepsilon_{DROP} A_{DROP} \sigma_B (\theta_R^4 - T_{DROP}^4) - \frac{dm_{DROP}}{dt} h_{fg} \qquad \text{Eq. 54}$$

(Ref 8,9, Faeth)

where h_{fg} is the latent heat of vaporisation. The rate of evaporation dm/dt, is calculated from the molar flux, as a function of the vapour concentration gradients

$$N_i = k_m (C_{iSURF} - C_{iAIR}) \qquad \text{Eq. 55}$$

C_{iSURF}, the vapour concentration at the droplet surface is determined from the ideal gas law:

$$C_{iSURF} = \frac{P_{SAT}}{RT_{DROP}} \qquad \text{Eq. 56}$$

C_{iAIR} is, of course, the result of previous mass exchange by other particles.

k_m, the mass transfer co-efficient uses a Nusselt correlation (Ref 8, Faeth), which is also dependent on the diffusion co-efficient of vapour in the bulk flow (Di) to consider the effect of convection

$$Nu = 2 + 0.6\,\mathrm{Re}_{DROP}^{0.5}\,Sc^{0.33} = \frac{k_M D}{Di} \qquad \text{Eq. 57}$$

Knowing N_i, the mass transfer of the droplet can be calculated over the integral time step,

$$\frac{dm_{DROP}}{\Delta t} = N_i A_{DROP} M_i \qquad \text{Eq. 58}$$

(M_i-molecular weight of drop)

and finally used in the heat transfer equation 54.

As has already been mentioned the main hindrances to evaporation are the blowing effect, and reduced temperature and pressure gradients due to other evaporating droplets in the near-field.

2.6.3 Boiling

The boiling law is implemented as soon as the whole droplet has reached saturated vapour temperature is reached, and is given as:

$$\frac{dD}{dt} = \frac{4k_{AIR}}{\rho_{DROP} C_{P,AIR} D}\left(1 + 0.23\sqrt{\mathrm{Re}_{DROP}}\right)\ln\left(1 + \frac{C_{P,AIR}(T_{AIR} - T_{DROP})}{h_{fg}}\right) \qquad \text{Eq. 59}$$

This term does not include radiative terms, and assumes a constant droplet temperature at boiling.

Using the information from all three laws, the equation for the coupling of the heat exchange between gaseous and liquid phase can be formulated as:

$$Q = \sum_{i}^{n}\left(\overline{m}_{i,DROP} C_P \Delta T_{DROP} - \Delta m_{i,DROP} h_{fg}\right) \qquad \text{Eq. 60}$$

where the first term is the heat exchange due to droplet heating, and the second term is the energy loss in the evaporation of molecules from the droplet surface.

2.6.4 Change of Characteristic Constants with Temperature and Pressure

The change in characteristic parameters with surrounding operating conditions can vary considerably from parameter to parameter. Almost all are subject to temperature change, and a number also vary with pressure. As pressure increases to 20bar, the lifetime of an evaporating droplet decreases, mainly due to the higher rates of

convection. A comprehensive study of these parameter profiles has been completed and is shown in the Appendices of the first technical report (Section 3.8).

2.6.5 Single Component / Multi-component fuels

As mentioned, certain inaccuracy is brought to the calculations with the simplicity of model using only a single compound and uniform temperature droplet. The difference between the evaporation curve (assuming the d-squared law) for a single compound, and a dual compound liquid can be seen in figure 12.

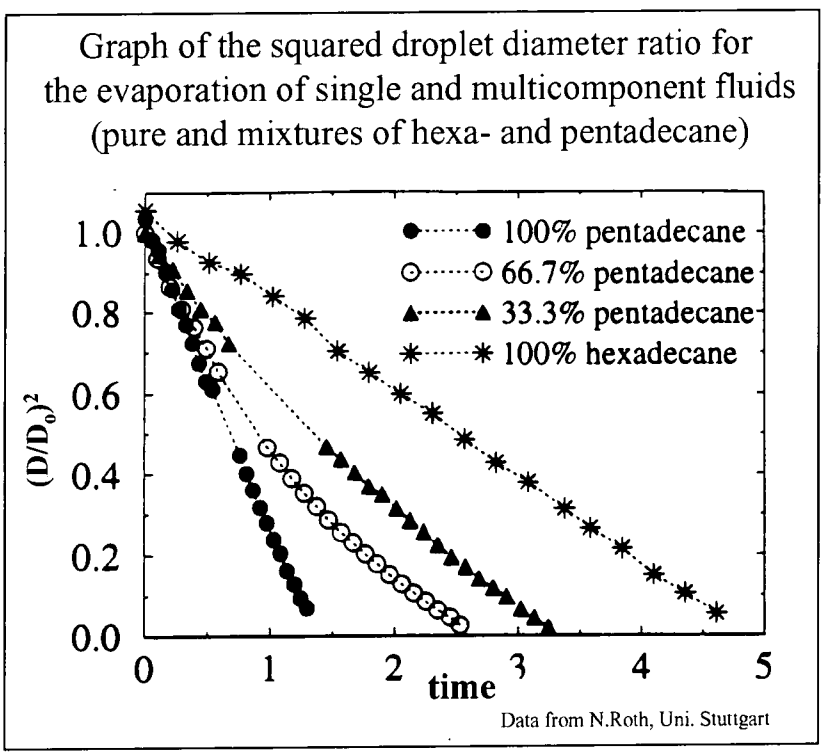

Figure 12

When moving to a multi-component model, there are two approaches that can be taken. Firstly if evaporation is relatively slow, diffusion within the droplet can be assumed rapid (known as the Rapid Mixing model – Ref 1, Abramzon et al), and concentration gradients negligible. In this case, a so-called boiling curve model can be used where the concentration of each component is recalculated at each time step. Each component evaporates separately, the most volatile first, one after the other, as the droplet rises to the corresponding species' boiling point. The droplet remains at that temperature until

the species is fully evaporated, and then heats up to the critical temperature of the next species. As a result, a multi-component fuel does not achieve a 'wet-bulb' state.

However, in the case of fast evaporation rates, the rapid diffusion of species to the droplet surface cannot be assumed. Diffusion is now the limiting mechanism, and the heat and mass transfer now needs to be calculated in the internal droplet volume. Such methods are normally 1D methods across the radius of the droplet. However, mass and heat transfer within a droplet can be very different. Mass diffusion is very slow compared to heat diffusion, so slow in fact, that the characteristic droplet diffusion time is often longer than the droplet lifetime. (Ref. 8, Faeth; Ref. 28 Sirignano). Unfortunately the diffusion limited model requires around 20 times more CPU time than the rapid diffusion model. This requires the discretization of the droplet, with new values for the concentration and temperature gradients to be determined at each time step. Figure 13 shows a representation of the two methods.

Present methods do not yet allow such a model to be simply implemented. Oil contains many compounds and this data would need to be implemented in some kind of lookup table. For the time being, the characteristics of tetradecane have to substitute oil. In reality, more volatile substances vaporise earlier, implying that as the droplet moves through the combustor gradually evaporating, there will be regions rich with less volatile components. This is somewhat compensated by the distribution in the initial droplet sizes.

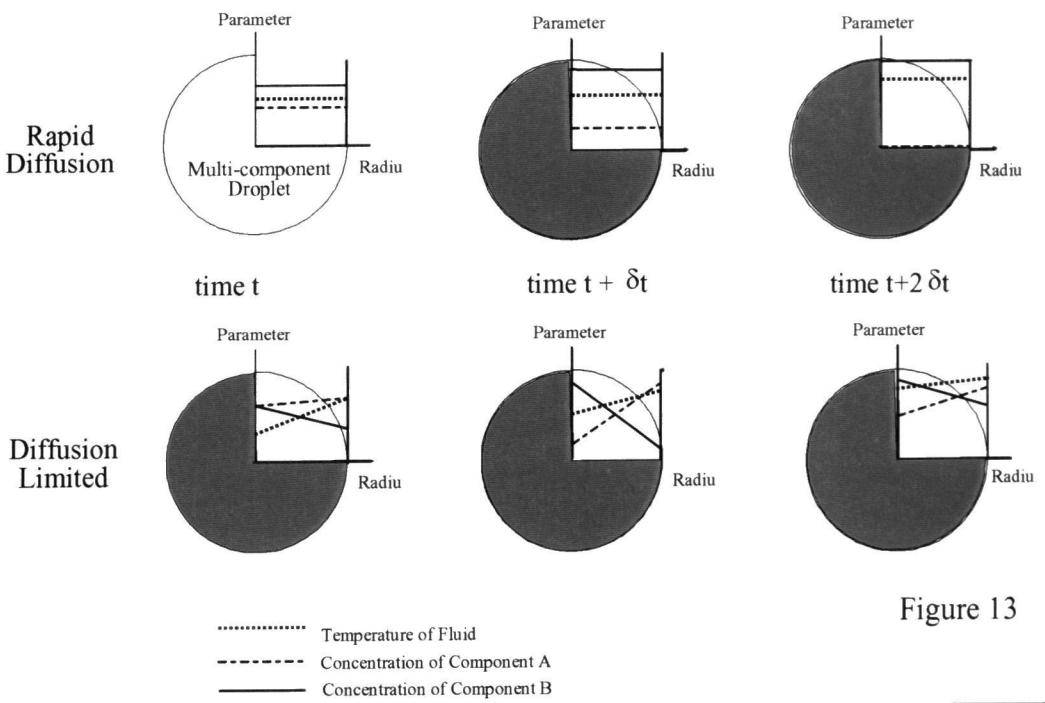

Figure 13

2.7 *Mixing*

2.7.1 Turbulent Particle Paths

In turbulent regimes, the continuous flow field has an influence on the droplet paths, as do the droplet's turbulence on the air flow field. However, within the coupled solution of the program used, there is no source term of turbulence supplied from the droplets, and only the effect of the air on the droplet trajectories is accounted for.

As the droplets continue their path through the turbulent field, their trajectory can be changed depending on the size of eddies. By using a random turbulent velocity, within the bounds of the local eddy turbulence, the turbulent dispersion effect can be accounted for if enough particle paths are computed. There are two ways of choosing the random turbulent velocity. These are known as the Eddy-Lifetime Model, and the Continuous Random Walk Model.

For the eddy lifetime model, a turbulent velocity will be chosen from random according to the Gaussian probability law at that local kinetic energy level. This turbulent velocity will be added to the mean velocity to create the particle velocity. This velocity lasts for the lifetime of the eddy or the length-scale of the eddy, which ever is shorter. On termination of that eddy, it will take on a new turbulent velocity, typical of its new local position and turbulent eddy characteristic.

The turbulent length scale is taken to be

$$T_L = C_\mu^{0.75} k^{1.5} / \varepsilon \text{ for the k-}\varepsilon \text{ model} \qquad \text{Eq. 61}$$

while the eddy lifetime is often a function of length-scale

$$\tau = T_L / (2k/3)^{0.5} \qquad \text{Eq. 62}$$

(Ref. 8, Faeth)

By contrast, the Continuous Random model chooses a new turbulent velocity every time integral. The time integral can be fitted to the turbulent length scale, and a Gaussian distributed random factor associated with the new turbulent velocity. However, this is more computational expensive, and therefore the Eddy-lifetime model was chosen in the burner computations.

Because the k-ε turbulent model has been used, isotropic velocities are assumed, although in reality mean velocity vectors can differ considerably in the three

dimensions. This also allows errors in the particle dispersion, although the more accurate RSM (Reynolds Stress Model) is not commercially available for dispersed phase calculations.

2.7.2 Vapour Mixing

Once in the vapour form, oil to air mixing is calculated as a two-species single-phase model which includes the full closures for turbulence, and solves the Navier-Stokes equations in the usual way. Mixing occurs through a convection-diffusion equation which calculates the mass fraction of each component.

2.7.3 Lambda value

This is defined as the actual air to fuel ratio divided by the stoichiometric air to fuel ratio, and gives an indication of the amount of excess air available in a combustion mixture, and the gradients show how homogeneous a mixture is.

$$\lambda = \frac{\left(M_{oil} / M_{air} \right)_{Mixture}}{\left(M_{oil} / M_{air} \right)_{Stiochiometric}} \qquad \text{Eq. 63}$$

2.8 Combustion

2.8.1 Adiabatic Flame Temperature

When a molecule of fuel is fully oxidised in the combustion process, an exothermic reaction takes place, and a certain energy release per molecule of fuel is given in the form of heat. Depending how much excess air ratio there is in the precombustion reaction, the heat released and the unused gases (such as oxygen) mix locally to create a new local temperature.

However, in practical combustion cases, it is uncommon to have total premixed combustion. For some reason there will always be lean and rich local spots, causing high and low local temperatures.

If one assumes that the combustibles are totally premixed, then knowing the energy release per molecule of fuel in combustion, and the excess air ratio in the mixture, an

average flame temperature can be calculated. This is known as the adiabatic flame temperature.

2.8.2 NOx formation

As mentioned earlier, NOx emissions are a main cause of concern for the Greenhouse effect and acid rain. In order to be able to reduce these emissions, one has to understand the chemical formation of these compounds, and reduce them through optimising the chemical kinetics of the combustion process for a given geometry. This can be done by reducing the formation of NOx, or by reducing NOx to less dangerous compounds.

NOx formation (and deposition) is a complicated process and occurs through a web of reactions. However it can be simplified to two areas. The first is known as thermal NOx, and is a result of high local temperatures, and secondly Prompt NOx which occurs from the reduction of combustable compounds containing Nitrogen.

2.8.2.1 Thermal NOx

Thermal NOx is the result of the following reactions:

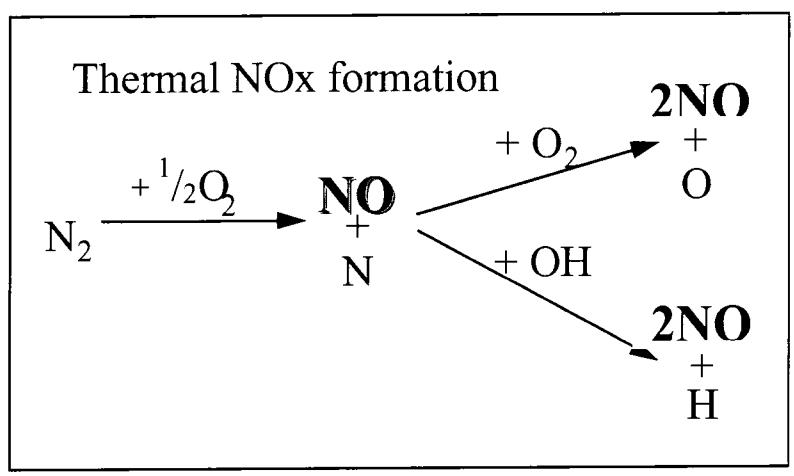

Figure 14

The reason for the name thermal NOx is due to the fact that the first reaction mechanism has a very high activation energy. This means that with typically high local flame temperatures, NOx is produced in high amounts. This is a main cause of concern when trying to run turbines at higher TIT values. For a similar reason, it is easier to create lower emission values at part load conditions than at full-load.

As all three reactions are fast, the first reaction, thus temperature, determines the NOx production rate.

2.8.2.2 Prompt NOx

This is considerably more complicated than the production of thermal NOx because of its reaction mechanism with CH radicals that can occur in numerous forms. However this can be somewhat simplified , and is shown diagrammatically below:

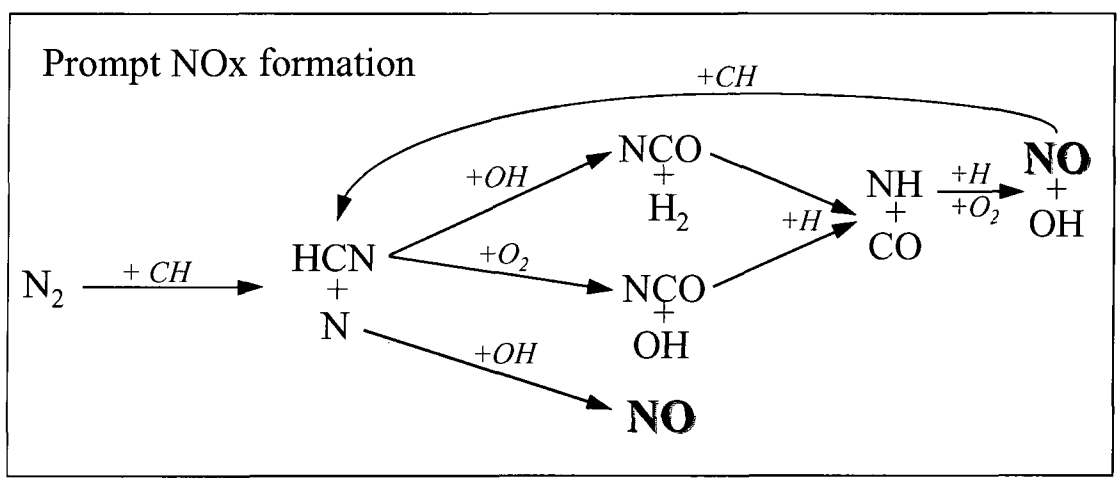

Figure 15

In this process the rate determining process is again the first reaction. This of course depends on the decomposition rate of the fuel hydrocarbon chain. However the production of HCN is also thermally dependent, although the activation energy is considerably lower than in thermal NOx production. As a result prompt NOx occurs at much lower flame temperatures (ie. 1200K)

2.8.2.3 NOx decomposition/reduction

One way of NOx minimisation is known as multi-staged combustion. In the first stage an over rich-mixture is burnt, in order to retain the N_2 in its stable form. In the second stage, a very lean mixture is combusted to create the stoichiometric conditions needed. In this way the flame temperature in the second stage remains low, and the chance for thermal NOx to be produced is reduced.

The addition of ammonia, which upon its oxidation produces N_2H, leads to a reduction of OH radicals and a secondary reaction ($N_2H+NO->N_2+HNO$). These are responsible for the suppressing of NOx production and direct NOx decomposition respectively.

Finally the use of catalysts in the exhaust gases can reduce the emissions, although this is considered a weak solution by combustion scientists due the expense of extra hardware installation and maintenance.

2.9 Resulting Consequences on Oil Combustion Design

Using the above information it can be concluded that it is necessary to keep the flame temperature as low as possible to avoid thermal NOx production. However it is not of benefit to reduce the adiabatic flame temperature, as this just translates into a reduction of power and efficiency, as well as the possibility of lean blow out of the flame. The problem that must be challenged is the reduction of high *local* flame temperatures. Local flame temperatures can deviate in hundreds of Kelvin from the adiabatic flame temperature, resulting from rich local spots. It is therefore necessary to create the most homogenous mixture possible shortly before combustion.

2.9.1 Restrictions of Design

- There are several difficulties in optimising the mixture homogeneity. Firstly the oil enters the burner in liquid form through a nozzle, normally at only one injection point. Oil nozzles have to be retractable for service reasons, and cannot, unlike the gas injectors, be a static feature of the burner. On injection, the oil must atomise and be distributed correctly throughout the burner. Throughout its path within the burner, the oil vaporises due to the high surrounding air temperature. This reduces the size of the droplets and the air momentum has a direct influence on the trajectory of the oil particle.

- All droplets must be fully evaporated before the flame front. Droplets are effectively very rich regions if found in the flame. NOx emissions would be excessive, and unburnt hydrocarbon content could be measured in the exhaust.
- The evaporation process cannot be considerably increased by increasing the initial temperature of the oil, due to the risk of coking on the nozzle. At temperatures higher than 130°C, oil is prone to oxidise and leave carbon deposits in the nozzle, gradually blocking the outlet.
- In an attempt to distribute the oil homogeneously across the cross-section of the burner, it is undesirable to have any droplets hit the walls of the burner. There are two reasons for this. Firstly a coking of the wall would take place, and after a considerable operation time, these solid coke deposits would remove, continuing through the turbine at high speed, damaging certain parts. However, more importantly is that on impingement with the hot burner walls, the majority of oil droplets are likely to evaporate immediately, leaving a rich concentration of oil vapour near the wall surface. As already mentioned, velocities in the mixing tube boundary layer are lower than the turbulent flame speed, and rich oil vapour concentrations create the risk of flashback; an undesired phenomena. The film-air holes found in the mixing tube help reduce this risk in three ways. Firstly they suppress the chance of a droplet meeting the wall, by introducing local high velocities. Secondly, they increase the boundary layer velocities, bringing the near wall velocities closer to the flame speed. Thirdly, the additional air weakens the mixture considerably, reducing the risk of auto-ignition and flashback.
- Finally, another major concern is to make sure the oil vapour has a lower residence time than self-ignition time. Self-ignition times are highly dependent on pressure and preheat temperature (see Chapter 6). At low pressure ratios (<20) and low preheat temperatures (<700K) this is not normally a problem. However with machines such as ABB's GT26, with pressure ratio of 30 and considerably higher inlet temperatures, self-ignition times can be reduced by a factor of 20. Self-ignition then becomes a major concern.

With this theory and the corresponding considerations, the aim of the work was defined.

3. AEV75 CFD - Oil Nozzle Prediction Technical Report

In order to understand the basic concepts of oil droplet evaporation in the AEV75 burner, a parametric study was undertaken, considering as many of the possible influences on fuel distribution likely to occur with a pressure swirl atomiser.
Knowing this information, along with experimental results of oil vapour distribution at the burner exit, the development time of an optimal nozzle design could be considerably reduced.

The following technical report, which appears in its raw form, was the result of numerical investigations on the AEV carried out by the author and Piers Allen (ABB Student 1996). The gridding and modelling of the continuous phase (air flow) was completed by the author, along with the first coupled case for the oil spray simulation. Under supervision of the author, the student collected important characteristics of oil and air across a broad temperature range, and completed the parametric study by changing certain variables (eg. droplet size). The technical report is a combined effort written by the author and student.

This report provides important information for the optimization of the AEV75 burner with oil combustion.

Technical Report

Reporting CRC (full name and address):

ABB Management Ltd.
Corporate Research Center Baden (CHCRC)
Segelhof
CH-5405 Baden-Dättwil Switzerland
Tel.: (+41 56) 76 84 11 Fax : (+41 56) 83 55 61

Responsible Person:	C.Steinbach				
Project Name:	Low NOx Combustors				
Document Title:	**Numerical Modelling of Oil Evaporation in the AEV Burner**				
Document Ref.No.:	ABB CHCRC 96-45	Reg:	T3-28-96	Page 1	
Date of issue:	15.5.96	Classification:	Normal	No. of pages:	54
Client:	ABB Stal				
Author(s):	J.Lloyd, P.Allen	Approved:	T. Sattelmayer	Order No.:	CHCRC.T3 96-07
Distribution:	see separate page				
Distribution page 1:	see separate page				
Keywords:	numerical modelling, oil evaporation, AEV burner				

Summary:

A numerical investigation was undertaken to help decide on the choice of oil nozzle needed for the AEV 75 burner. This included the validation of CFD with experimental results under atmospheric conditions, and the investigation of certain important parameters under operating conditions. Finally a suggestion was made, to what the *ideal* nozzle parameters might be used for the AEV burner.

The desired result was taken to be a constant lambda value across the end of the mixing tube.

It was seen that the most influencing parameters were those of operating pressure and average droplet size. As a result, atmospheric experimental tests must be treated with care when deciding on the choice of nozzle.

The air preheat temperature (set by the operating conditions of the machine) also has a major influence on the oil distribution within the mixing tube, as higher preheat temperatures mean much faster evaporation.

The other two parameters investigated, injection angle and injection velocity, have less impact on the results, although they can be useful as a refinement tool.

Contents

3.1 Introduction

The intention of this work was to use the available software, literature and knowledge, to give some conclusive information in order to help choose the type of design needed for an oil injection nozzle for the AEV burner.

However, applying the correct modelling laws and using the appropriate parameters, while keeping within the limits of the software, was decisive in the accuracy and reality of the results. Not only have the results a direct influence on the burner design, but hopefully this report (along with that from S.Marten et al. - Ref.1) can be used as a base for further CFD work on oil combustion within the gas turbine combustion.

3.2 Motivation

Burner efficiency and exhaust emissions rely partially on oil droplet distribution and evaporation. The development of a dry-oil low NOx gas turbine burner (eg. the AEV75) requires an examination to the fate of injected oil droplets in order to select an injection nozzle that gives the most even distribution of light oil vapour, taken on a cross-section across the end of the mixing tube. (Light oil has a complicated chemical structure and for these tests Tetradecane was used due to its similarity in physical properties). These tests had 4 stages.

Part 1) The modeling of droplet injections in a 2D duct at atmospheric pressure and a temperature of 651 K to examine the effects of changing droplet injection velocity on droplet evaporation time.

Part 2) The modeling of droplet injections in the AEV burner in an atmospheric pressure flowfield to obtain CFD results for the fuel/air distribution at the exit of the burner. These results could then be compared against the atmospheric test-rig data in order to relate the accuracy of the CFD results to reality.

Part 3) The modeling of droplet injections in the AEV burner at a pressure of 14 bars and temperature of 651 K to investigate different important parameters and help decide on the choice of nozzle.

Part 4) The modeling of droplet injections in the AEV burner with a higher preheat temperature of 750K and an air pressure of 14 bar.

3.3 Theory

The code used for the modeling was the commercial package Fluent, Version 4.3.2.

3.3.1 Modeling of the Dispersed Phase

The solver uses a two way coupling to model the droplets of oil in the continuous phase. It integrates the forces balance in a Lagrangian reference frame. This equation is in terms of particle momentum exchange:

$$\frac{du_P}{dt} = F_D(u_A - u_P) + g_x\left(\frac{\rho_P - \rho_A}{\rho_P}\right) + F_x \qquad \text{Eq. 64}$$

where subscript $_A$ are properties of the air and subscript $_P$ are the properties of the particle.

F_D is the drag force on a particle where the drag co-efficient is defined by the equation of Morsi and Alexander. g_x is the gravitational force, and F_x are all additional forces. These additional forces are made up of

i. the force required to accelerate the fluid surrounding the particle

$$F_{x.i} = \tfrac{1}{2}\frac{\rho_A}{\rho_P} u_A \frac{d}{dt}(u_A - u_P) \qquad \text{Eq. 65}$$

ii. Pressure gradients in the fluid

$$F_{x.ii} = \left(\frac{\rho_A}{\rho_P} u_A \frac{\partial u_A}{\partial x}\right) \qquad \text{Eq. 66}$$

iii. Electrostatic forces

iv. Thermophoretic Force

$$F_{x.iv} = D_P{}^T \frac{1}{T}\frac{\partial T}{\partial x} \qquad \text{Eq. 67}$$

Integration of the trajectory equation 64 is done over discrete time steps, and from dx/dt = Up, the position of the particle can be predicted.

For a group of droplets (all with the same injected velocity vector), a mass flow rate is set together with a mean diameter size, $\overline{D}$. If the Rosin-Rammler type distribution is set, then the mass fraction of droplets with a diameter greater than D can be expressed by

$$M_D = e^{-\left[\left(\frac{D}{\overline{D}}\right)^N\right]} \qquad \text{Eq. 68}$$

3.3.2 Laws used in Droplet Evaporation

In order to model the heat and mass transfer between particles and the continuous phase, and in order to model the evaporating droplet, 'laws' have to be integrated into the solver.

There are several set laws and user-defined subroutines available, but only those relevent to oil evaporation are described below.

3.3.2.1 Law 1. Inert Heating & Cooling

These laws are valid so long that the temperature of the droplet is lower than the so-called 'vaporisation temperature' - a theoretical temperature at which the vaporisation law comes into effect. The heat transfer to the droplet is modelled by :

$$m_P C_P \frac{dT_P}{dt} = hA_P\left(T_A - T_P\right) + \varepsilon_P A_P \sigma\left(\theta_R^4 - T_P^4\right) \qquad \text{Eq. 69}$$

where ε_P - emissivity of the particle

h - convection heat transfer co-efficient from the

Correlation of Ranz and Marshall

σ - Boltzmann's constant

θ_R^4 - radiative temperature = $\frac{I}{4\sigma}$ Eq. 70

(I-radiation intensity, sigma - Stefan-Boltzmann constant)

This assumes that the droplet has a uniform temperature.

3.3.2.2 Law 2. Vaporisation

This law comes into affect as soon as the 'vaporisation temperature' is reached and stops when either the boiling temperature is reached or the whole of the droplet has evaporated.

Mass transfer through vaporisation is calculated using the formula

$$N_i' = k_c (C_{iP} - C_{iA}) \quad \text{Eq. 71}$$

where N_i' is the molar flux,

C_{iP} is the surface vapour concentration of the particle

C_{iA} is the vapour concentration in the continuous gas

and k_c is the mass transfer co-efficient.

C_i can be calculated using the gas law and k_c is calculated from a Nusselt correlation.

From this the mass reduction can be calculated through

$$m_P(t+\Delta t) = m_P(t) - N_i A_P M_i \Delta t \quad \text{Eq. 72}$$

Also calculated is the renewed droplet temperature according to the previously shown heat transfer function with an additional rate of evaporation term.

3.3.2.3 Law 3. Boiling

As the boiling temperature is reached the evaporation model is halted and replaced by the following law describing the reduction in droplet diameter.

$$\frac{dD_P}{dt} = \frac{4k_{GAS}}{\rho_P C_{P_{GAS}} D_P}\left(1 + 0.23\sqrt{\mathrm{Re}_D}\right)\ln\left[1 + \frac{C_{P_{GAS}}(T_{GAS} - T_P)}{h_{fg}}\right] \quad \text{Eq.73}$$

where k = thermal conductivity

and h_{fg} = latent heat

Once it has started, the boiling law is applied for the rest of the particle trajectory.

These three laws mean that from injection to total phase change the particles have a definite history (if they don't meet a boundary). This can be represented as below.

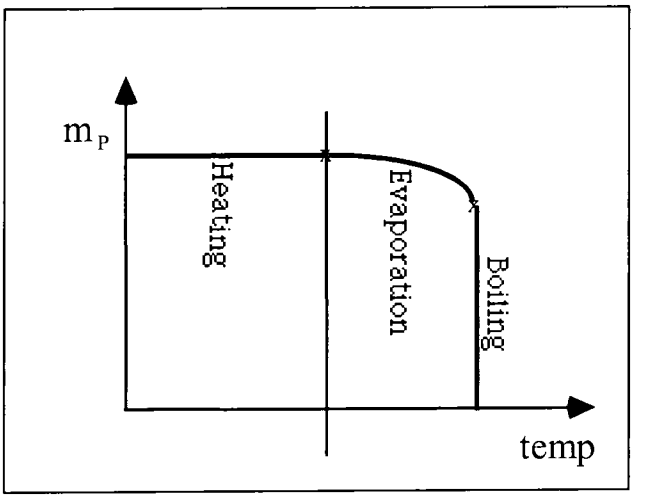

Figure 16

As can be noted from the theory and also seen in the calculations, the value of evaporation and boiling temperatures have a great influence on the solution of the problem.

The two way coupling process is achieved by having two exchange equations:

one for momentum

$$F = \sum \frac{18\mu C_D \,\mathrm{Re}}{\rho_P D_P^2 24}(\mu_P - \mu_{AIR})\dot{m}\Delta t \qquad \text{Eq. 74}$$

and one for heat.

This is solved by calculating trajectories of droplets inbetween solving the continuous phase.

3.3.3 Second Phase Boundary Conditions

There are 4 alternative models for dealing with the dispersed phase as it interacts with the ambient fluid and the geometrical and computational boundaries (eg. surfaces) :-

1) Reflect - rebounds the particle off the boundary in question with a change in its momentum as defined by the Coefficient of Restitution.

2) Trap - evaporates the entire mass of the droplets (upon impact with the wall) instantaneously passing its mass into the vapour phase.

3) Escape - allows the droplet to disappear out of an exit at the domain.

4) Saltate - is a development of reflect, but as well as bouncing the droplet it allows the droplet to instantaneously jump in from the wall.

At the high wall temperatures involved in this project instantaneous evaporation is the most realistic model for the droplet as they hit the burner walls, hence Trap was chosen as the Boundary condition of the walls.

3.4 Part 1 - Calibrating the Droplet Model

An initial calibration of the droplet model was done by comparing evaporation times in a simple 2D duct with the work of S. Martens (Ref. 1), who estimated droplet evaporation times in a laminar flow at both 14.5 bars & 1 bar. In that case a special model was developed that allowed more physically accurate and realistic evaporation models.

3.4.1 Checking Oil Droplet Evaporation Times

The 2D duct was modeled using a uniform structured grid of 20 x 10. The length of the duct was five times the height. Air flowed from left to right with the upper and lower boundaries being walls.

The main stream flow was modeled as air with an inlet velocity of 50 m/s and a temperature of 651K.

Droplets of 350K were injected parallel to the main flow in the middle of the duct 10mm downstream of the inlet. (See Figure 17)

Figure 17 - 2D Duct

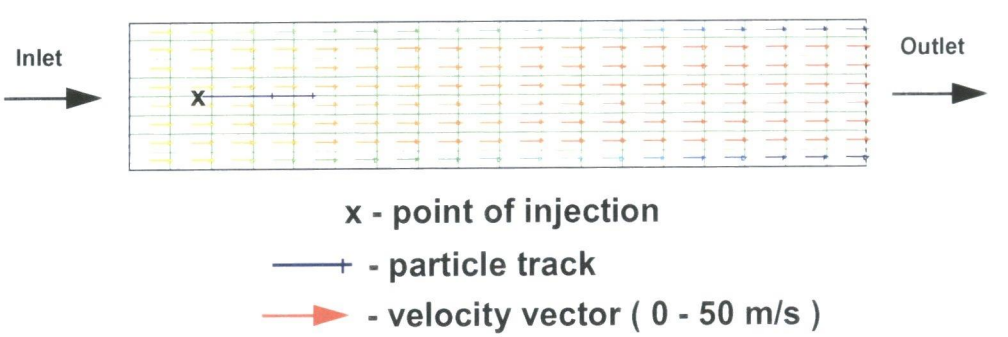

As Marten injected droplets at 250m/s *perpendicular* to the main flow of 60 m/s, the relative speed was calculated to be 257 m/s. Therefore, taking account of the main air flow, the droplets in the 2D Fluent case were injected with an absolute speed of 307m/s.

For the cases of both 1 bar and 14 bar, a series of different injection velocities were tested for the 16 μm droplet.

3.4.2 Results to Part 1

As Martens could not couple his solution (i.e. the droplet/gas interaction was not included), the Fluent case was also not coupled. The laminar model was used. The results can be seen in the following graphs. (Figure 18)

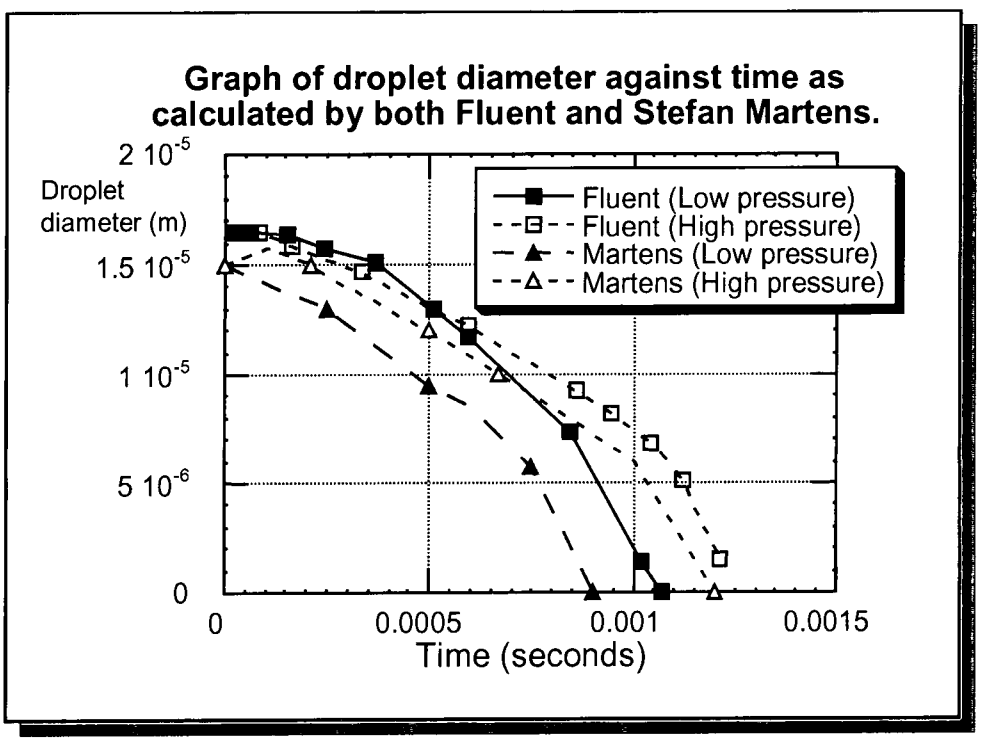

Figure 18a

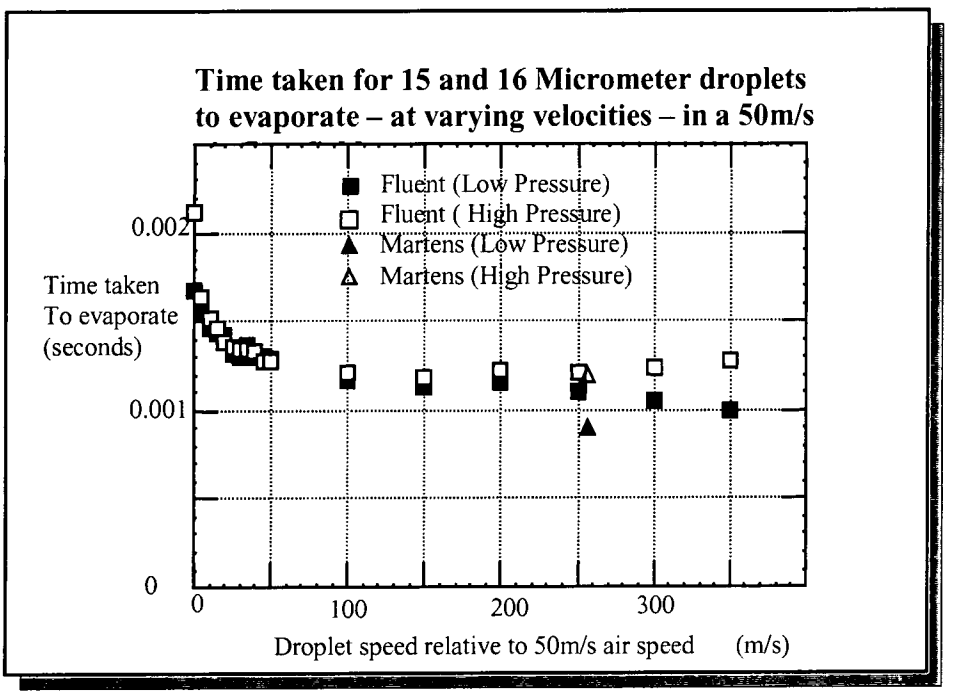

Figure 18b

It can be seen that the results agree in the main. Reasons for the results not being perfectly matched lie in the following points:

i. Martens injected perpendicular to the flowfield in contrary to this case which injected parallel to the flowfield. This means that different forces would be exerted on the droplets causing different evaporation times.

ii. A slightly larger droplet was modelled in the Fluent case ($16\mu m$) than in the Martens case ($15\mu m$). This could cause around 6% difference in evaporation times.

iii. Extrapolation and integration of evaporating times could be slightly inaccurate due to numerical errors and lack of grid refinement.

It can be concluded that the Fluent models and subroutines describe the droplet evaporation satisfactorily, with the assumed set of parameters (physical properties) used.

3.5 Part 2 - Modeling Oil Evaporation in the AEV Burner

In attempts to reduce NOx emissions whilst increasing efficiency, the design of the EV burner has been refined to the AEV 4 slot burner. Responding to this evolution of design an examination of the effects of varying droplet diameter, velocity of injection and spray angle on droplet evaporation is required. The aim of manipulating droplet sizes and spray angles is to find a combination which causes all the droplets to have evaporated evenly across the exit of the burner, just upstream of the flame front.

The results of the numerical model need calibrating. However, to examine the accuracy of the high pressure model would require a large amount of expensive high pressure test rig data. Hence the need for the second stage of the tests - to model an atmospheric flowfield and droplet injections and examine these against results obtained cost effectively in an atmospheric rig.

3.5.1 Preparing the calculation.

Modeling of the AEV burner flow field is a complicated 3-D grid generation problem. Considering that the grid had to later cope with second phase oil droplet injections, at the time of writing a structured grid was the only available option. It was due to the skewed triangular/tetrahedral geometry within the connecting piece, that gridding problems occured. Highly skewed cells in this region led to rapid divergence in the solver. Finally a satisfactory grid was evolved by the appropriate curvature of certain sub-domains edges. Slices through the grid are shown in figure 19. The grid evolves through the swirl generator, then the transition piece and into the mixing tube.

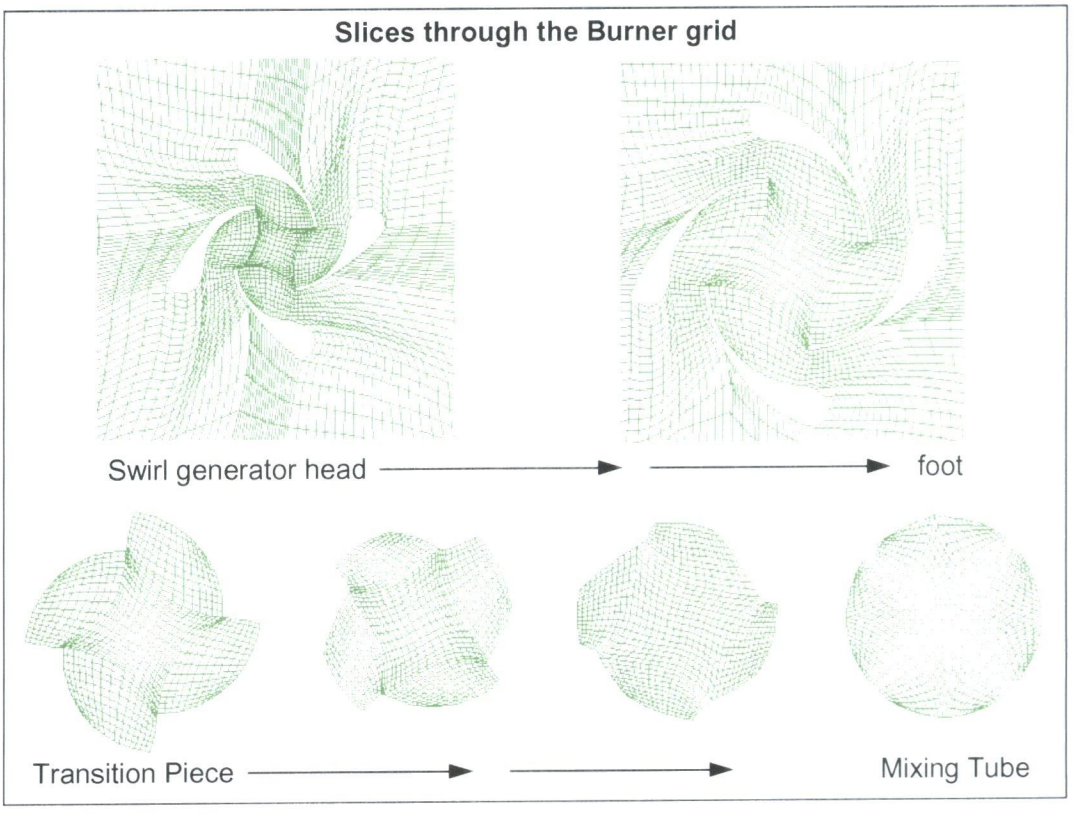

Figure 19

The whole geometry consists of a low NOx burner (AEV75/12.5/100) surrounded by a 200mm x 180mm box (as in Figure 20). One side of the box consists of the inlet (shown in blue) while the other five sides are set as walls. The outlet is taken as the end of the mixing tube. (shown in green)

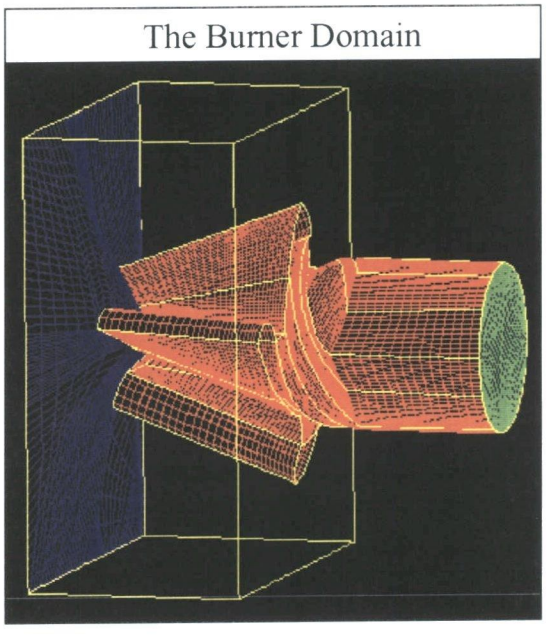

Figure 20

When evaluating the results, one should be aware of the boundary conditions within the restriction of this geometrical setup. The inlet condition was a velocity boundary condition, with vectors parallel to the axis of the burner. However due to the proximity of the inlet to the burner head, there will in reality be a slight upstream effect in this area, and 100% of the flow will not be normal to the inlet.

There is a second simplification in the geometry that can be seen on the outer side of the swirl generator shell. Here the outer surface has been smoothed off to allow for easier mesh generation.

Finally, the outlet has an even pressure distribution default. There is no sudden expansion modeled after the mixing tube and no chance for a vortex breakdown to occur. This means the flow in the last few cells close to the outlet could portray a false flowfield.

The Fluent Unstructured code should soon offer the Lagrangian Dispersed Phase Modeling. It is recommended that for future calculations, due to meshing, that this solver is used. Not only is the main geometry meshing easier, but film layer holes and head injection can be added. More detail can be included, and the refinement can easily be applied to the correct areas (see Figure 21) The disadvantage of this solver lies in the difficulty of simple geometric changes and the inability to patch certain regions and easily view slices (eg. inlet slots)

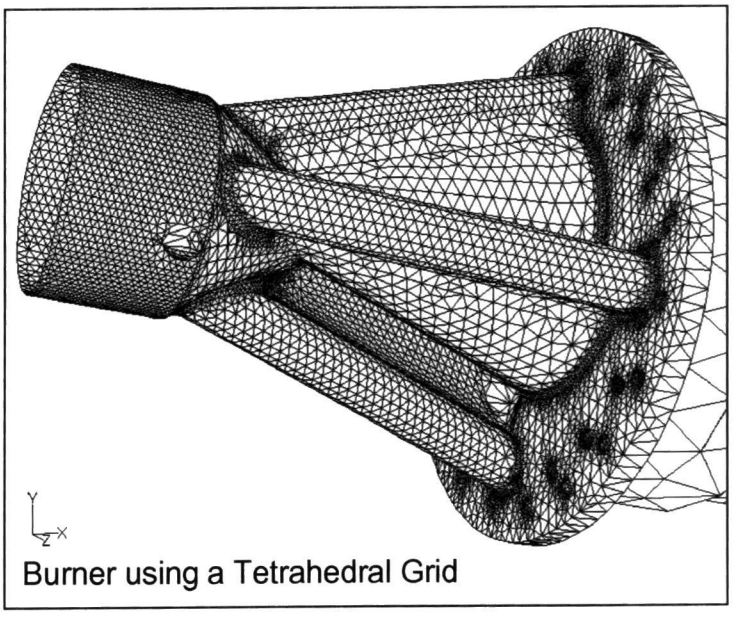

Figure 21

A convergence problem was encountered when using a flat nose to the nozzle. Recirculation around the nozzle tip caused disturbance in the injected droplets. The nozzle was altered to a spherical end profile. (Shown in Figure 22)

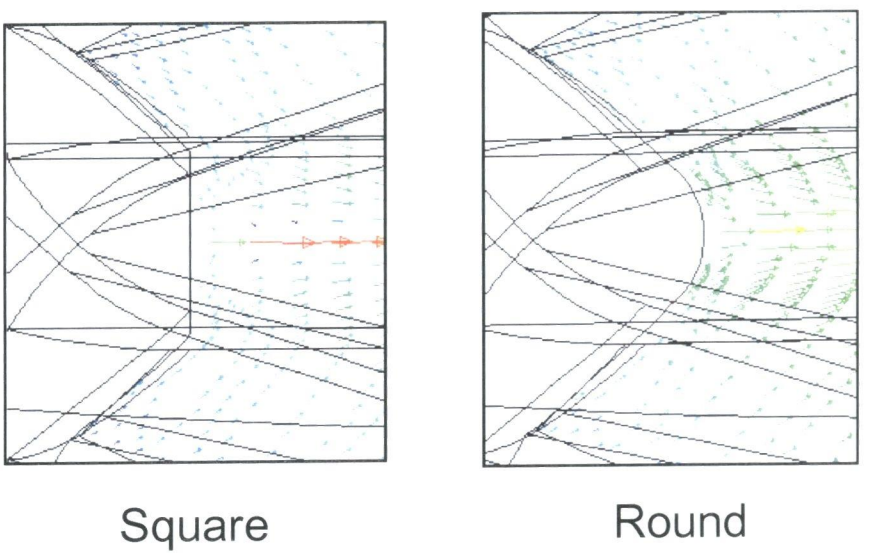

Figure 22

Having set up the grid, the physical models and governing equations to be used in the calculation must be input into the solver.

The air flow is turbulent and there are 3 turbulent models that can be used:-

1) the K-epsilon model,
2) the RNG K-epsilon model,
3) the Reynolds stress model.

With a 7 equation model of turbulence the Reynolds stress model is the most realistic turbulence model (in that it makes less of an assumption that turbulence is isotropic) but also the most burdensome in terms of CPU time, making it unnecessarily slow for our low levels of turbulence. The K-epsilon model and the RNG K-epsilon model are both similar in that they use a 2 equation model of Turbulence. However the Renormalised Group (RNG) model gives improved results over the standard K-epsilon model, whilst only slightly increasing demands on the processor time, making this the model chosen for the calculation.

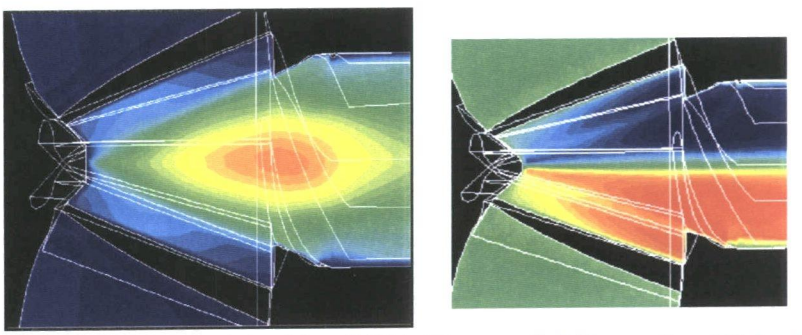

Axial Normalized Velocities (U/ U_m) Tangential Normalized Velocities (W/U_m)

BLUE = 0 ; RED = 3 **CFD** BLUE = -1.2 ; RED = 1.2

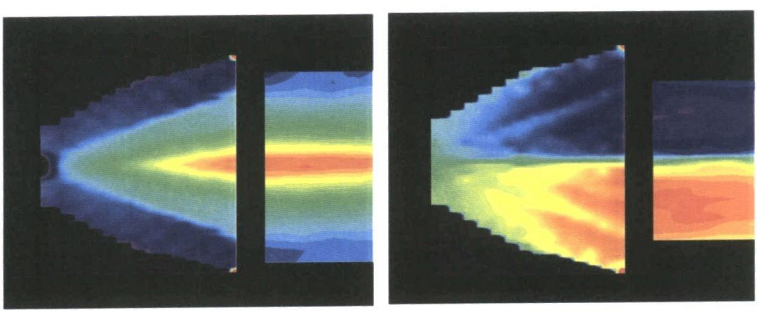

Axial Normalized Velocities (U/ U_m) Tangential Normalized Velocities (W/U_m)

BLUE = 0 ; RED = 3 BLUE = -1.5 ; RED = 1.5

Water Tests

Internal Burner Flowfield

Figure 23

The CFD results for the 14 bar air flowfield are shown in figures 23 & 24. As can be seen they are comparable to the LDA results from the water tests although not exact; a gradual rise in axial velocity along the axes to 2.2 times the normalised velocity and then dropping away in the mixing tube. The swirl number was from the CFD results was calculated to be 0.45 towards the outlet of the mixing tube. This is in the same range as the results from the water test.

There does appear to be an irregular/asymmetric flowfield close to the domain boundary due to the complex gridding in this region. This is due to the highly skewed cells and the high aspect ratios found in this region.

Figure 25 shows the comparison of LDA measurements with CFD results for the slot. An overall good comparison is achieved. The results were used as a base to the second phase calculations.

Next, the solver had to be set up to calculate 2 species (tetradecane and air), temperature and swirl. For each species, values of their physical constants had to be input, whilst the boundary conditions of the inlet, outlet and walls also had to be defined. It is worth noting that some of the boundary conditions varied with pressure and a complete list of the values used is contained in the section 3.8.1 entitled *Boundary Conditions*. Knowing the mass flow of air, the mass flow rate of oil was set to give average lambda value (λ) of 2.4 for the atmospheric case.

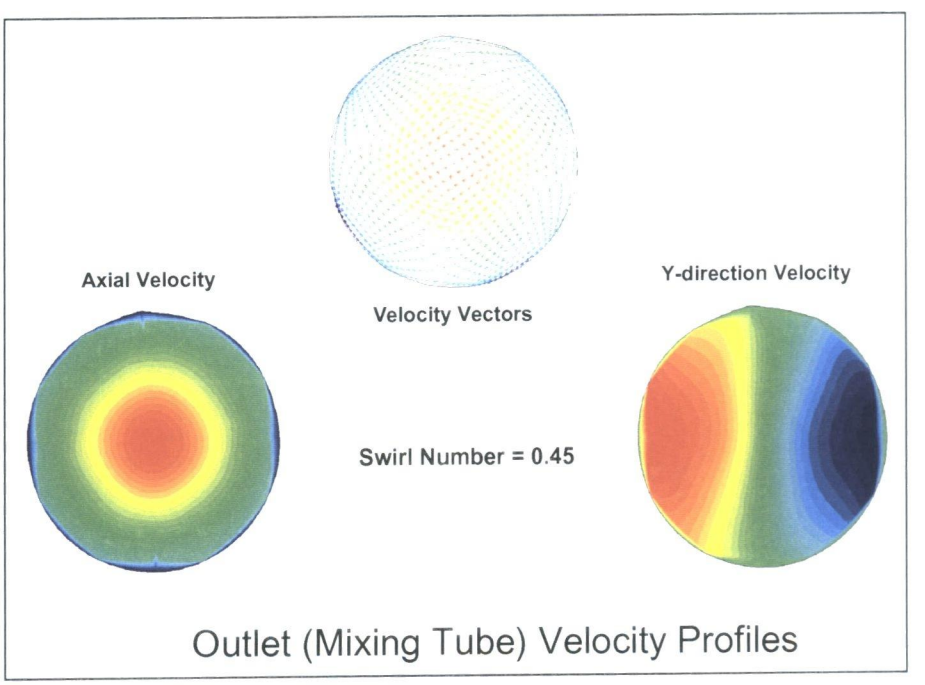

Figure 24

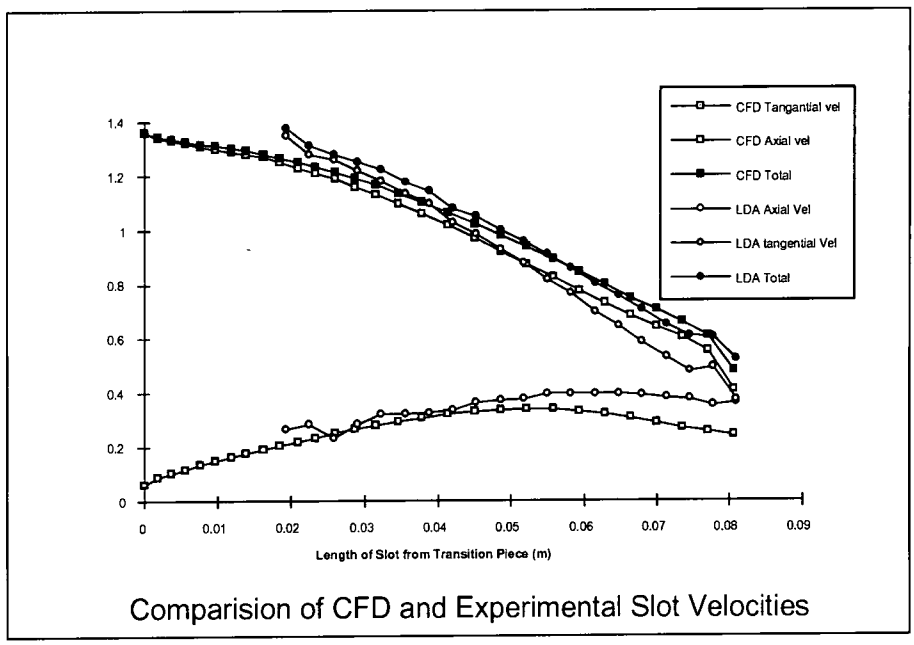

Figure 25

3.5.2 Method

The process of calculating the droplet trajectories can be broken down into 2 major stages.:-

1) Initial iteration of the air only flowfield, requiring roughly 2000 iterations.

2) Iteration of flowfield with intermittant droplet injections.

Although it is not necessary to break up the process, calculating the air flowfield before injecting the droplets significantly speeds up the total time taken for the calculation and reduces the risk of the solution diverging.

3.5.3 2-Way Coupling

To calculate the air only flow-field 1600 iterations were computed to satisfactorily converge the solution.

The next stage was to inject droplets. These injection calculations have been broken down into a further 2 stages - the first using a droplet injection every 500 iterations and the second using a droplet injection every 100 iterations.

The dispersed phase physical constants input are listed in the section entitled *Boundary Conditions*.

The solver performs a species 2 calculation (i.e. droplet injections) for every specified number of species 1 calculations.
Before inputting how regularly droplet injections are to be made it must be considered that a constant stream of injected droplets will change the air flow field in three ways :

1) By imparting some of their momentum onto the surrounding air, they will create a localised high velocity current in the air flow field.
2) Droplets are injected along similar paths. Droplet evaporation along these paths will be marked by a high mass fraction of tetradecane in the surrounding air. This will raise the evaporation time of successive droplets.
3) The temperature at local points in the flowfield will be reduced, the higher the concentration of oil droplets present.

Therefore it is insufficient to inject just one set of droplets on the existing flowfield as the twentieth injection will result in a different evaporation time to the first. A series of droplet injections must be made, with 2-way coupled air calculations in order to calculate the flow field when there are droplets in the surrounding air field for a sustained period of time. It may appear that a constant spray of droplets is best modelled by droplet injections on every iteration. This is unnecessary as the software will take roughly 400 iterations to converge the flowfield with an injected set of droplets. After each injection the solution develops towards the stable, well-developed flowfield of a constant spray. As the flowfield develops in response to the droplets, fewer iterations between injections are needed, and flowfield iterations can be reduced to around 100 for every injection step. Eventually the final air flowfield is converged into which droplets can be injected and whose resulting paths can be studied. This is a coupled solution where the flowfield is not altered by new droplet injections.

3.5.4 Nozzle / Spray Modeling

The tetradekane droplet injections had to be set up in the solver. Each injection consists of 48 groups, each of 20 Rosin Rammler distributed droplets. All characteristics of each group are the same except for the direction in which the group is injected. This varies between 48 directions radially from the tip of the nozzle (see Figure 26).

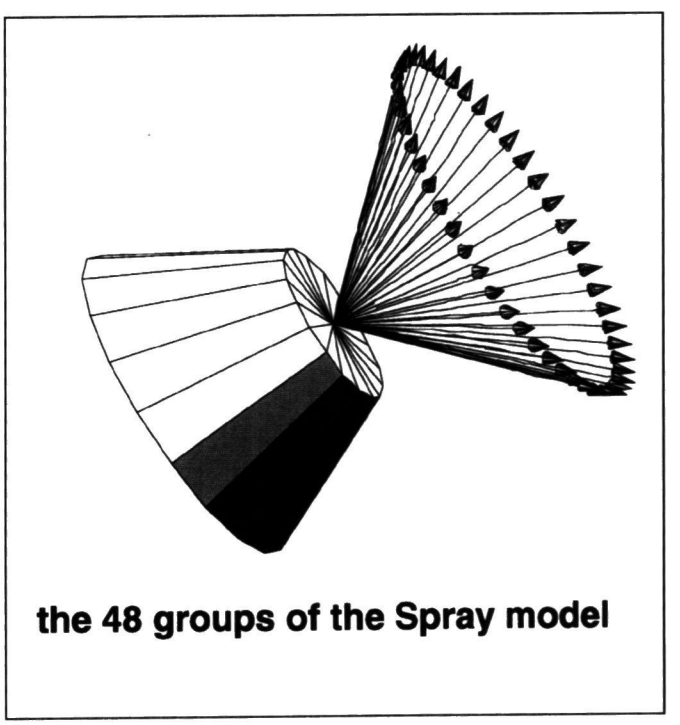

Figure 26

The arrows mark the injection angle of a single group of 20 droplets. Within each group of droplets, there are a range of droplet mass flowrates as defined by the equation in the Theory (Section 3.3.1). n, the spread factor, was in this case taken to be 3.5. This gives a droplet distribution similar to that shown in figure 27.

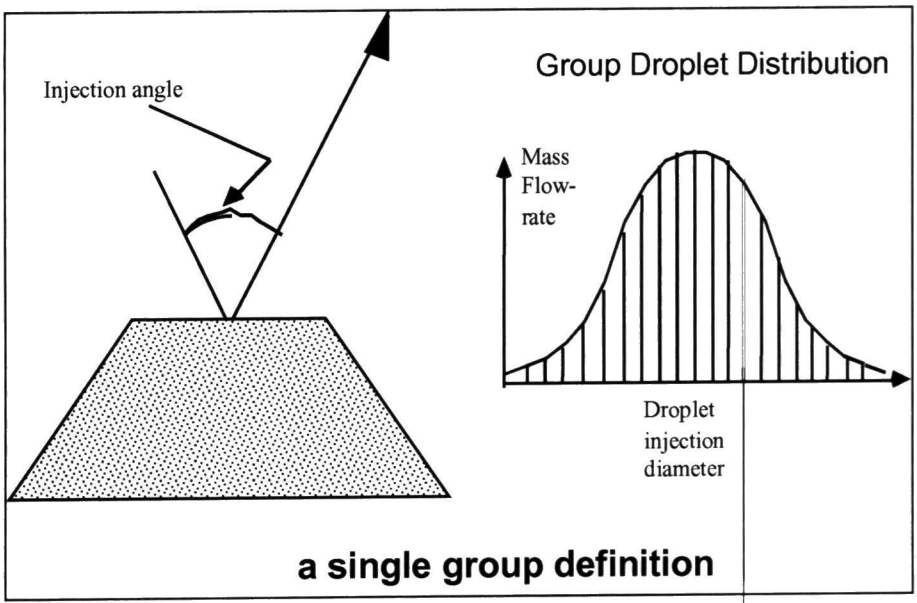

Figure 27

For different oil inlet pressures and spray angles there will be different values of U, V and W velocities for each of the 48 groups - as defined by the equations:-

$$U_1 = ACosV_z$$

$$V_1 = ASinV_z$$

$$W_1 = -Cos(SprayAngle * B)$$

Where: Eq. 75

$$A = Sin(SprayAngle * B)$$

$$B = \sqrt{\left(\frac{2 * Oil\,\mathrm{Pr}essure * (1 - 0.25) * 100{,}000}{850}\right)} = V_{max}$$

(B incorporates 25% pressure loss)

Using the appropriate values of Spray angle, oil pressure, oil temperature, mean droplet diameter, oil mass flowrate and X;Y and Z injection position the parameters can be calculated.

3.5.5 Procedure

The droplet injections from 2 nozzles were examined, one which created a 30 degree spray angle and another which created a 60 degree spray - as these were the most common spray angles. Further for each nozzle 4 different average droplet sizes were tested - 45, 30, 23 and 15 microns.

3.5.5.1 Part 2 - Modeling Oil Evaporation under Atmospheric conditions.

The atmospheric air pressure tests were interlinked by using an oil pressure of 320 bars for 15 micron averaged oil droplets, 250 bars for 23 micron averaged oil droplets, and a pressure of 190 bars for 30 microns averaged oil droplets; all were set with a spray angle of 30 degrees.

3.5.5.2 Part 3 - Modeling Oil Evaporation in the AEV burner at 14 bar

With the new oil and air pressures, the property values needed changing. Due to the rise in pressure and therefore density, the mass flow of air altered, as the velocity flowfield was kept roughly constant. The mass flow of oil was set to give an average lambda value of 2. A list of these values is contained in the section entitled *Boundary Conditions.*

3.5.5.3 Part 4 - Modeling Oil Evaporation at a higher Air Preheat Temperature of 750K

In this case the pressure loss was kept similar to that in Part 3. Pressure loss can be related to mass flow rate, effective area and density by the following formula.

$$\dot{m} = A_{eff}\sqrt{2\rho\Delta p} \qquad \text{Eq. 76}$$

Due to the drop in density, and for a constant pressure loss, the air mass flow rate must fall. With it the velocities rise by around 7%. Therefore in order to keep an average lambda value of 2 constant, the mass flow of oil must drop.

In reality the 750K preheat case shall be run at 20bar meaning that the density will rise. The Weber number

$$\mathrm{We} = \frac{\rho u^2 D_{DROP}}{\sigma} \qquad \text{Eq. 77}$$

(which gives an indication of the droplet size) is proportional to density. This can only help the situation in providing more resistance and consequently smaller droplets.

3.5.6 Post Processing

Having successfully calculated the first and second phase solutions it remains to examine the results. Of interest were images of :-

a) Mass Fraction of Tetradekan in the vapour phase.

b) Droplet trajectories

c) Temperature distribution inside burner

d) Lambda profile of the cross section of the end of the mixing tube.

3.6 Results

3.6.1 Results to Part 3.5.5.1 - Comparing CFD Results against Expermental Results

The results to Part 2 are shown in figures 29-31 , Cases 1, 2 & 3.

The oil pressures were set to a value needed to create the corresponding droplet size. This was known as it had been tested and validated in a PDPA experimental rig.

This part of the investigation was to calibrate the experimental results of nozzles in the PDPA against the CFD calculations for a simple nozzle.
Figure 28 shows the comparison of lambda values between the two techniques.

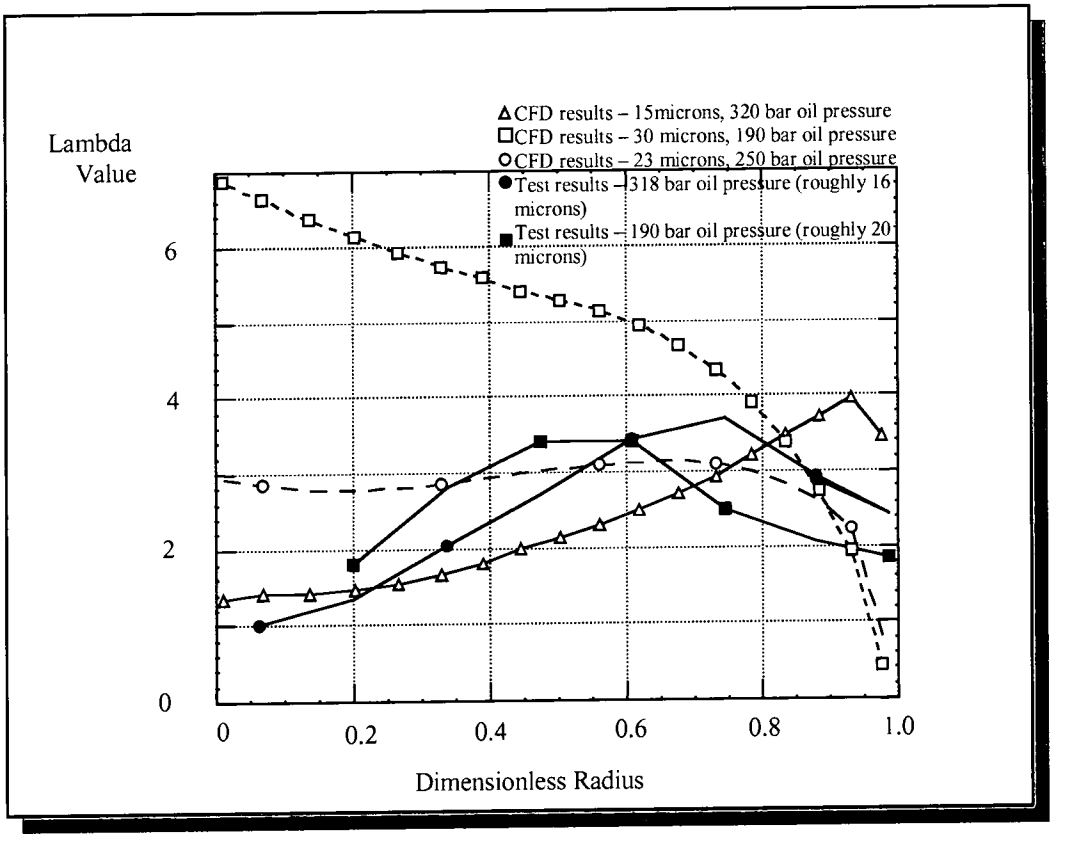

Figure 28

From the experimental tests, it is hard to determine the exact average size of the injected droplets due to the intolerances in the measurement technique coupled with the quality of the nozzle exit ; it is taken to be around $20\mu m$ for an oil pressure of 190 bars.
If this is taken into consideration, the CFD results lie well in the range of lambda values expected within the limits of experimental accuracy. The lower size droplets create a fairly rich centre of almost stoichiometric mixture becoming gradually leaner with increase in radius, until the near-wall region that is enriched by the small amount of droplet-remains that immediately evaporated after hitting the hot-metal wall. The larger the average droplet size, the leaner the centre region.

However, by comparing the three cases, it can be seen that the droplet size has a very large influence on the oil distribution at the end of the mixing tube. At one extreme it can be seen that small droplets do not have the momentum to drive through the air coming in the slots, and are immediately carried away and stay on the axis. At the other extreme, large droplet sizes have too much momentum, plunge through the air and hit the wall before they are fully evaporated. On collision with the 650K wall the droplets are expected to evaporate almost immediately. This causes a very rich mixture in the near-wall region and causes concern over flash-back due to the low velocities in the boundary layer.

To conclude, within the accuracy of computational and (especially) experimental results, the calibration was good enough to continue a qualitative investigation into the 14 bar case. However, more accurate methods should be found for determining the exact droplet distribution for certain nozzles, in order to make a firmer validation between experimental and computational results.

3.6.2 Results to Part 3.5.5.2 - Oil Evaporation at 14 bars

The results to Part 3.5.5.2 (Cases 4 - 8), along with the atmospheric cases are shown in figures 32-36. Table 1 shows in a simple form, which cases were tested.

Table1

Air Pressure	1 bar	14 bars	
Angle of Injection (degrees)	30	30	60
Average Droplet Diameter / Oil Pressure (bars)			
15 um / 100			
320	Case 1		
23 um / 100			Case 7
250	Case 2		
30 um / 100		Case 4	Case 8
190	Case 3	Case 5	
45 um / 100		Case 6 Case 9 (Preheat)	

There are five main variables:

i. Air pressure
ii. Average droplet diameter
iii. Angle of Injection
iv. Oil Pressure
v. Air Preheat Temperature

(Case 9 and Air Preheat Temperature shall be discussed in Part 4)

The following table shows which cases should be looked at to compare certain variables.

Table 2

Variable to be Compared	Cases to be compared
Air Pressure	Cases 3 & 5
Average Droplet Size	Cases 1,2 & 3 or Cases 4 & 6 or Cases 7 & 8
Oil Pressure	Cases 4 & 5
Angle of Injection	Cases 4 & 8
Preheat Temperature	Cases 6 & 9

1 bar Air pressure. 30° Spray angle. 15 um Average Droplet size. 320 bar Oil pressure.

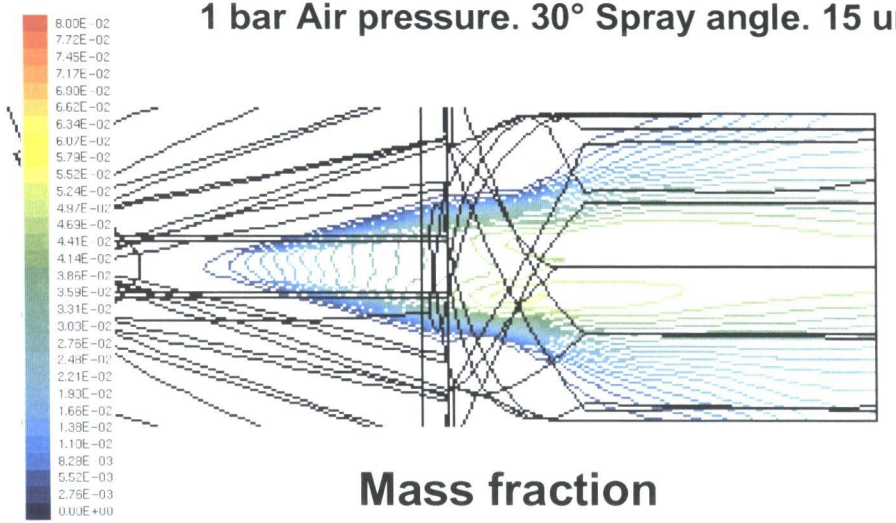

Mass fraction

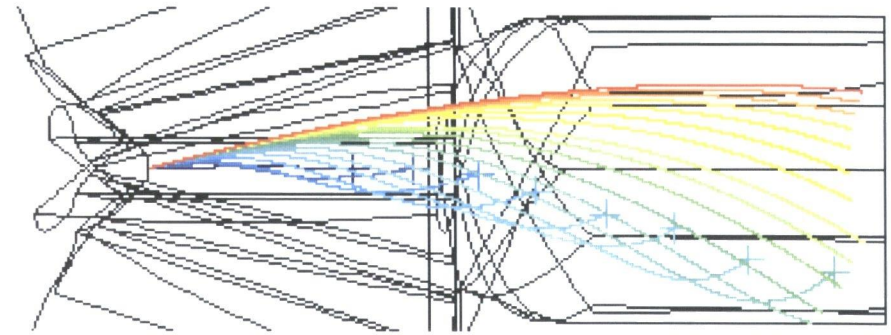

Particle tracks

Temperature

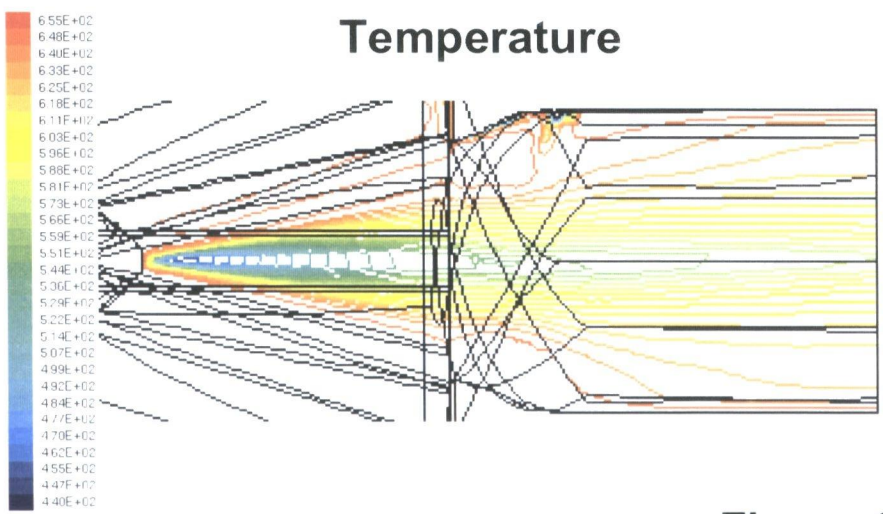

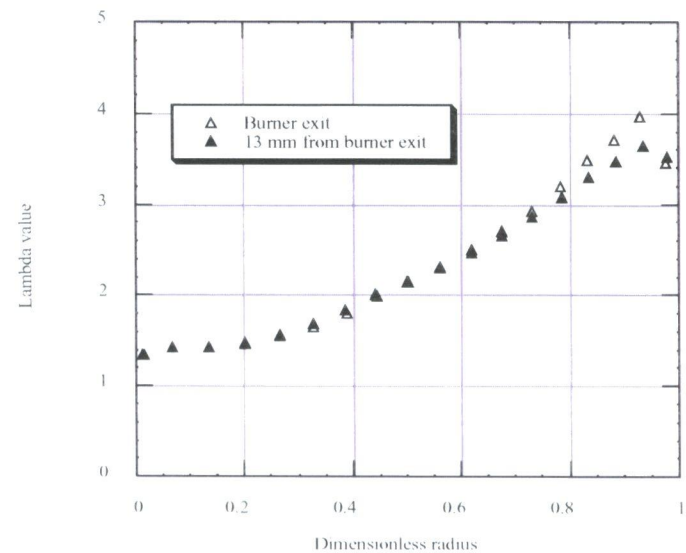

Figure 29: Case 1

1 bar Air pressure. 30° Spray angle. 23 um Average Droplet size. 250 bar Oil pressure.

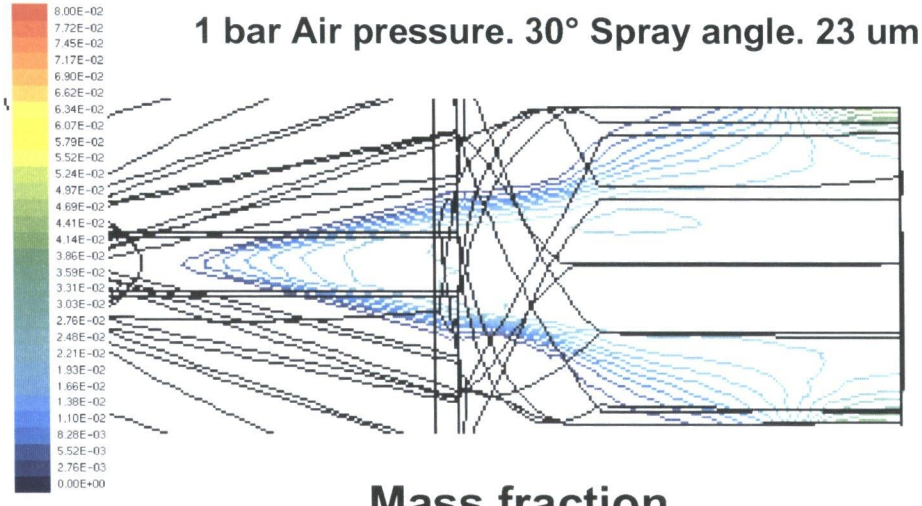

Mass fraction

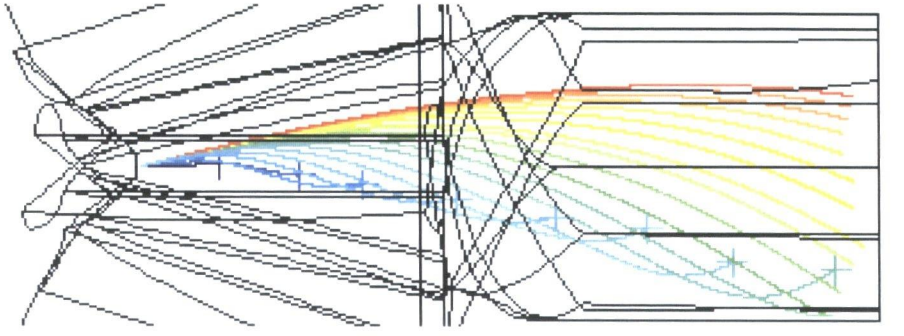

Particle tracks

Temperature

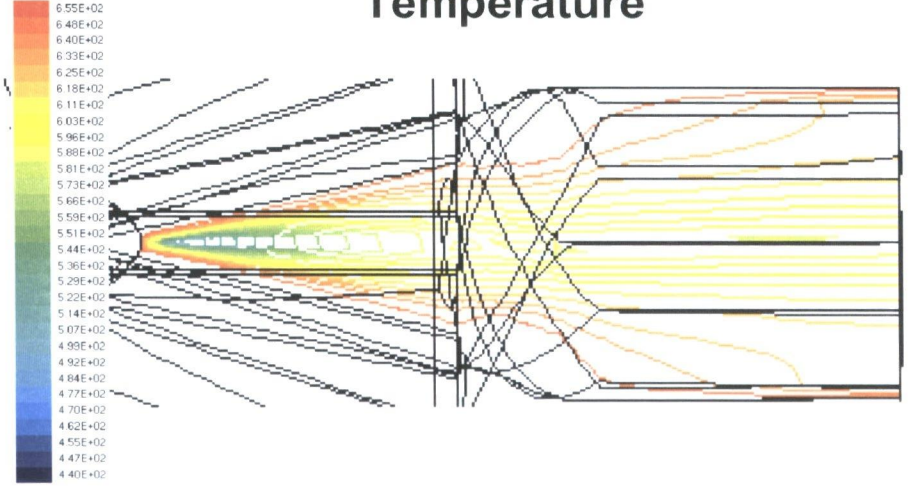

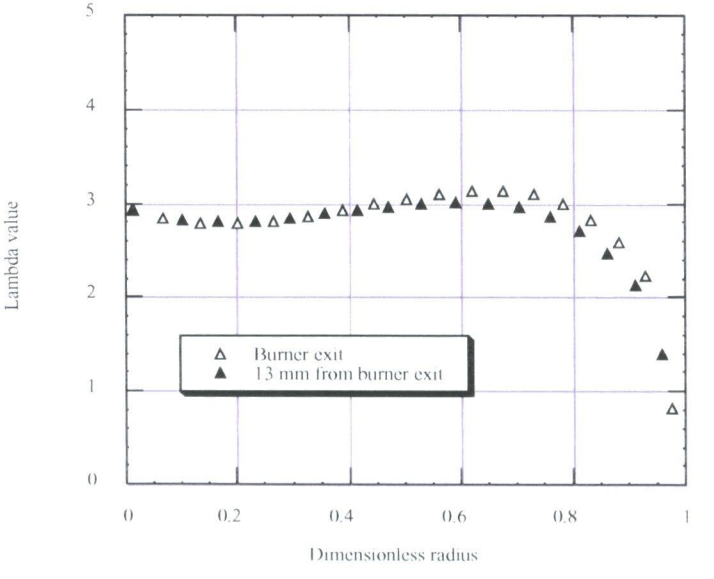

Figure 30 : Case 2

1 bar Air pressure. 30 Spray angle. 30 um Average Droplet size. 190 bar Oil pressure.

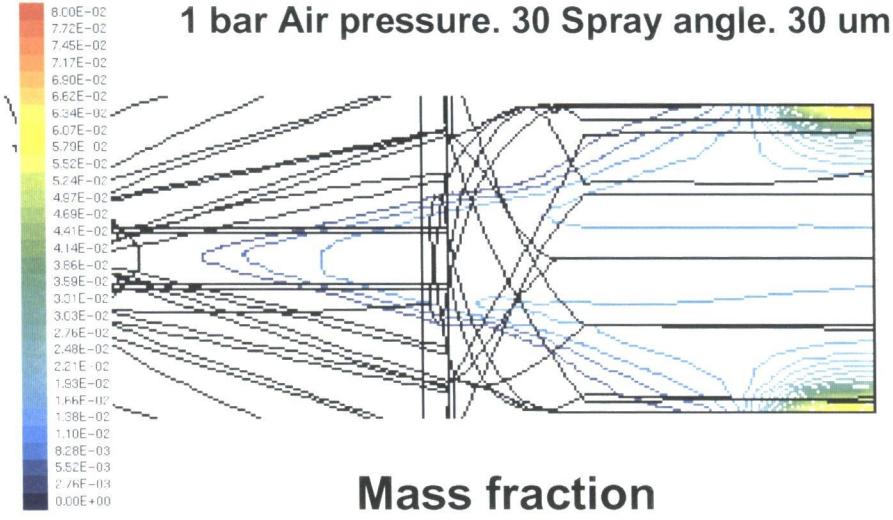

Mass fraction

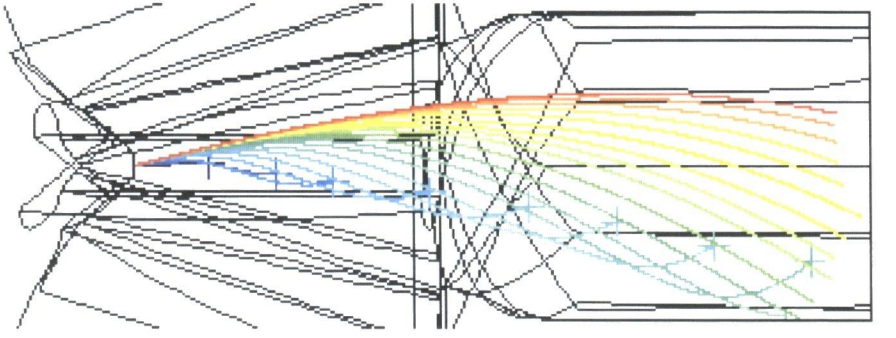

Particle tracks

Temperature

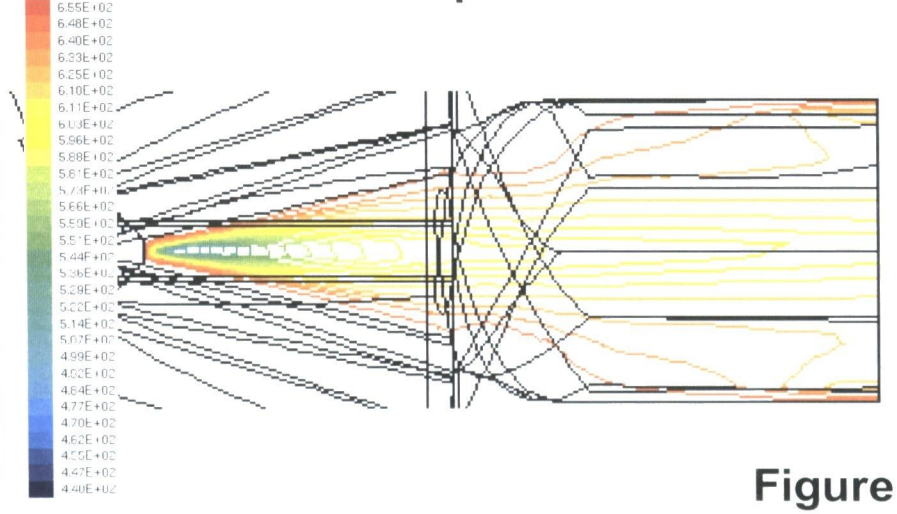

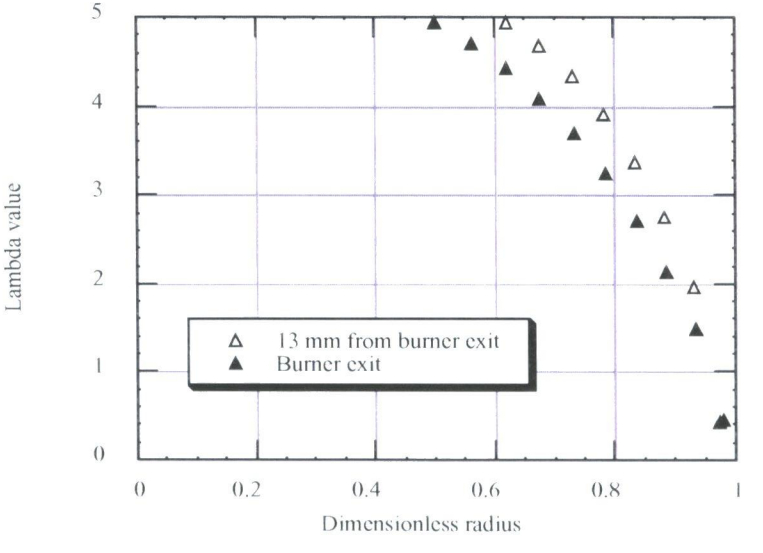

Figure 31 : Case 3

14 bar Air pressure. 30 Spray angle. 30 um Average Droplet size. 100 bar Oil pressure

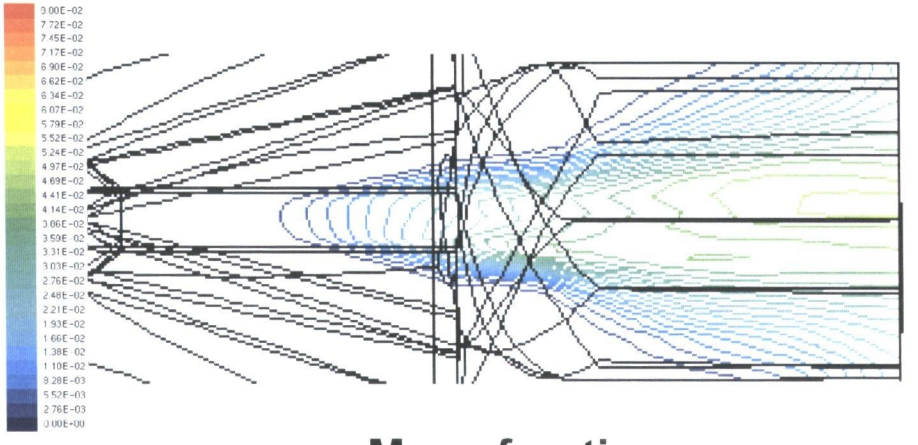

Mass fraction

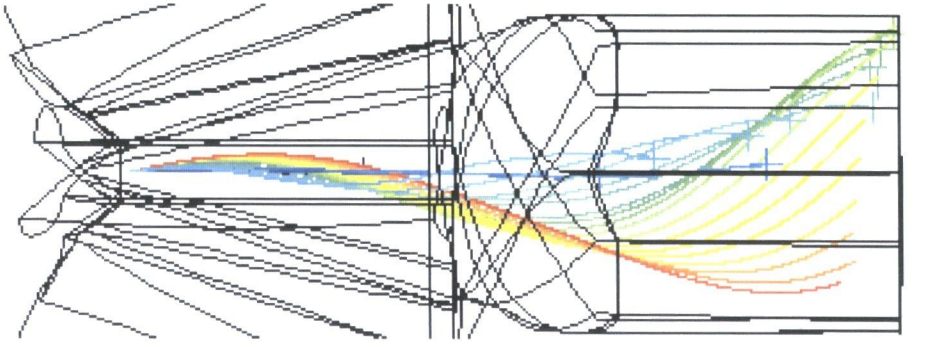

Particle tracks

Temperature

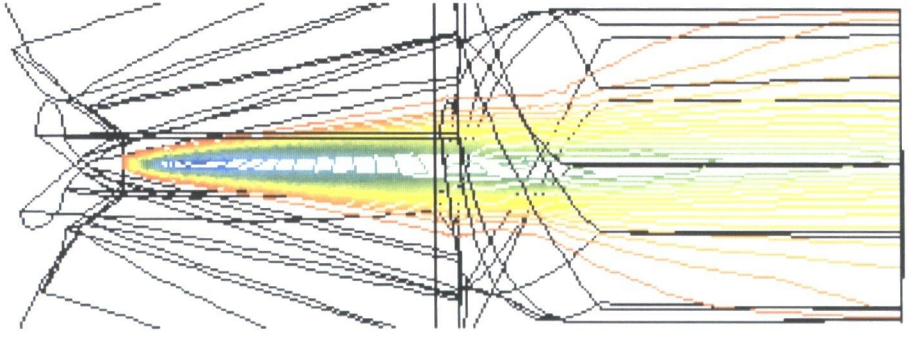

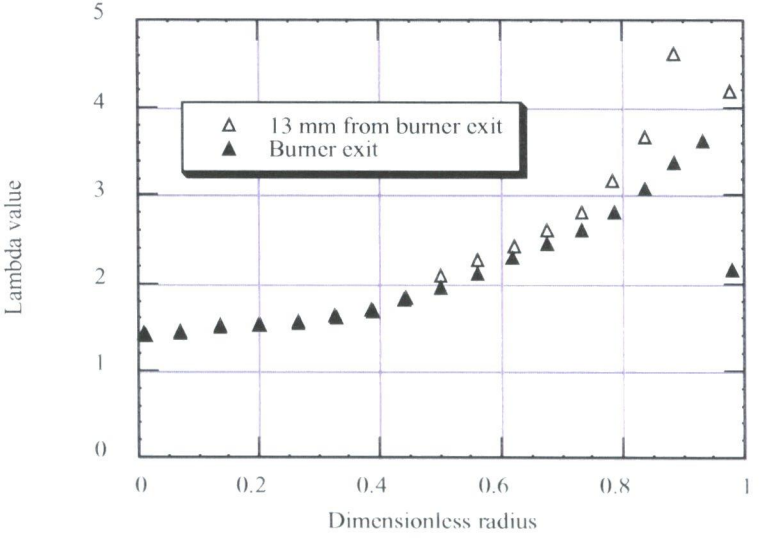

Figure 32 : Case 4

14 bar Air pressure. 30° Spray angle. 30 um Average Droplet size. 190 bar Oil pressure.

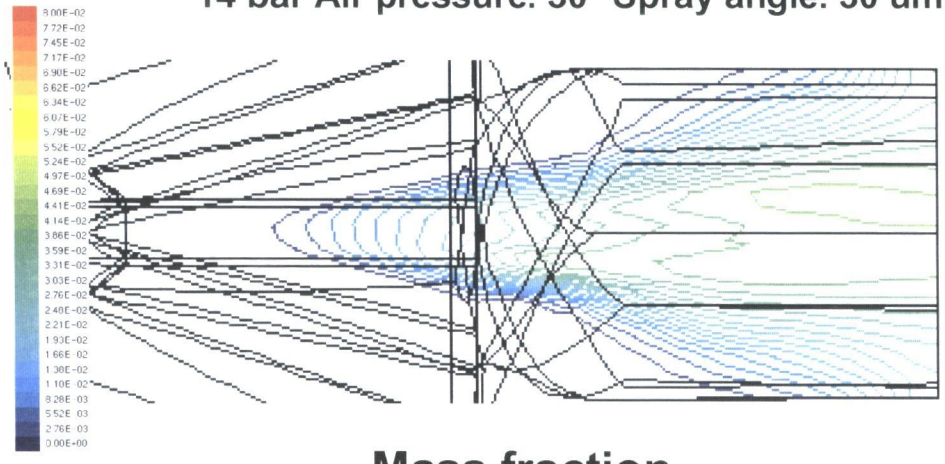

Mass fraction

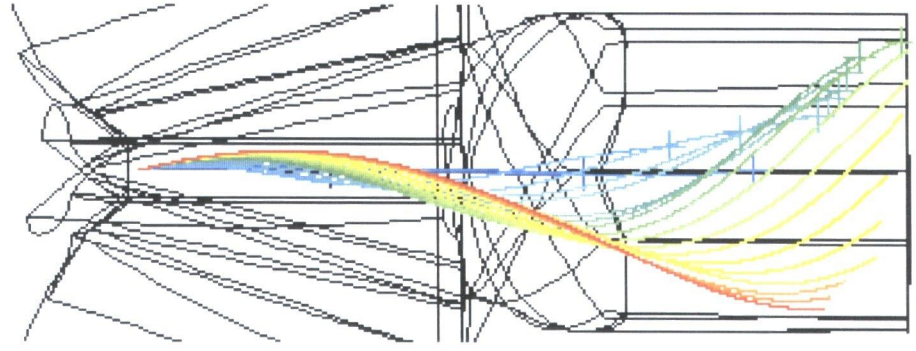

Particle tracks

Temperature

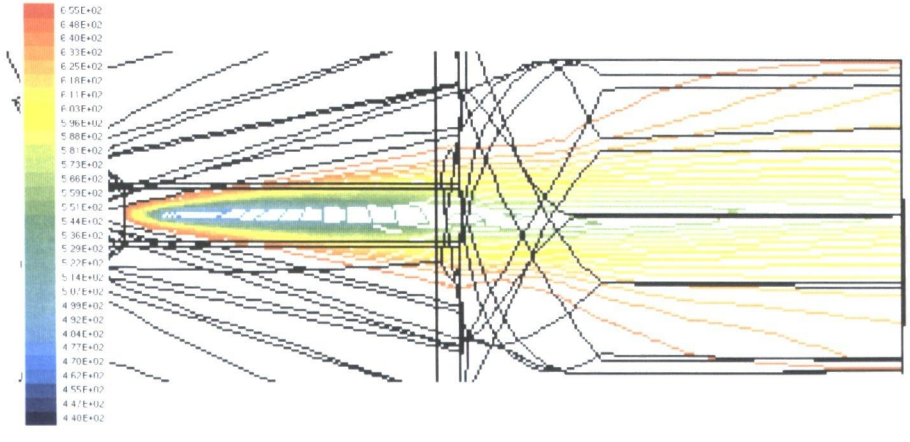

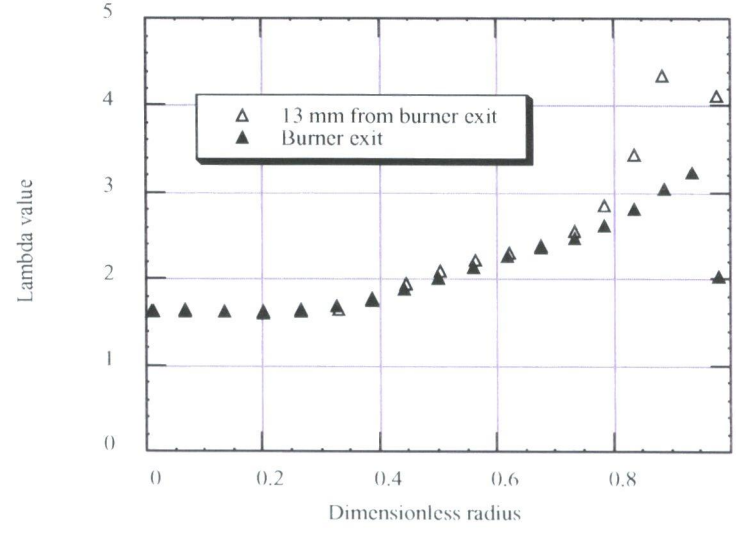

Figure 33 : Case 5

14 bar Air pressure. 30° Spray angle. 45 um Average Droplet size. 100 bar Oil pressure.

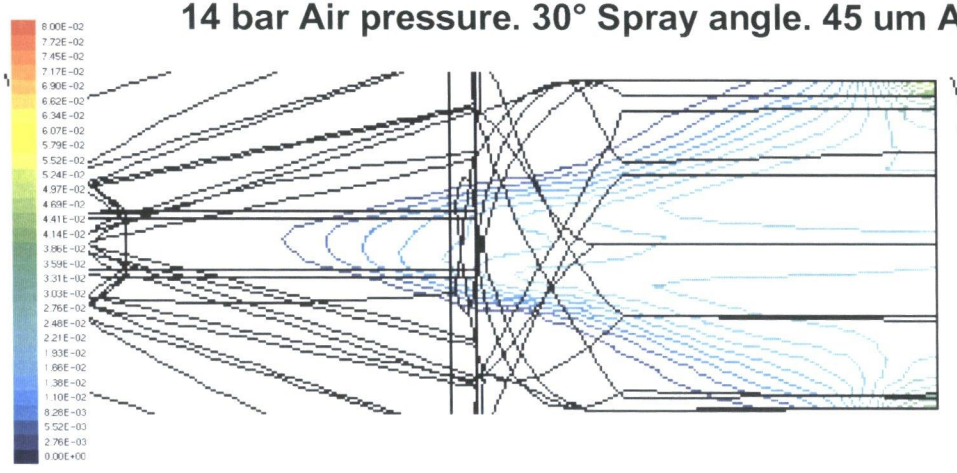

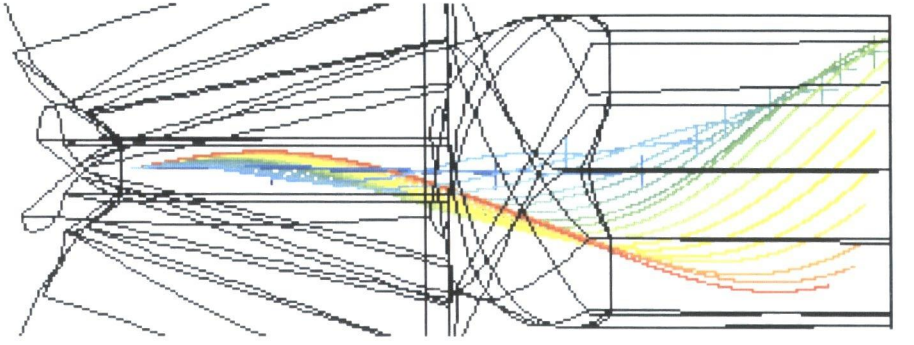

Mass fraction

Particle tracks

Temperature

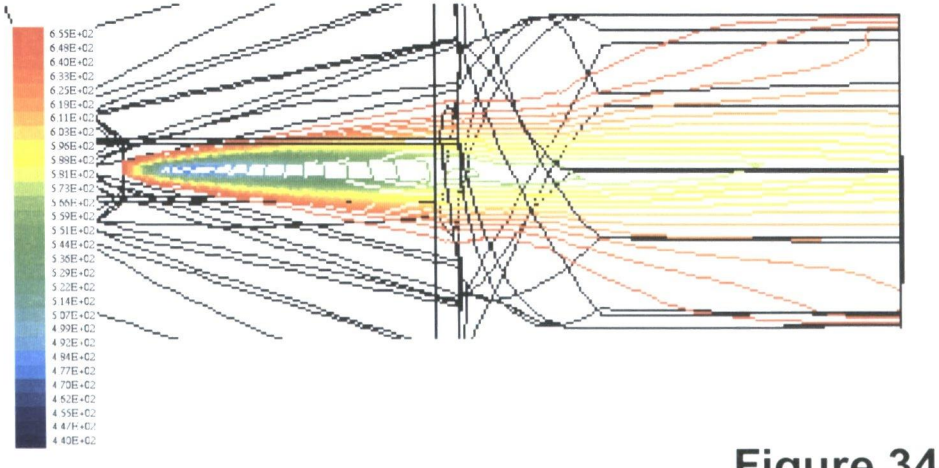

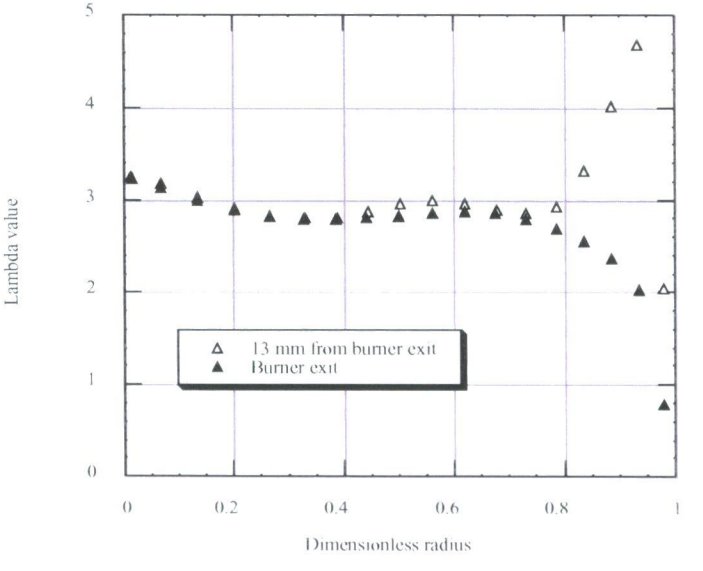

Figure 34 : Case 6

14 bar Air pressure. 60° Spray angle. 23 um Average Droplet size. 100 bar Oil pressure.

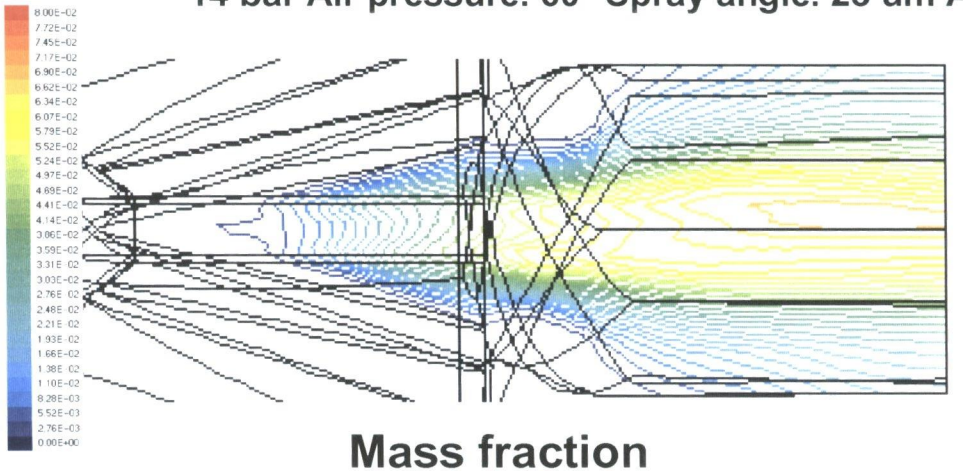

Mass fraction

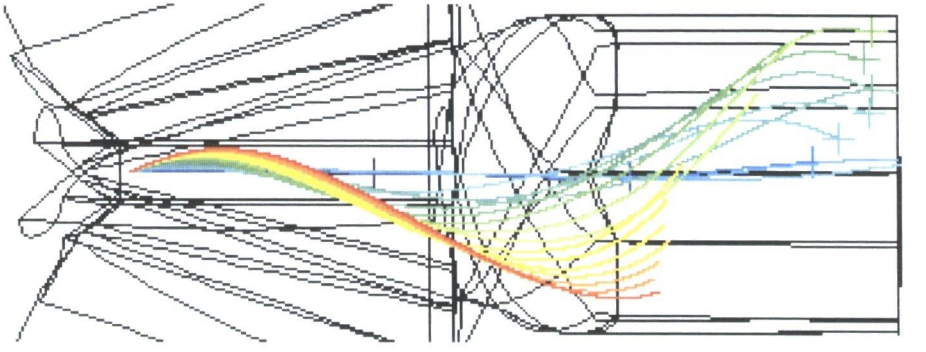

Particle tracks

Temperature

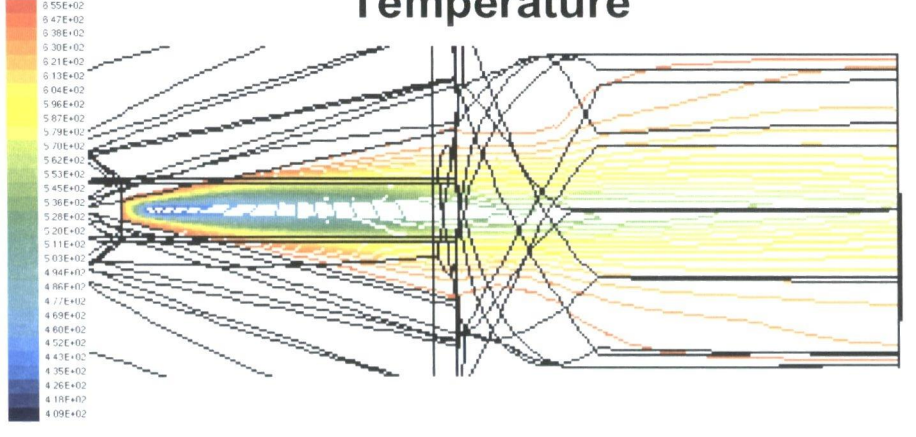

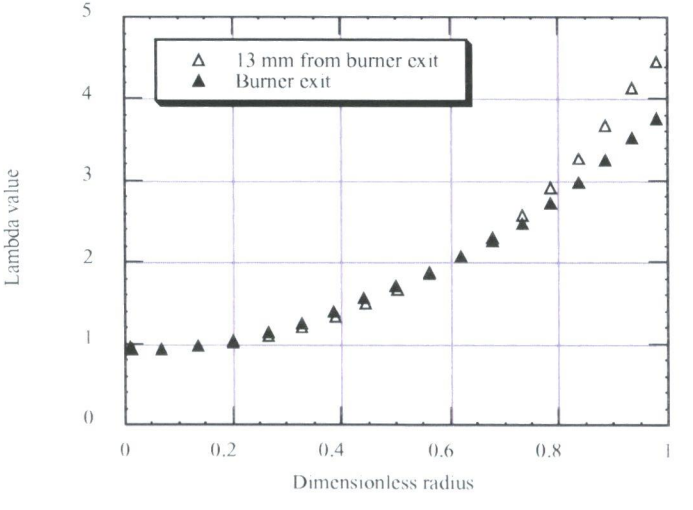

Figure 35 : Case 7

14 bar Air pressure. 60° Spray angle. 30 um Average Droplet size. 100 bar Oil pressure.

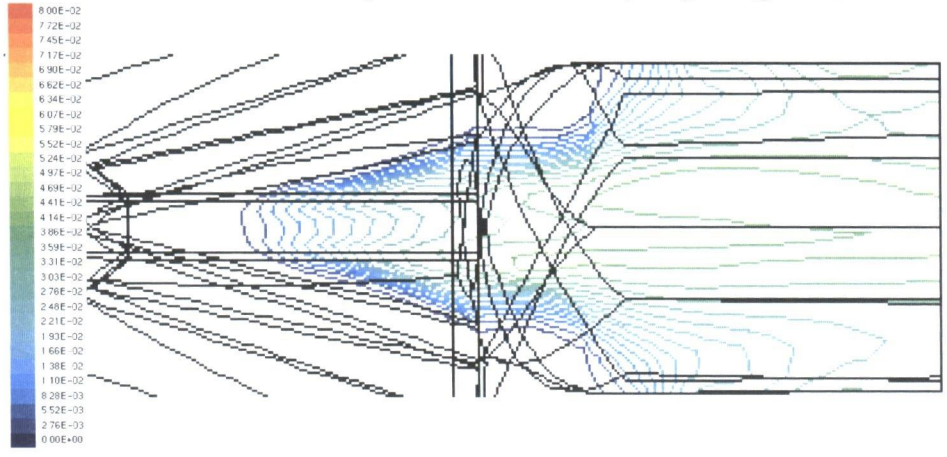

Mass fraction

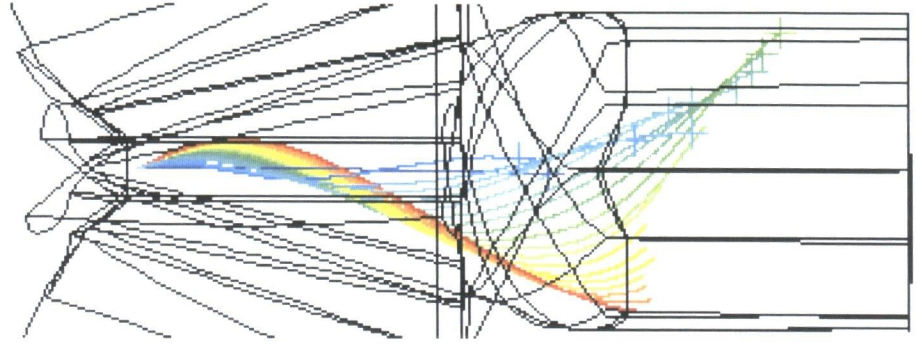

Particle tracks

Temperature

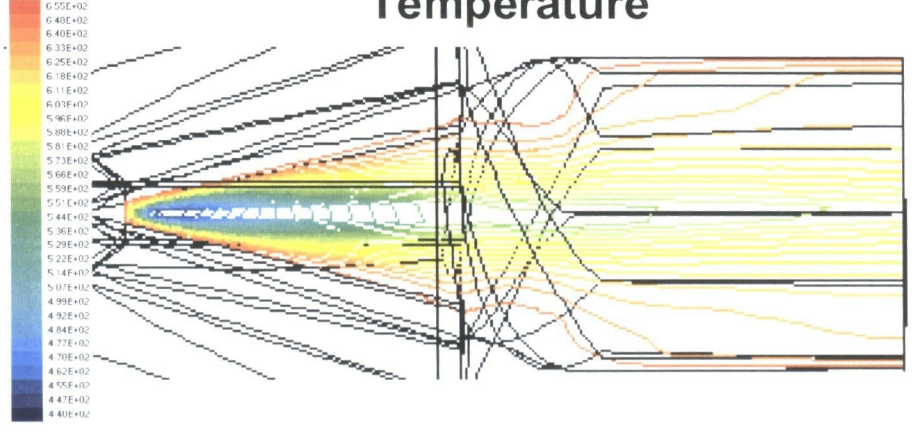

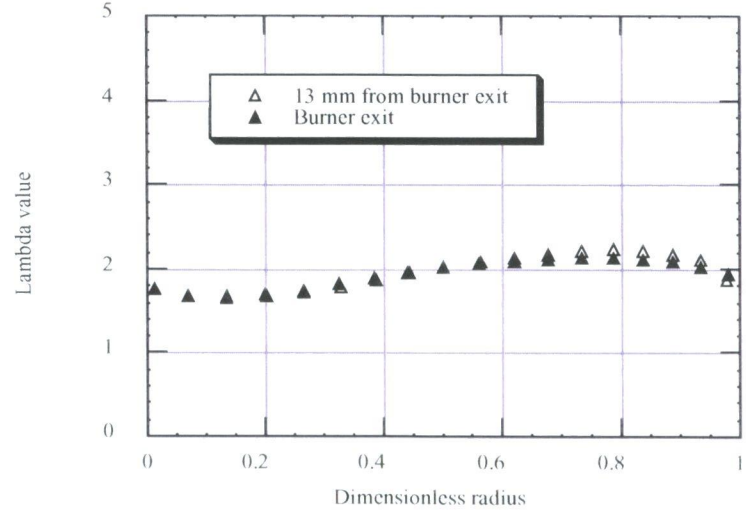

Figure 36 : Case 8

14 bar Air pressure. 30° Spray angle. 45 um Average Droplet size. 100 bar Oil pressure. 750 K preheat.

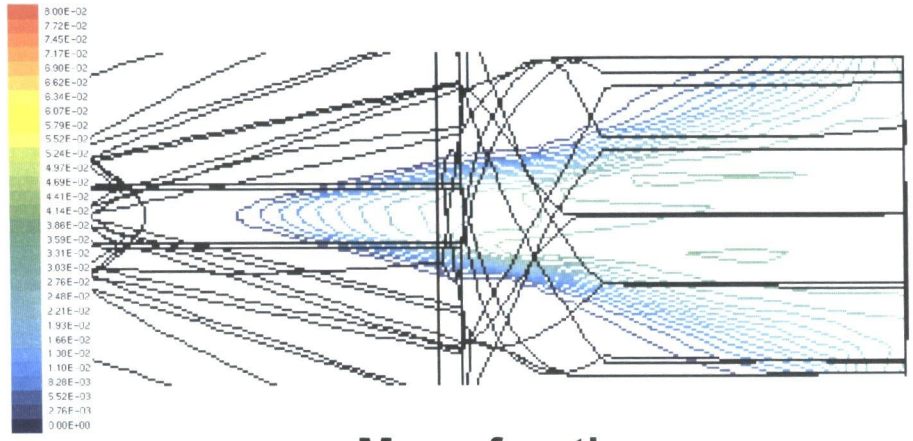

Mass fraction

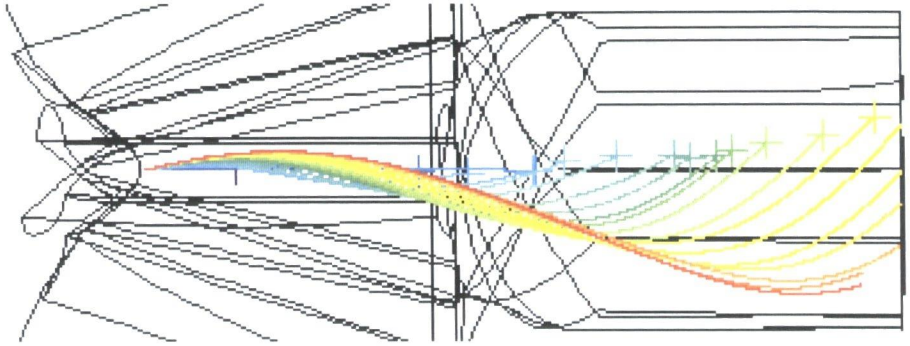

Particle tracks

Temperature

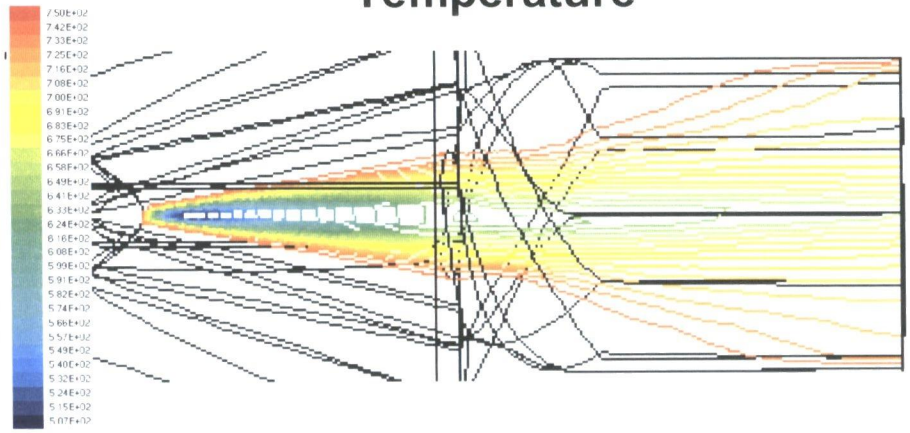

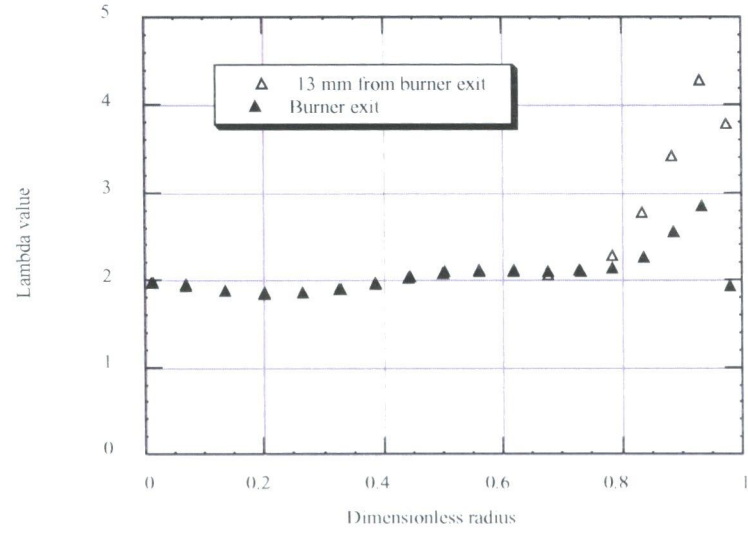

Figure 37 : Case 9

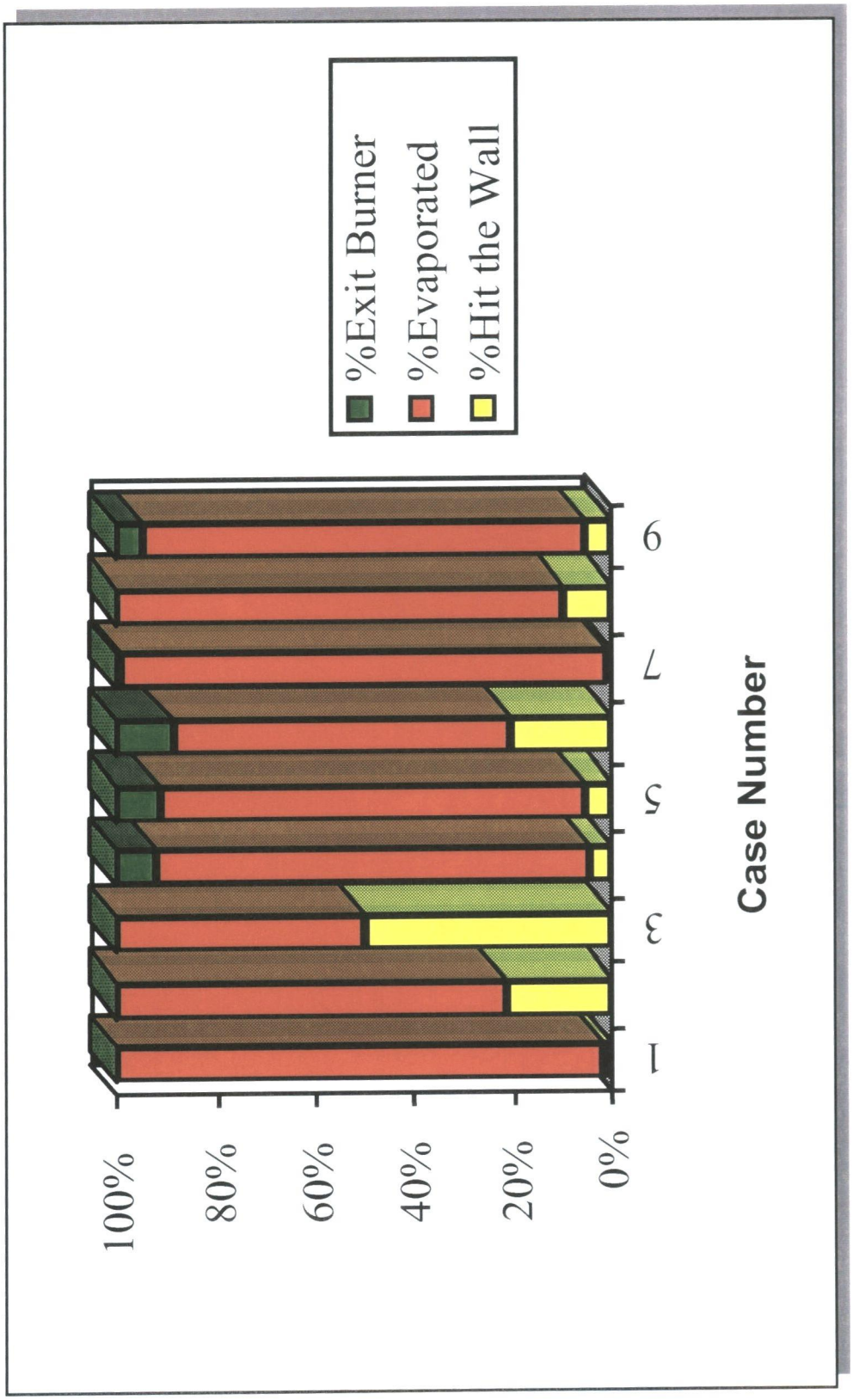
%Exit Burner
%Evaporated
%Hit the Wall
100%
80%
60%
40%
20%
0%
1
3
5
7
9
Case Number

Figure 38

3.6.2.1 Influence of Operating Pressure (Air Pressure)

Comparing Cases 3 & 5, one can see the large difference the operating pressure has on the oil distribution within the burner. From the particle tracks of Case 3, it can be seen that the air has little influence on the droplets, which drive through the flow hitting the wall before fully evaporated. In the high pressure Case 5, the air carries the droplets with it, keeping them on the axis. Due to the higher pressure and therefore the higher density, the air has more momentum making it more difficult for droplets to escape to the regions away from the axis.

This difference is so marked, that there is a total reverse in the trend of the lambda values with the respect to the radius at the outlet of the mixing tube. It has shown that any results taken experimentally under atmospheric conditions can only be used qualitatively with respect to the momentum ratio, and high pressure test must be done to make the final nozzle decision. It means that a nozzle operating at 1 bar conditions is unlikely to be suitable in machine conditions.

(When comparing the two operating pressure, it should be kept in mind that more droplets evaporated at 14 bars due to the higher fuel/air ratio.)

3.6.2.2 Influence of Average Droplet Size

As already discussed in Part 2, average droplet sizes play an important role in the lambda distribution at the end of the mixing tube.

Should they be too small (as shown in Case 7), they evaporate quickly and have not enough momentum to carry them to the outside wall. There then appears a very rich region in the centre, with values of lambda lower than stoichiometric 1. This will lead to high fuel concentration at the flame front and results in high NOx emissions. Local flame temperatures will be far too high and the thermal NOx production will be large.

Conversely, if the average size is too large, (as clearly shown in Case 3), the droplets are flung to the outside of the mixing tube. As the majority of them have not had time to fully evaporate, they collide with the wall, where upon they evaporate. However due to the low velocities in the boundary layer close to the wall, the oil vapour is not quickly

carried away but builds up. This leads to rich regions, where flashback occurs, resulting in pulsations which can be catastrophic.

There is an optimum value of average droplet size for a specific operating pressure. The droplet size has a very important role to play: small droplets are required for quick evaporation, whereas large droplets supply a more even profile due to their larger momentum.

3.6.2.3 Influence of Oil Pressures

In reality, the oil pressure has an influence on both the droplet size and the velocities at which they are injected into the main flowfield. The higher the pressure the higher the velocities and the lower the droplet size. Computationally they can be set separately, and in the computational calculation oil pressure only influences the injection velocities.

Comparing Cases 4 & 5 where two different oil pressures of 100 and 190 bars were used correspondingly, it is shown that this has little effect on the overall oil distribution. There is a slightly better distribution with higher inlet velocities as the droplets have more momentum to carry them to the outer region. Also with higher velocities there is the tendency for the oil to evaporate faster due to the higher surface friction created, although this effect fades out at high relative velocities (see Figure 18b)

Thus, for the nozzle type studied here, oil pressure (injection velocity) is not a vital parameter, although could be used as a refinement tool once the main parameters are set. Influence could be different for other nozzle types such as plain jets, prefilmers, etc.

3.6.2.4 Influence of Injection Angle

Two injection angles were tested: 30^{o} and 60^{o}. Again this is not a major parameter although it does have an influence in the lambda profile.

For the high pressure case, the small droplets have no momentum to drive through the field, and as a result, the angle of injection tends to have little influence on their path.

However for large particles with higher momentum, the angle of injection makes a big difference. Larger angles cause the droplets to hit the wall region at a much earlier point than with small angles. This results in low lambda values against the wall.

Therefore injection angle can also be used as a refinement parameter, especially to change the oil concentration in the outer region away from the axis. One should be careful, as although a good lambda profile is achieved, it could mean a lot of droplets already hit the wall in the transition piece.

3.6.3 Results to Part 4 - Higher Preheat Temperature of 750K

The result to Part 4 (Case 9), is shown on page 80, figure 37.

3.6.3.1 The Influence of Air Preheat Temperature

The comparison of cases 6 & 9 gives an indication on the influence the air preheat temperature has on the lambda value at the end of the mixing tube.
The particle tracks stay roughly similar, although the evaporation times are considerably reduced due to the hotter air. In the case of 750K preheat only 5% of the oil mass hits the wall compared to 20% with 650K preheat air.
This results in a more even distribution of the oil vapour at the end of the mixing tube, due to the less rich zone next to the wall.
The parameters chosen in Case 9 (namely 14 bars operating pressure, $45\mu m$ average droplet size, a 30^{o} injection angle and a air preheat temperature of 750K) lead to an almost perfect oil distribution. (as seen in the lambda plot)
For a larger droplet diameter, a good oil distribution can still be obtained by using a higher preheat temperature.

3.7 Conclusion

Using the 2D duct simulation in **Part 1**, the Fluent code was validated against S. Martens results for his more detailed droplet evaporation model. This was found to fit reasonably well, and therefore a study of evaporation in the AEV burner could be undertaken.

Part 2 calibrated the CFD AEV burner model against experimental results at atmospheric operating conditions. Within the error of experimental results, it was seen that the two methods show similar trends in lambda distribution. This also provided some important data concerning the influence of droplet size.

In **Parts 3 & 4** several parameters were investigated in order to help decide on the correct choice of nozzle for the AEV burner.

Operating pressure (i.e. air density) has a large influence on the lambda distribution at the burner exit. The higher the operating pressure the higher the oil concentration close to the axes. This is due to the rise in density and momentum of the air, which have more control over the droplet tracks, especially for small droplets.

The higher the **Average Droplet Size**, the more droplets appear in the outer region next to the wall. This is due to their higher momentum and centrifugal forces that drive them through the air. The amount of droplets actual hitting the wall should be minimized, as the oil vapour is not carried away in this region due to the low velocities in the boundary layer. This can lead to flashback and pulsations.

The **Angle of Injection** has less effect, although can help in refining the distribution. By increasing the angle, the profile of the outer region can be changed. However the profile near the axes is likely to stay similar. For 60^{o} spray angle, droplets already hit the wall in the transition piece.

By **Preheating** the Air to a higher temperature, one obtains faster evaporation of droplets and a distinctly different distribution of oil. There is a tendency for less mass of oil to collide with the walls of the mixing tube and a higher fuel concentration on the burner axis.

Increasing the injection velocity of oil (by increasing the **oil pressure**) has little effect, although a slight improvement can be seen due to the increased mass transfer at higher relative velocities and thus a minor decrease in evaporation time.

3.7.1 Recommendations

The qualitative results of this investigation are more important than the quantitative results. For an accurate determination of the quantitative results, a much more detailed validation of the codes must be considered, possibly along with additional correction models. Also a highly detailed and reliable set of experimental results is needed for the validation and for the definition of boundary conditions. However, the above investigation is shown to be within a reasonable range of experimental error, and guides in the right direction in terms of nozzle choice.

If one could choose parameters independently, from all the cases investigated, the best nozzle selection for the AEV burner running under 14 bars operating conditions would appear to be a nozzle with 30^{o} spray angle, $45\,\mu m$ average droplet size, a high injection velocity and an air preheat temperature of 750K.
Due to the fact that the air temperature is set by the machine conditions, it is unlikely to achieve such a preheat temperature for the GT10 machine. Another possibility to obtain a similar effect (i.e fast evaporation while retaining the other parameters), but with a more realistic 650K preheat temperature, would be to preheat the oil. This is under investigation.
There are other problems in choosing a nozzle with such high average droplet sizes. Maybe a more desired solution would be much smaller droplets (for quicker evaporation) injected in a different manner (eg. a 4 hole nozzle), in order that they reach the outer

zones. By doing so, the centrifugal forces of the mixing tube are not used to create an even lambda profile. This is also being considered.

When choosing a dry-oil nozzle for the GTX or GT24 machines, which run at even higher pressures, the following points should be noted:

i. The higher operating pressure results in higher air density and momentum meaning more droplets will stay close to the axes.

ii. For large droplet sizes the self ignition time of the oil is likely to be shorter than the full evaporation of the droplets (especially in the GT24/26). Consequently there will be high NOx production and the risk of flashback.

iii. The higher preheat temperature will help faster evaporation for corresponding droplet sizes, but higher partial pressure increases the time for full evaporation.

vi. A higher injection angle and velocity might help the distribution in the outer region.

3.8 Appendices

3.8.1 Appendix A - Boundary Conditions

3.8.1.1 Conditions common to both high and low pressure tests.

Temperature Boundary Conditions

Zone	Temperature
Walls	653 K
Inlet 1	653 K

Species molecular weight.

Species name	Molecular weight
C14H30	198 g
Air	288 g

Viscosity Definition for Tetradekan

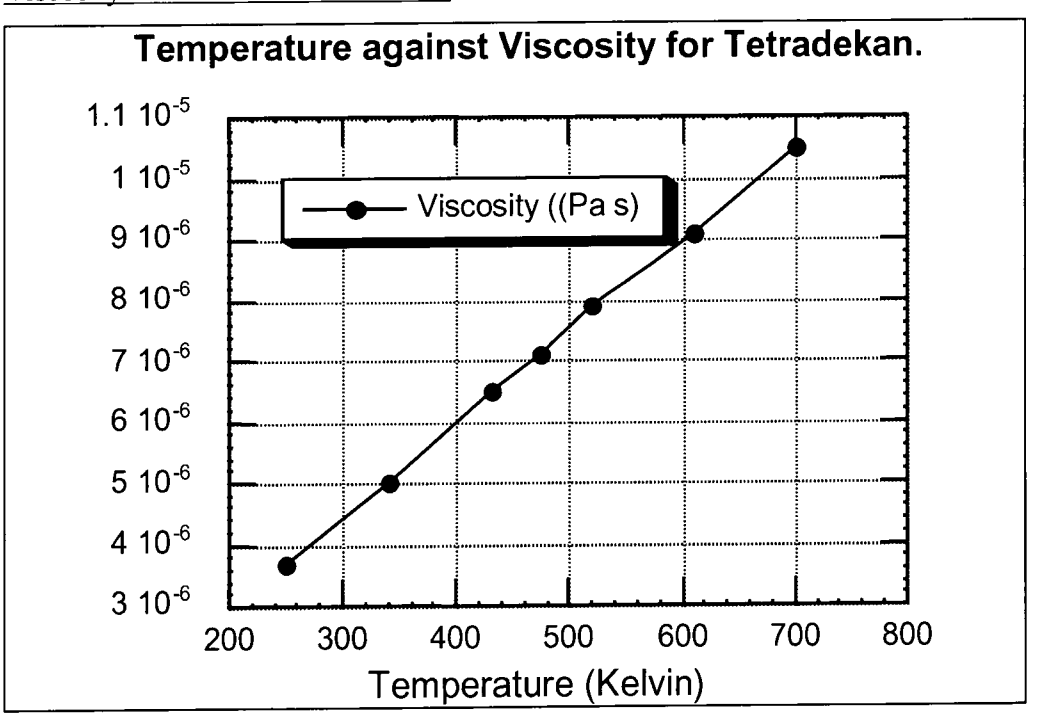

Figure 39

Particle droplet boundary conditions.

Zone	Boundary condition
Walls	Trap
Outlet	Escape
Inlet	Live

Particle Laws activated for user-defined history

Inert	YES
Vaporise	YES
Boiling	YES
Devolation	NO
Burnout	NO
Inert (Law 6)	YES

Second Phase Particle / Droplet Properties

Thermal Conductivity

K = 0.078 W/mK

Vapour Pressure

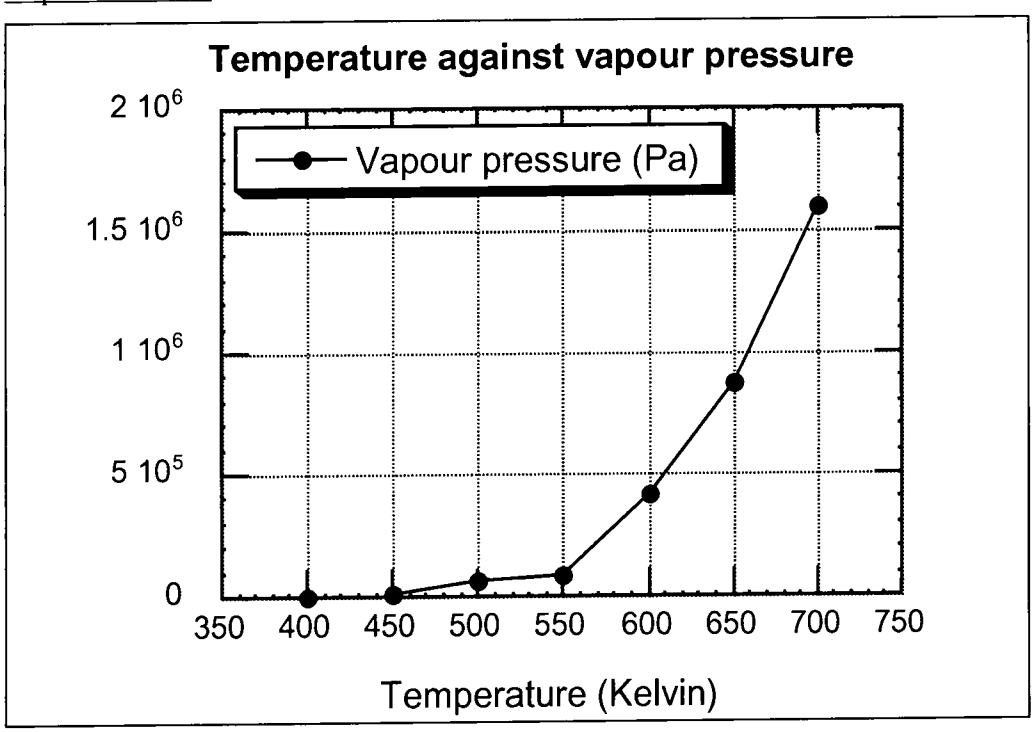

Figure 40

3.8.1.2 Boundary Conditions which varied with pressure.

Velocity Boundary Conditions for 1 bar

Zone	U-Vel	V-Vel	W-Vel
Walls	0	0	0
Inlet 1	0	0	10.98 m/s

Velocity Boundary Conditions for 14 bars

Zone	U-Vel	V-Vel	W-Vel	Normal
Walls	0	0	0	N/A
Inlet 1	0	0	10.2 m/s	N/A

Specific Heat for Tetradekan

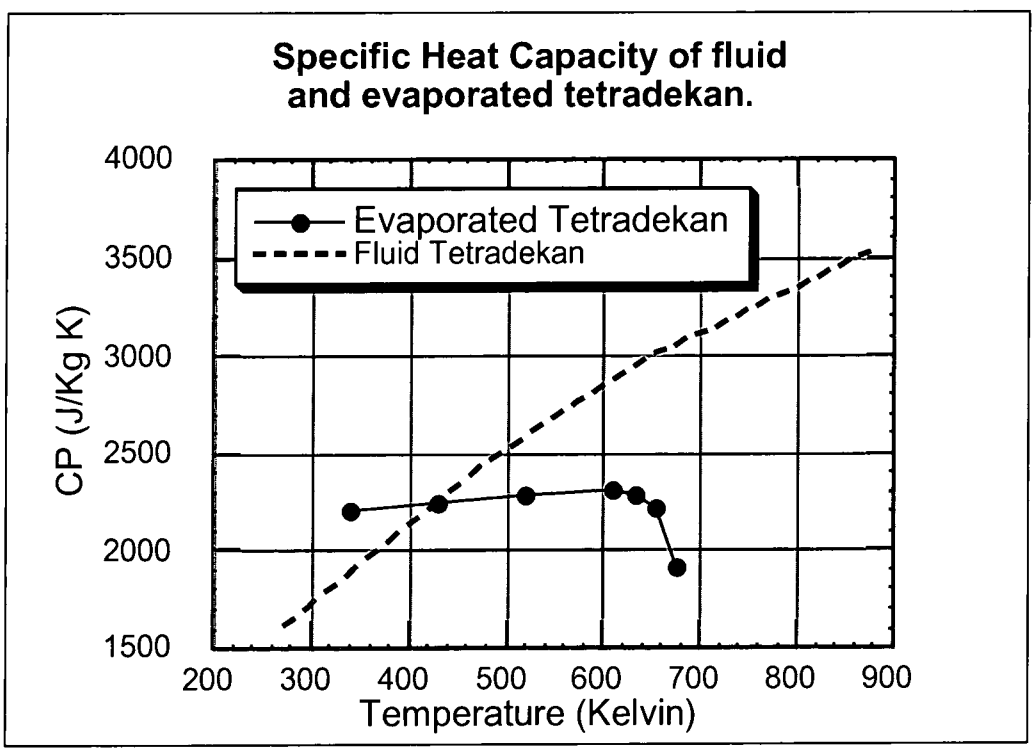

Figure 41

Specific Heat Definition for Air

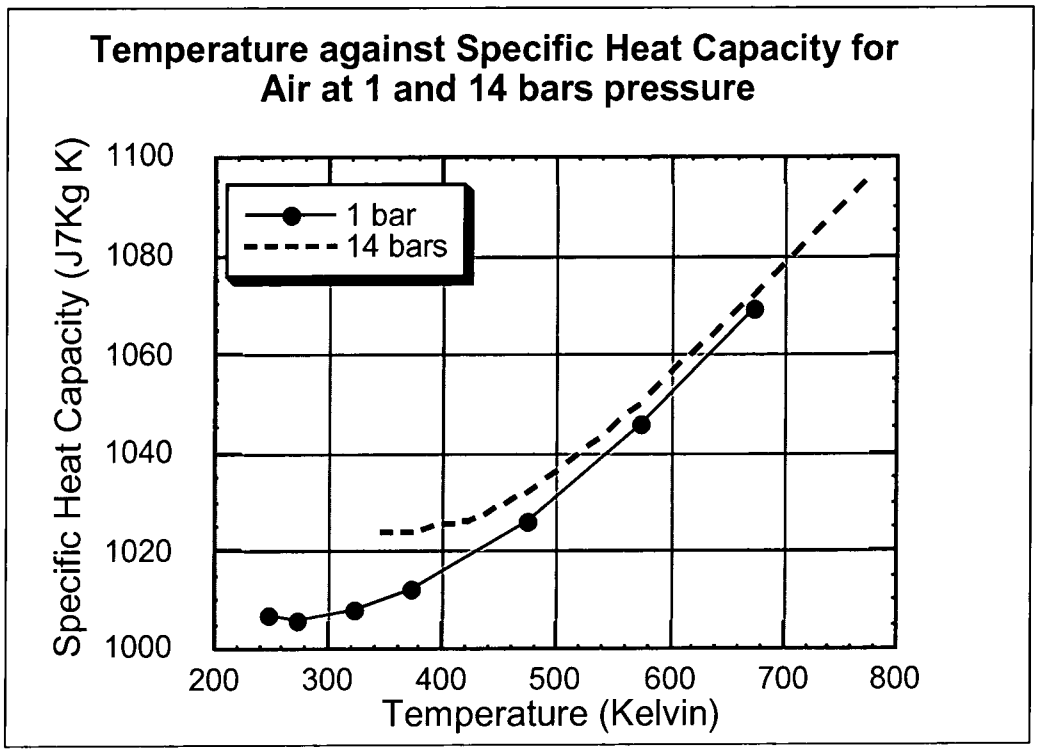

Figure 42

Binary Diffusivity Coefficient

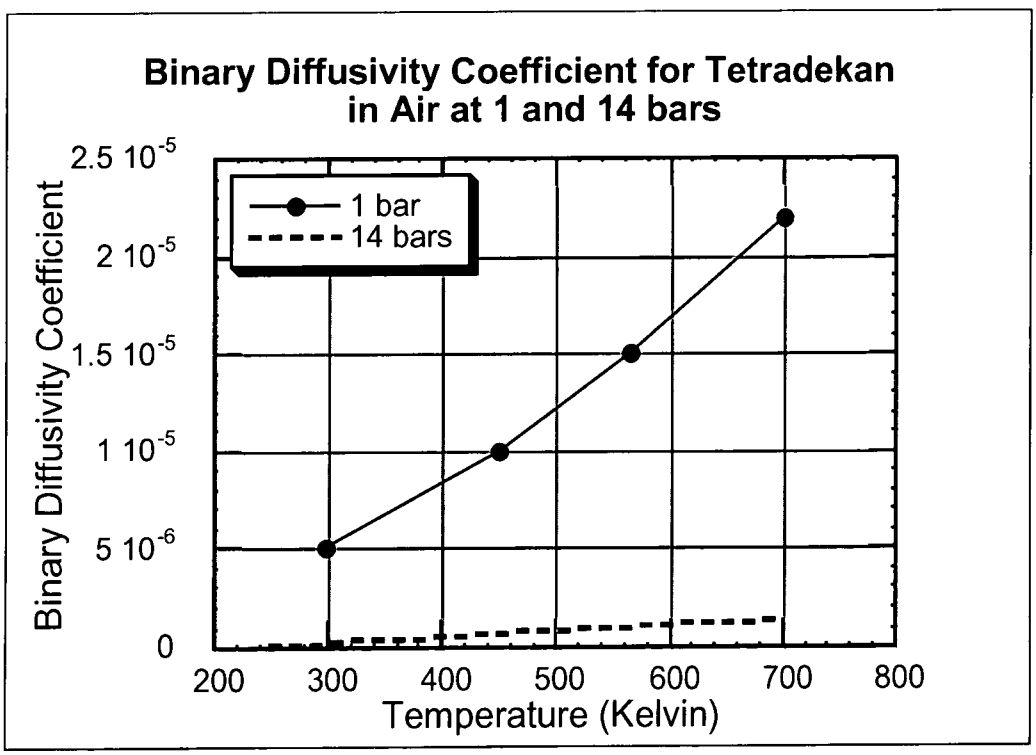

Figure 43

Viscosity Definition for Air

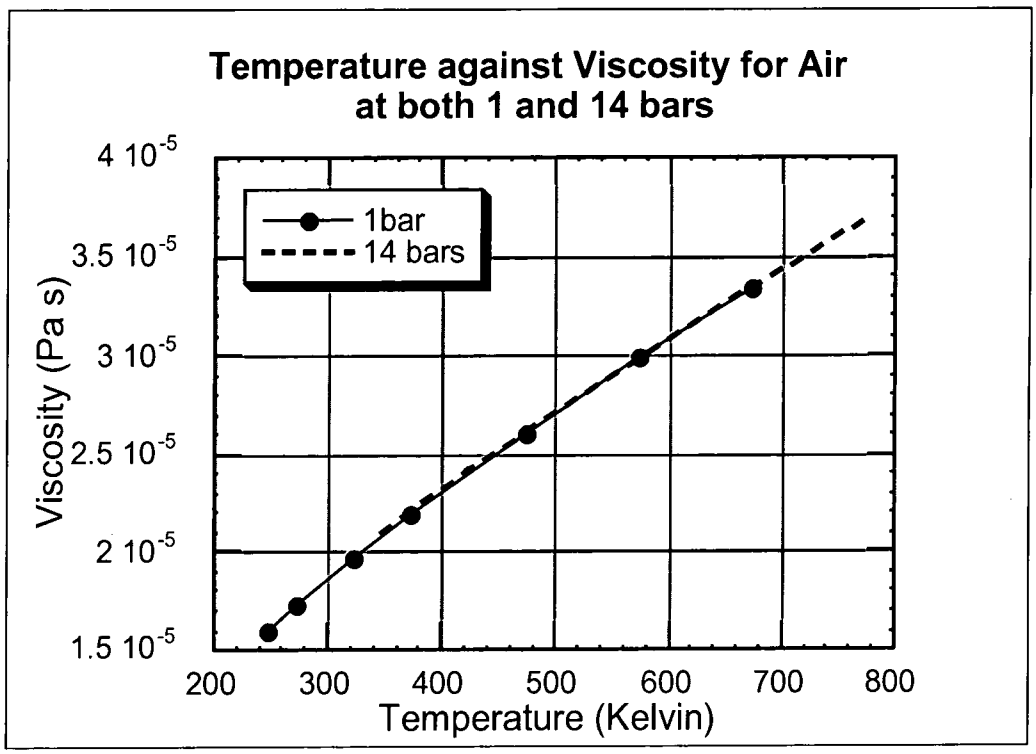

Figure 44

Thermal Conductivity Definition for Tetradekan

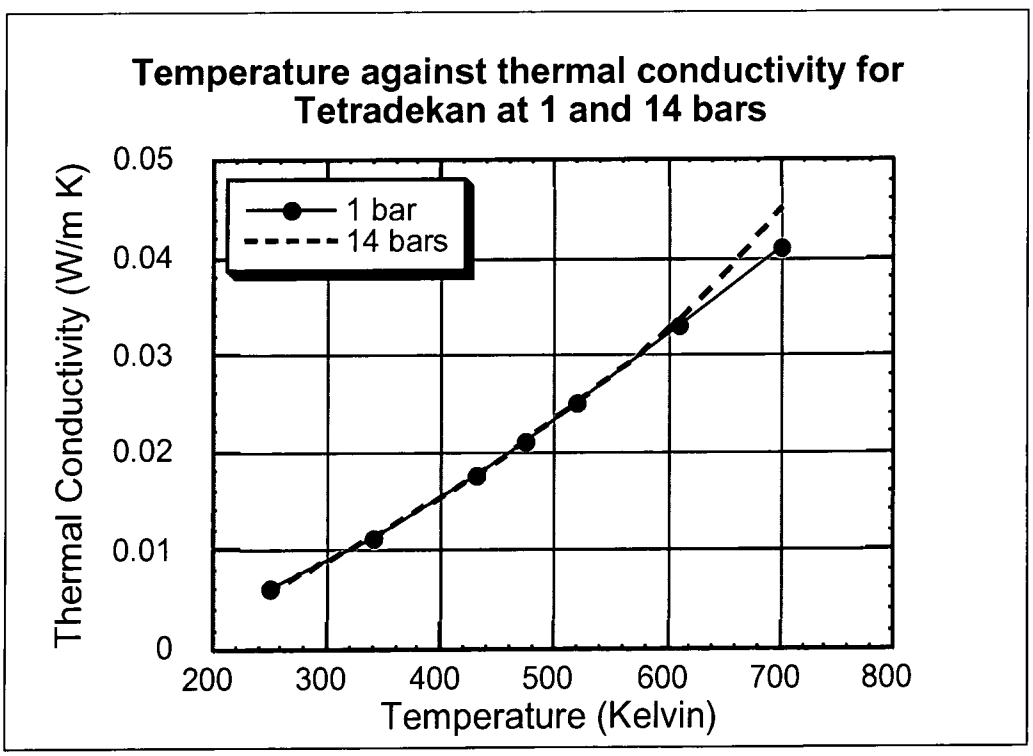

Figure 45

Thermal Conductivity Definition for Air

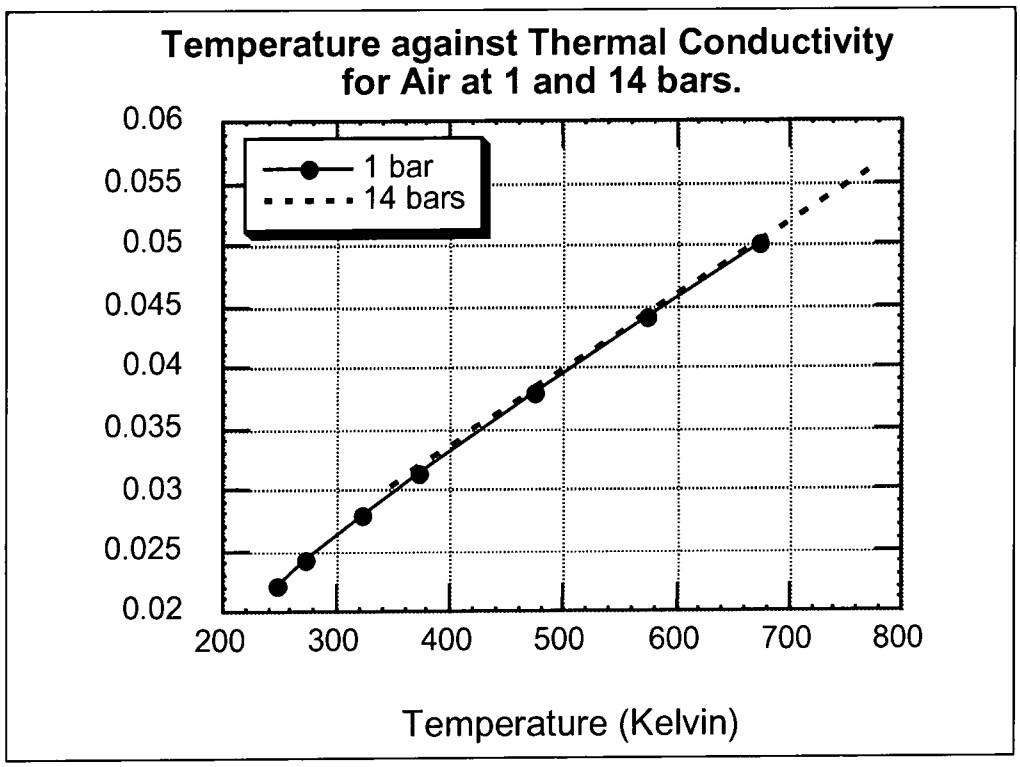

Figure 46

Second phase particle droplet properties at 1 bar

Mass Flow Rate	0.0055 kg/s
Particle density	720
Boiling point	525
Latent heat of vaporisation	1.768E5
Vaporisation temperature	350
Fraction volatile component	1
(Mass Flow Rate of Air	0.195 kg/s)

Second phase particle droplet properties at 14 bars

Mass Flow Rate	0.092 kg/s
Particle density	720
Boiling point	690
Latent heat of vaporisation	1.768E5
Vaporisation temperature	450
Fraction volatile component	1
(Mass Flow Rate of Air	2.73 kg/s)

3.9 References

1. Martens S., Berechnung der Bewegung und Verdampfung von Brennstofftropfen in Heißgasstömungen hohen Druckes, ABB Research Report - CRBT 92-10, 1992

2. Fluent User Manual, Version 4.3, January 1995

4. AEV75 CFD - Further Results and Model Limitations

4.1 CFD Prediction for Preheated Oil

In the parameter study it was seen that increasing the air preheat temperature caused faster evaporation of the droplets resulting in an influence on the fuel distribution. What was not considered was the option of increasing the oil preheat temperature as a means of faster evaporation. The main part of the heat transfer to the droplet contributes to the heating of the droplet. As soon as the droplet reaches a certain temperature, evaporation occurs faster and faster. This is due not only to the rise in temperature and energy, but the decrease in droplet size, which therefore means that the drop requires less energy per degree for heating. If the heating process could be speeded up, faster evaporation could take place, allowing larger droplets in the spray and deeper penetration.

An additional calculation has therefore been completed to investigate the effect of an increased preheat oil temperature. However the oil temperature is limited due to the danger of coking the nozzle.

The air pressure remained at 14 bars, spray angle 30 degrees, average droplet size 45μm, and oil pressure at 100 bar.

The oil was preheated to 130°C, as opposed to the previous 80°C - an increase of 50°C. Coking should not occur at this temperature.

This case can be compared to Cases 6 & 9 in Chapter 3. It is difficult to make a direct qualitative comparison between an increase in the air preheat temperature and an increase in the oil temperature.

However, the trend shows a similar tendency in results (see Figure 47) : due to the smaller evaporation time, the oil mass fraction on the axis is increased, while in the wall region, less oil mass hits the wall. In this case the lambda profile was improved in relation to non-preheated oil (Case 6), although results were not as good as the air

preheated case. This is due to the smaller temperature rise, and also that the air contains more heat capacity per volume flow rate than the oil.

In summary, oil preheat is also an option for changing the lambda profile at the burner outlet. How it is achieved in practice is separate problem. Expensive heaters need to be used, which cost power and money. In a single cycle machine, turbine exhaust gases may be used, but this is not viable in a combined-cycle.

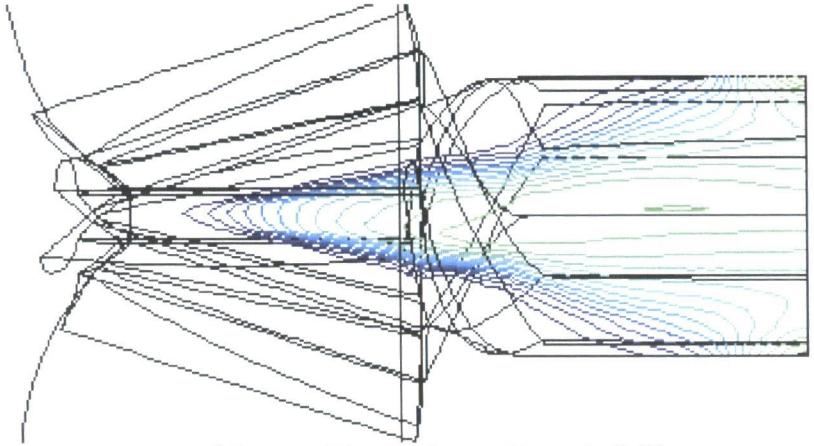

Mass Fraction (0 - 0.08)

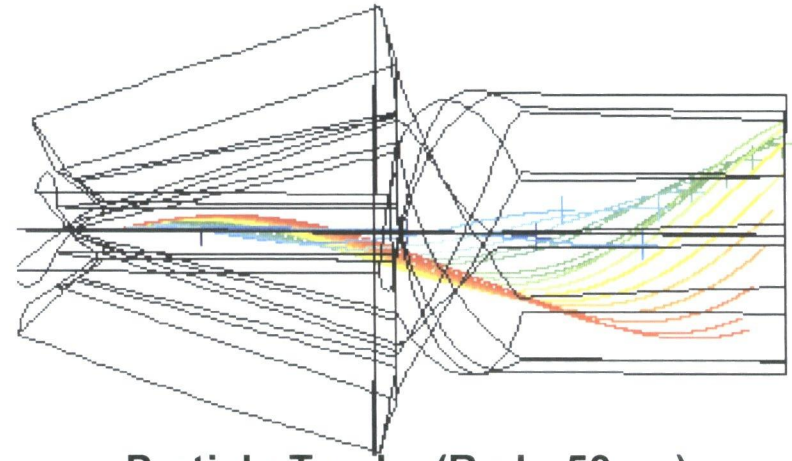

Particle Tracks (Red - 50um)

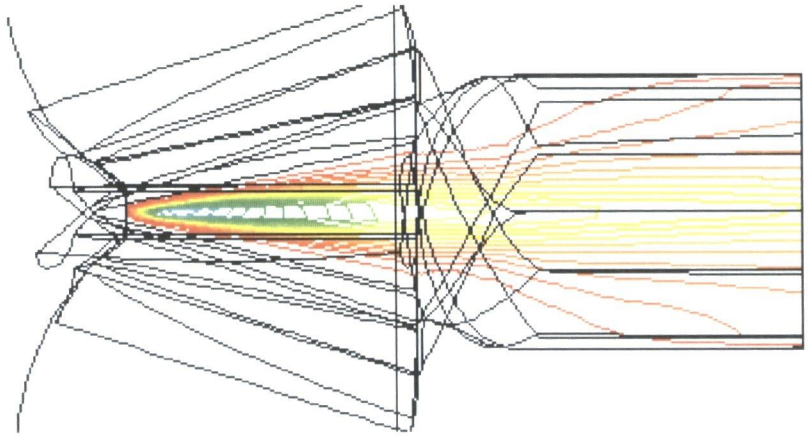

Temperature (440 -650 K)

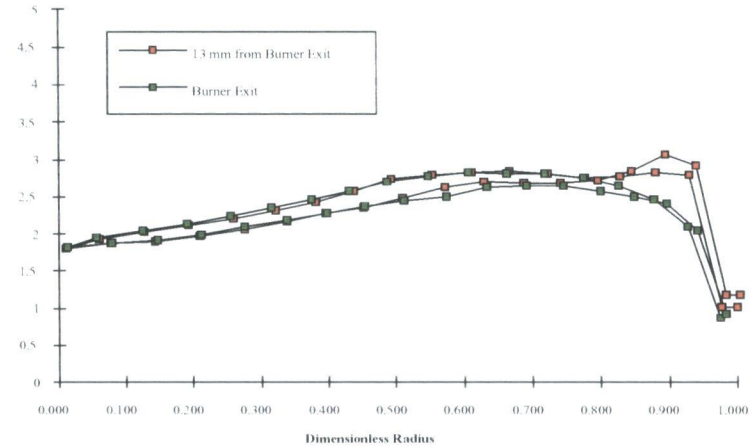

Lambda Values

14 bar Air Pressure. 30° Spray Angle. 45um Average Droplet Size. 100 bar Oil Pressure

Fig 47 - AEV75 CFD Oil Preheated to 130°C

4.2 Limitations, Inaccuracies and Assumptions in the AEV75 CFD Modelling

There are two main sources of inaccuracies occurring in the described model used for evaporation in the AEV burner.

i. In the continuous phase flow-field modelling.

ii. In the dispersed phase models and coupling

4.2.1 The Continuous Flowfield

Looking at the solution in figure 23, there appears to be minimal inaccuracies occurring in the flow-field of the numeric model until the transition piece. Slot velocities compare very well to those from the water channel tests (see figure 25). Also the internal burner flow inside the swirl generator compares well. Problems occur in the axial region downstream of the transition piece. Here swirl appears to be lost due to numerical dissipation. The peaked tangential velocity rising sharply from the axis gradually spreads radially, the further downstream one goes from the transition piece. With it there is the spreading of axial velocity leading to a reduction in the stream-wise direction.

One of the problems lies in the grid. In the region of concern (i.e. along the burner axis), the grid is too coarse. There are cells lying on the axis in the transition piece that have widths up to 4mm. This means that within 3 cells, the high gradients of tangential velocity and swirl must be solved. Here the numerics cannot be solved accurately enough leading to the loss of axial velocity and swirl. This is likely to be the main reason for the discrepancy between experimental and computational results. A better grid should be made by adapting the axial region. Also the highly skewed cells in the boundary regions should be improved.

Other discrepancies could lie in the simplification of the geometry which was implemented to help the ease of gridding. In the case calculated no boundary layer

bleed holes were included and geometrical errors could have been present in other areas (such as the transition piece).

The use of a tetrahedral unstructured grid should overcome these problems. This has already been modelled, although the similar dissipation problems along the axis occurred due to the lack of refinement in the corresponding area. (although the aim of that model was not an accurate internal burner flow, but the inlet modeling and external aerodynamics)

The turbulence model is another likely source of error. The turbulence model used was the k-ε RNG. The RNG version has the advantage of predicting swirling flows with much higher accuracy than the normal k-ε. Another advantage that RNG k-ε has over RSM is its ability to model near wall flows to predict heat, mass and momentum transfer. This is important in the case of oil droplets hitting the walls of the AEV. However it is limited in not considering the rotation forces and the RSM model is known to predict swirling flows even better than k-ε RNG. The main disadvantage of the RSM is the high CPU time needed. Also convergence is more difficult to achieve with RSM, especially with such a complicated geometry. Considering the number of cases needed to be computed, the RNG option was taken. The k-ε model certainly over-predicts the production of turbulent energy (and therefore turbulent viscosity) where high shear effects occur. This leads to a less peaked tangential velocity profile causing a reduction in total pressure across the radius and therefore reduced axial velocity. Correctly predicting the turbulent viscosity in these regions is vital. Both the RNG k-ε and the RSM attempt to do this. Literature and experience claims that RNG k-ε is only marginally worse than the RSM model. A validation of RSM to RNG should be done, although the present version of Unstructured Fluent has not yet implemented the RSM.

For structured grids, higher order schemes should be used due to the fact that the main flowfield is not aligned with the grid (i.e. streamlines cross cells at an angle). Either the second-order upwind scheme or QUICK (Quadratic Upwind) should be used.

For higher accuracy of droplet dispersion in further work, a more accurate continuous flowfield should be obtained.

4.2.2 The Dispersed Phase Models

When considering dispersed phase calculations, there are two main options: an Eulerian or Lagrangian modelling approach.

The Eulerian approach should be used when the dispersed phase appears in high volume fractions, typically above 10%.

In the Eulerian approach the different phases are all calculated as continuous functions by using a volume fraction concept. Each set of phase equations have similar terms solved for momentum and continuity. This also allows some form of droplet influence in the turbulent flow-field which is not seen in the Lagrangian model. Here the droplet / droplet interaction can be accounted for.

Reasons for Inaccuracies in the Dispersed Phase Model

1. The question remains to whether the volume fraction is low enough to validate the use of the Lagrangian model. In the near nozzle region (the first few mm) this is not the case due to the density of droplets close to the injection point, although the rapid dispersion of the droplets in the burner brings the local volume fraction of droplets to air quickly below the aforementioned 10%.

There are however limitations within the Fluent Euler model that made it invalid for such modelling; notably the inability to use the RSM model and the fact that phase change is not allowed.

2. This gave way to the use of the Lagrangian model. This allows a 2-way coupling to achieve the impact of the dispersed phase on the continuous phase and visa-versa. The trajectories injected in the dispersed phase, along with their heat and mass transfer, can be calculated (Heat, Mass and Momentum exchange calculated). The influence that the turbulence in the continuous phase has on the droplet dispersion is accounted for, although the trajectories have no influence on the turbulence levels in the continuous phase.

3. Fluent calculates trajectories by equating the forces that act upon a particle. These equations are shown in the Theory section (Chapter 2.5) and include the drag force of the particle (most important), gravity, and extra terms including the force required to accelerate surrounding fluid, pressure gradients in the fluid and thermophoretic forces. The first two extra terms are almost negligible as they are proportional to the air to oil density ratio which is around a 10/1000. The thermophoretic term is also negligible as it is proportional to 1/T, which can be as little as 1/600. Therefore this was not included in the solver. However the blowing effect (the influence of evaporating fuel on the boundary layer characteristics) is important, and the simple correlation described in the theory section should be implemented in order to increase the accuracy.

4. Although the particle track plots show the trajectories using the mean fluid phase velocity, the calculations were done using tracking in turbulent flow. Random Walk Methods (either discrete or continuous) can be used to predict the dispersion of droplets due to turbulence from the continuous phase. The model chosen here was the Eddy-Lifetime model, as the Continuous Random Walk model this takes computationally longer, even though it is more realistic.

5. The boundary conditions are also subject to error. For atomisation characterisation the Rosin-Rammler equation is generally accepted as a way of describing the droplet distribution.

However the two vital parameters that have to be input (namely SMD droplet size and the spread factor – Eq. 20) are to be questioned. For these calculations, a spread factor of 3.5 has been taken. This may seem high to start with, although this result was obtained by measuring spray in a cross flow with PDPA equipment. A best-fit curve gave a spread factor of 3.5.

6. Another assumption in the boundary conditions of the nozzle is that all droplets are injected with the same half angle. In reality there is likely to be a slight distribution of droplets in the angular spectrum. This is not accounted for in the modelling and is also likely to have an effect on the droplet history. There will be less

droplet/droplet interaction as a result and less penetration of the spray into the air flow-field due to the reduced continuous inertia.

7. The other parameter that can be difficult to determine is the mean droplet size. Mean droplet size used depends not only on the accuracy of the measuring technique, but also on the quality of the nozzle tip. Similar nozzles with different tip quality (surface roughness) can vary in mean droplet size. More experimental investigations need to be considered. It can be seen from the CFD results that this is a critical parameter in the distribution of oil vapour.

It is highly important that the starting conditions for the nozzle are accurately determined, else an accurate simulation of the AEV burner for oil operation can never be achieved.

8. The wall condition should also be considered as a region for errors, as the wall plays an important role in the AEV burner. Here the walls were taken to be so hot that any droplets that came into contact with them would immediately evaporate leaving the corresponding vapour in the neighbouring cell. In reality other effects could take place: bouncing before evaporation, partial evaporation, break-up, etc. These phenomena could be considered further.

9. Another weakness in the modelling appears in the evaporation model. This simplistic model actually ignores any evaporation of the droplet until a certain 'vaporisation temperature' (see Section 2.6). Until this point only the heating of the droplet is considered. In reality this is not the case; there will always be evaporation especially in multi-compound liquid like light oil. Even if this model is used, there is the question to what value the 'vaporisation temperature' should be set. As it is a theoretical number there are no known values for it. It is also likely to vary considerably with pressure. Calibrating this value is vital to the model. The lower the vaporisation temperature, the earlier the decrease in droplet size. Certainly the evaporation model needs some more detailed consideration.

The use of tetradecane as the compound for modelling also included assumptions. While the physical constants of tetradecane correspond to light oil well

(i.e.. density, viscosity), the complex makeup of the liquid fuel means that the evaporation curve will be somewhat different; the smaller chain compounds will evaporate quicker, while the longer chain compounds will take longer. The correct oil mixture is complex to model, as it means describing a new evaporation curve, as mentioned in the theory chapter.

In summary there are certainly simplifications and weaknesses in the model. However, how important they are, and how far they are from reality can only be studied from further evaluations.

El Banhawy and Whitelaw (Ref. 9) completed a similar study involving a swirling spray along an axis from a swirl-atomizing nozzle. It was found there were discrepancies between the computations and the measurements. These were attributed to the large grid spacing near the nozzle, evaporation rate uncertainties, lack of adequate information on nozzle exit conditions, and limitations in the k-ε turbulence model.

Although many points have been listed here it is important to note the weight that each carries. The initial conditions of the spray (size and spread) have the most influence on the result.

5. AEV100 CFD - Oil Nozzle Prediction Technical Report

In order to have a flexible burner, scaling needs to be possible as power demands for different machines vary. Therefore it was necessary to scale the AEV75 burner upto AEV100 (corresponding to an increase in burner diameter from 75 to 100mm).
Along with the scaling come practical problems of reoptimizing the oil operation. While retaining similar operating conditions to the AEV75 optimization (pressure and preheat temperature), dimensions are increased. Oil penetration to larger diameters is needed. On one hand this could be achieved by increasing droplet size, although more droplets are likely to hit the wall. Alternatively a totally new concept may be required.

The following technical report describes numerical simulations undertaken to optimize oil operation for the AEV100. It is solely the work of the author, and alongside being work for this thesis, is an important practical part of the burner development.

Technical Report

Reporting CRC (full name and address):

ABB Management Ltd.
Corporate Research Center Baden (CHCRC)
Segelhof
CH-5405 Baden-Dättwil Switzerland
Tel.: (+41 56) 76 84 11 Fax : (+41 56) 83 55 61

Responsible Person:	P.Jansohn				
Project Name:	3rd Generation Burner NG/Oil				
Document Title:	**AEV100 Oil Nozzle Prediction** (Setup & Results only)				
Document Ref.No.:	ABB CHCRC 97-26	Reg: T4-32-04		Page 1	
Date of issue:	21.3.97	Classification:	Normal	No. of pages:	33
Client:	KWR-T				
Author(s):	J.Lloyd	Approved:	K.Döbbeling	Order No.:	CHCRC.T3 97-05
Distribution:	see separate page				
Distribution page 1:	see separate page				
Keywords:	AEV100, Oil Evaporation, Numerical Modelling, Lambda Profiles				

Summary:

A numerical investigation has been completed to evaluate the viability of obtaining good NOx emissions when running oil No.2 in the AEV100 (a scaled version of the present AEV75). The main criteria used to assess this, was the degree of mixed oil vapour at the end of the mixing tube of the burner.

After calculating and comparing the main air flow field in the burner, oil was injected through two different types of nozzle. Firstly, a standard hollow cone nozzle was modeled, similar to that presently used in the AEV75. This was seen to give undesired results, leading to very lean regions near the burner walls.

Secondly, a four hole solid cone injection system was simulated. Due to the many different geometrical possibilities, a parameter study was undertaken, to optimise the nozzle design. It was seen that the parameters that have a major influence on the final oil vapour profile are injection angle, individual spray angle, droplet size and the droplet range. Optimised profiles can be obtained, although trends are often not as expected. Other parameters also investigated were tangential angle, pressure loss and the back pressure.

The perspective for Dry Low NOx Oil operation with the AEV100 would appear optimistic and realisable.

Contents

5.1 Introduction

In a study to establish the viability of a scaled version of the AEV75, a AEV burner of mixing tube diameter 100mm will be produced and tested for its characteristics. As well as being able to combust natural gas, it is also required that it can run on oil No. 2 with satisfying NOx emissions without the addition of water injection.

In order to implement Dry Low NOx Oil into the AEV100 burner, it is necessary to make a prediction of the lambda profile at the end of the mixing tube, as a means of assessing which nozzle can help produce the lowest NOx emissions.

It can be predicted that due to the increase in dimensions over the AEV75, considerable problems could be caused in penetrating the oil far enough radially into the air flow to obtain an even vapour distribution at the burner outlet. The optimum nozzle type should be defined through the use of CFD before testing in order to help produce the best results for the burner.

By using CFD, a wide variety of nozzle parameters can be evaluated, both giving qualitative trends, and quantitative results. An initial comparison in the DIVA (high pressure) test rig will give an indication of the quantitative accuracy. From there on, the qualitative results can swiftly guide us to the correct choice of nozzle.

5.2 Continuous Phase

The continuous phase results were computed on a scaled up version of the AEV75 case. This corresponds to a mixing tube diameter of 100mm, mixing tube length of 137mm, zero gradient pressure outlet (i.e. no sudden expansion),and slot widths of 16.6mm. The single block grid can been seen in Fig.48.

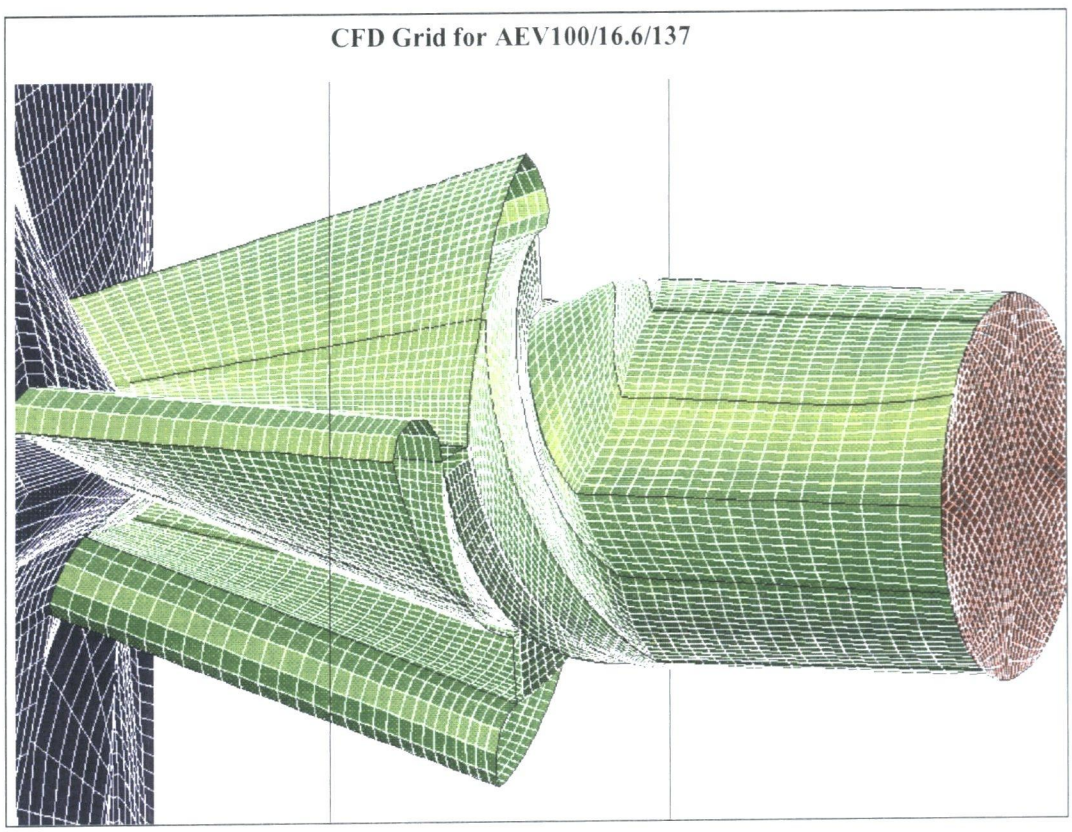

Figure 48

The air was calculated at 15 bar and a compressor outlet temperature of 763K. The mass flow rate of 3.65 kg/s per burner has been taken. This gives the average velocity (68m/s) and temperature, at corresponding DIVA (high pressure test rig) experimental conditions (13 bar).

A turbulent intensity of 5% was used at the inlet with a turbulent length scale of 0.007m (calculated from 0.07L = 0.07 x 0.1m)

For a turbulence model, the RNG K-e model was used, known to perform better at solving swirling flows, separated flows and stagnation flows. Apart from that, it is the only turbulence model able to easily converge this case.

The solver also included the Non-equilibrium Wall function, i.e., where turbulent dissipation at the wall is not equal to the turbulent production, in order to improve the boundary layer modelling. This option was used.

Although certain inaccuracies occur in this grid, a good result has been achieved for the continuous phase. The numerical dissipation that sharply reduced axial and tangential velocities near the centre region of the AEV75, did not occur in this case. A comparison between normalised AEV75 velocity profiles from the *water rig* and normalised computational AEV100 results (shown here in Fig. 49), confirms the close agreement of numerical and experimental results. The continuous phase results, a major inaccuracy in the AEV75 results, can in this case, be relied upon to give an effective base for coupling between oil and air. This means that the quantitative results should have a much higher accuracy.The swirl number for the CFD case is calculated to be 0.58.

The swirl number can be defined as: $\frac{AngularMomentum}{r_{outer} \cdot AxialMomentum} = \frac{\int_0^r uwr^2 dr}{r \cdot \int_0^r u^2 r dr}$

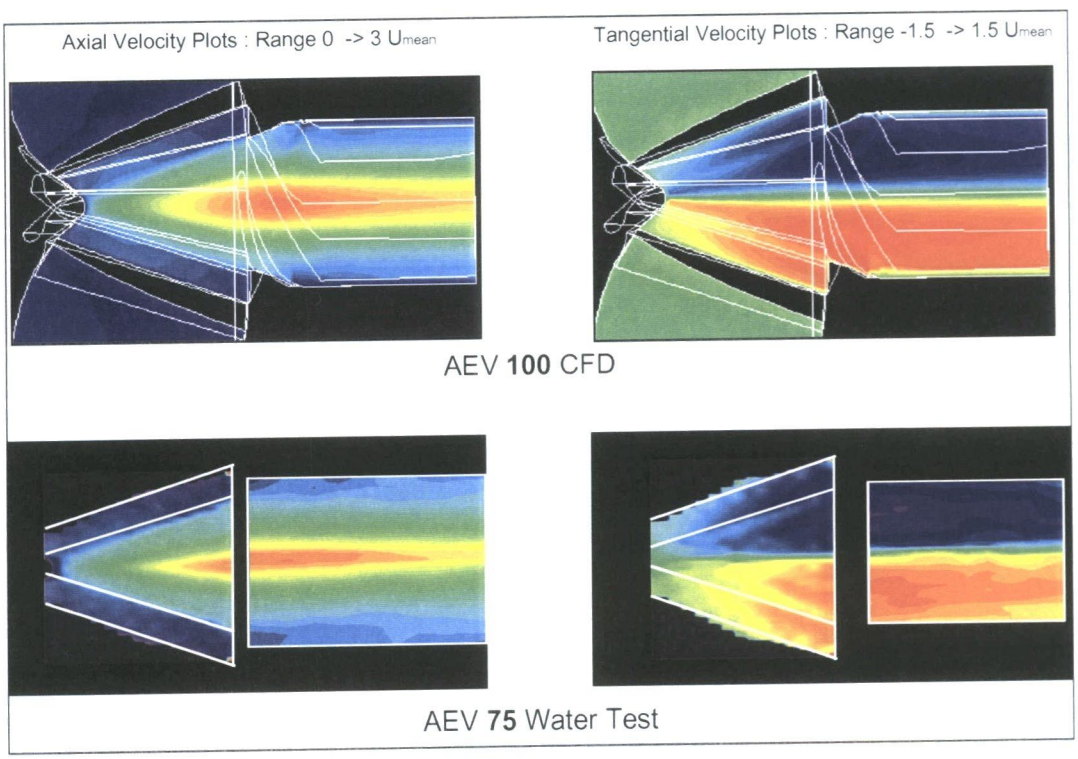

Figure 49

5.3 Coupled Phase

The standard models for two phase flow incorporated in Fluent were used. They comprise of three evaporation phases, namely heating, evaporation and boiling, all based around a Lagrangian particle tracking model (momentum, heat and mass exchange). For further information, refer to Ref. 3., or the Fluent manuals (Ref. 1).

5.3.1 Hollow Cone Sprays in the AEV100

In order that a direct computational comparison between previous and present results could be seen between the AEV75 characteristics and the AEV100, a similar single hole, hollow cone nozzle was chosen as a test case. Due to the increased dimensions of the AEV100, it was predicted that the droplet size needed to be large in order to bring oil to the outer regions of the burner. A small droplet size would evaporate too quickly, and also be too influenced by the air momentum, thereby remaining in the axis region of the burner. With this in mind, a hollow cone spray of full angle 30°, SMD value 45μm, and spread factor of 3.5 was taken for the comparison. A realistic value of 100 bar back pressure, with a mass flow rate of 110 g/s was used. The spray was divided into 48 separate groups (as in Ref.3) and had an injection temperature of 353K.

The results can be seen in Figure 50. In the AEV100 case, lambda profiles are taken at 125mm downstream of the transition piece; in the AEV75 90mm downstream of the transition piece. In both cases very little liquid oil escapes out the exit of the burner. However this is where the similarity ends. In the AEV75 case the larger droplets tend to reach the outer region near the wall, seen by the particle tracks (crosses represent the position of a fully evaporated droplet). The overall lambda profile is relatively flat, from which low NOx emissions might be expected. Looking at the AEV100 profile it can be seen that the oil concentration is considerably stronger in the middle of the burner than at the outside. 99.7% of the spray mass evaporates before the outlet. This is firstly due to the larger dimensions, giving droplets more time to fully evaporate. Secondly, the first few centimeters of the AEV100 slots, have less swirl component

than the AEV75 (again due to the dimensioning). This momentum ratio in the AEV100 tends to retain droplets nearer the axis region than the AEV75.

It is clear that the profile obtained is not optimised for the AEV100. The centre is rich and the outer region too lean. The situation will become even worse if one was to go to higher air pressures and temperatures. Air density and momentums will rise, leading to a richer burner axis region.

In these calculations the film air holes were also not taken into account. This will also make the near wall region leaner.

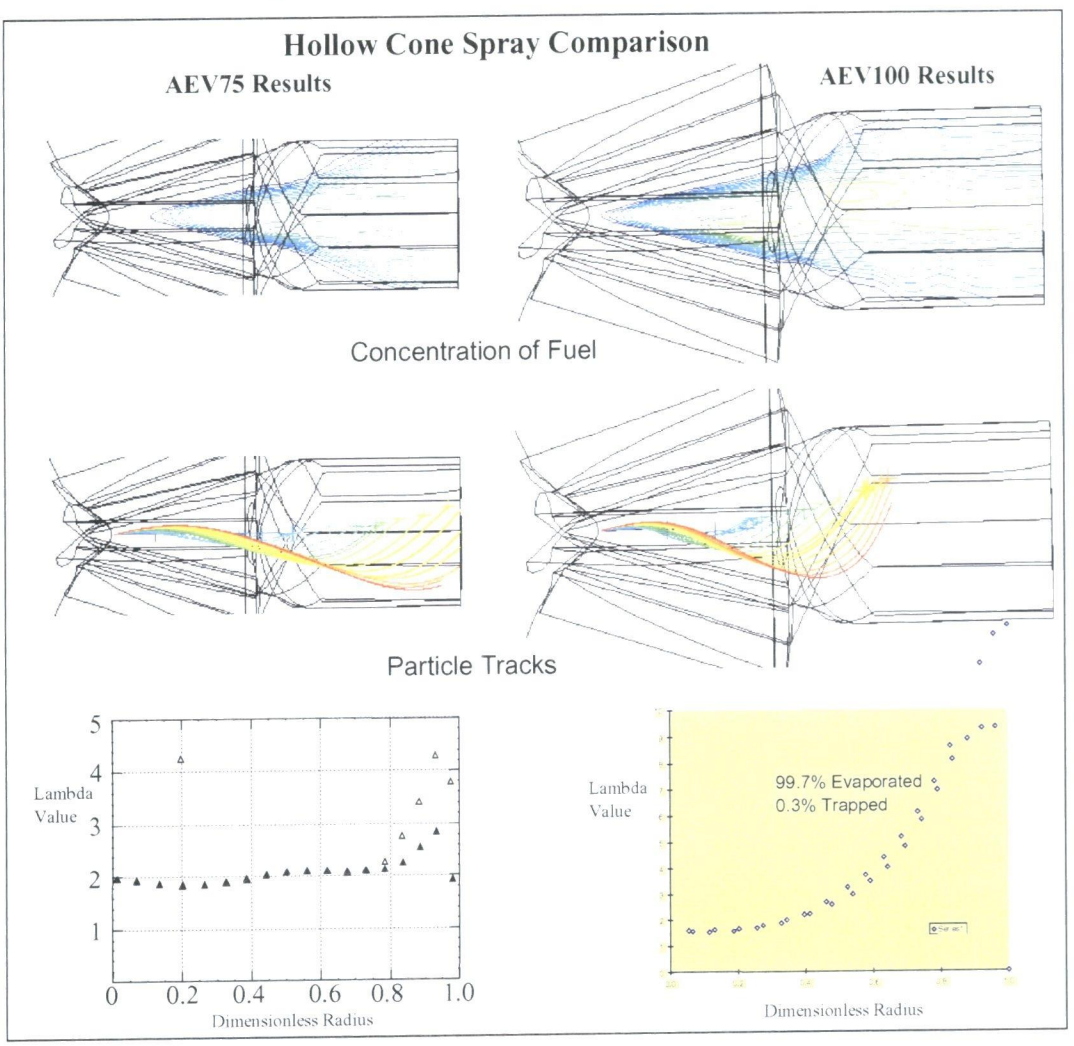

Figure 50

One option to improve the profile would be to increase the oil penetration depth by increasing the SMD of the spray. However the danger of self-ignition occurring with sprays larger than 45um SMD, is too high to consider. The time for a large droplet to

fully evaporate, is longer than the time taken for it to spontaneously combust in a 763K air field. Self ignition causes high temperatures inside the burner mixing tube leading to very high NOx emissions, and is therefore undesired. Also, in order to provide a nozzle with larger droplet sizes and a similar mass flow and angle, oil pressure would have to be reduced. This would lead to a decrease in oil momentum, partly counteracting the positive effect of the increase in droplet size.

An increase in angle or a decrease in the injection temperature of the oil may contribute to improvements in the end lambda profile, but basically a different injection system needs to be considered to make a major step forward.

5.4 Four Hole Nozzle

For this reason, the four hole injection system has been considered, each jet being a turbulent enhanced spray (seen in Fig.51).

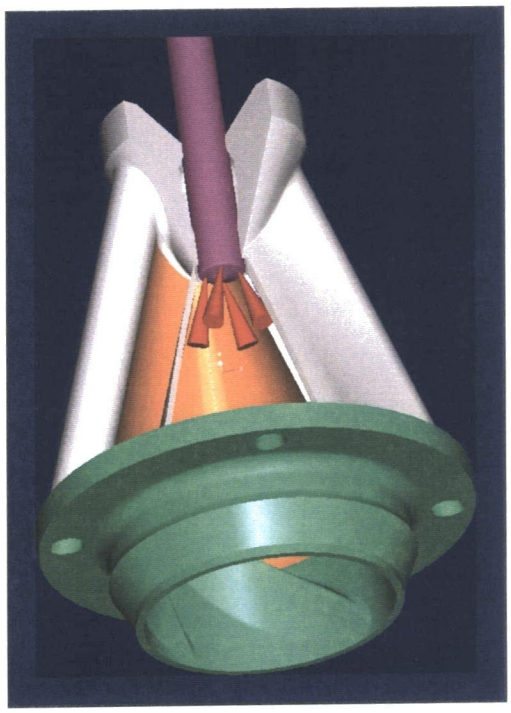

A slice through an AEV burner showing:
i. the swirl generator (white/orange)
ii. the transition piece (green)
iii. a 4-hole nozzle (pink)
iv. the sprays (red)

Figure 51

It has the following advantages and characteristics:

i. a four hole system is as symmetric as the burner requires, i.e. the burner has four slots.

ii. four single holes can be positioned at larger starting radii than a single hole nozzle, thus allowing further penetration to the outer regions.

iii. four single holes allow air to flow between each spray, filling the centre region, and not necessarily influencing all the oil. With a single hollow cone, the only way for the air to reach the burner axis is directly through the spray, taking much of the smaller droplets with it, which in turn creates a rich centre zone.

iv. four single sprays create a much fuller patternation and even distribution on a circular cross section than a single ring. (Consider 4 overlying circles as opposed to a thick single ring).

v. With a four hole design, the possibilities of optimisation are much larger. There are considerably more parameters that can be altered. These include axial angle, tangential angle, circumferential angle and single jet angle.

The following parameters have been investigated:

i. the axial / radial spray angle (see Fig. 52b)

ii. the tangential spray angle (see Fig. 52c)

iii. the circumferential positioning of the nozzle (see Fig. 52a)

iv. the angle of a single jet (see Fig. 53)

v. SMD and spread factor (see Fig. 54)

vi. droplet size range (see Fig. 54)

vii. oil back pressure

viii. oil pressure loss in nozzle

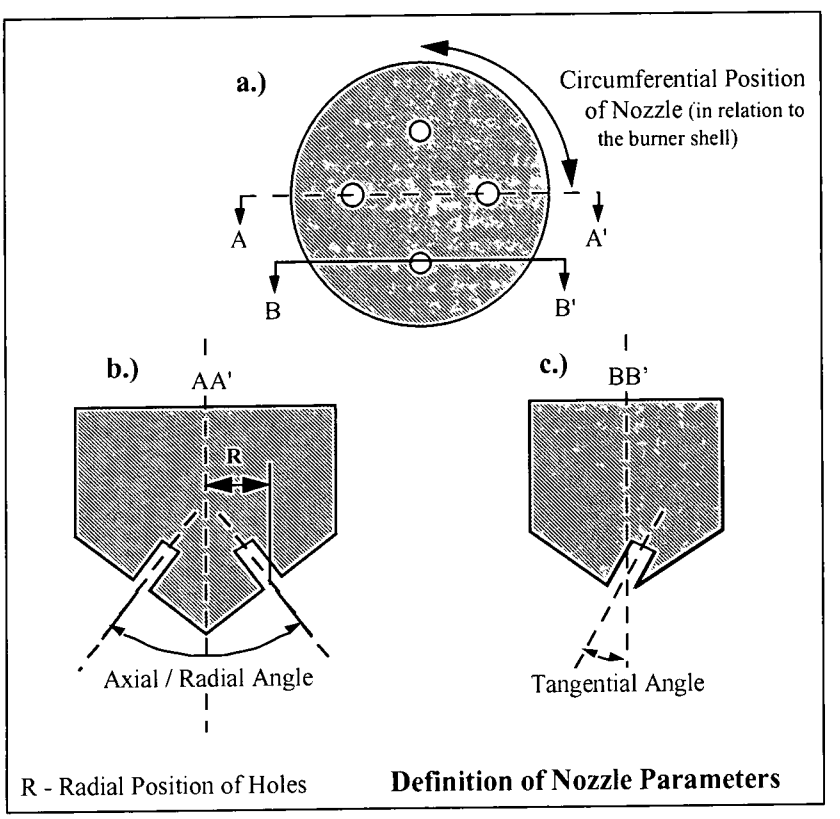

Figure 52

Additional possibilities would be to look at the radial position of the holes with respect to the axis line, the axial position of the nozzle, and the result of a decreased mass flow rate for part load.

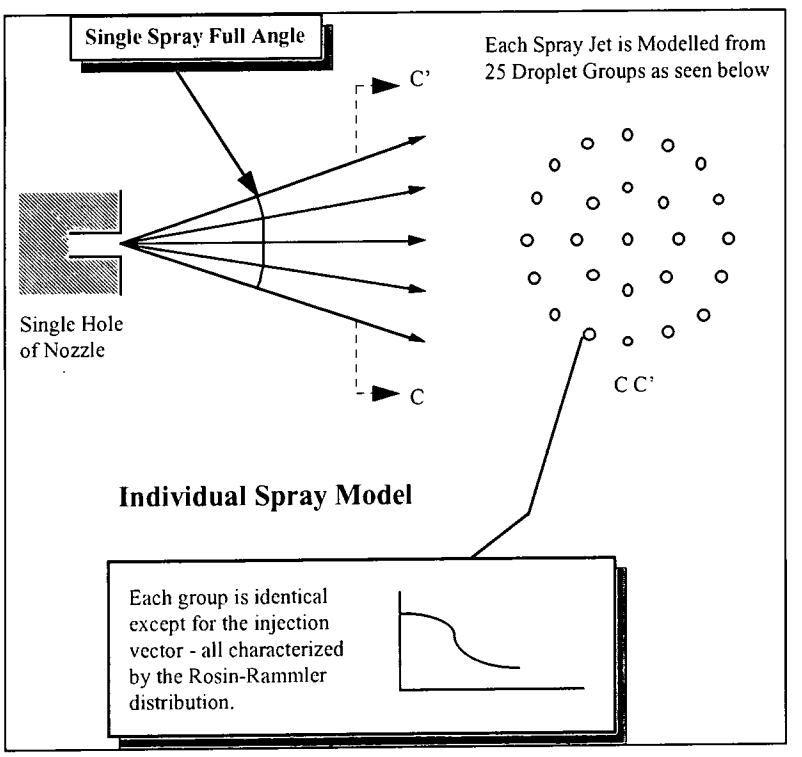

Figure 53

The remainder of the report concentrates on the parameters in the last paragraph, and what influence they play on the lambda profile at position 125mm in the AEV100 mixing tube.

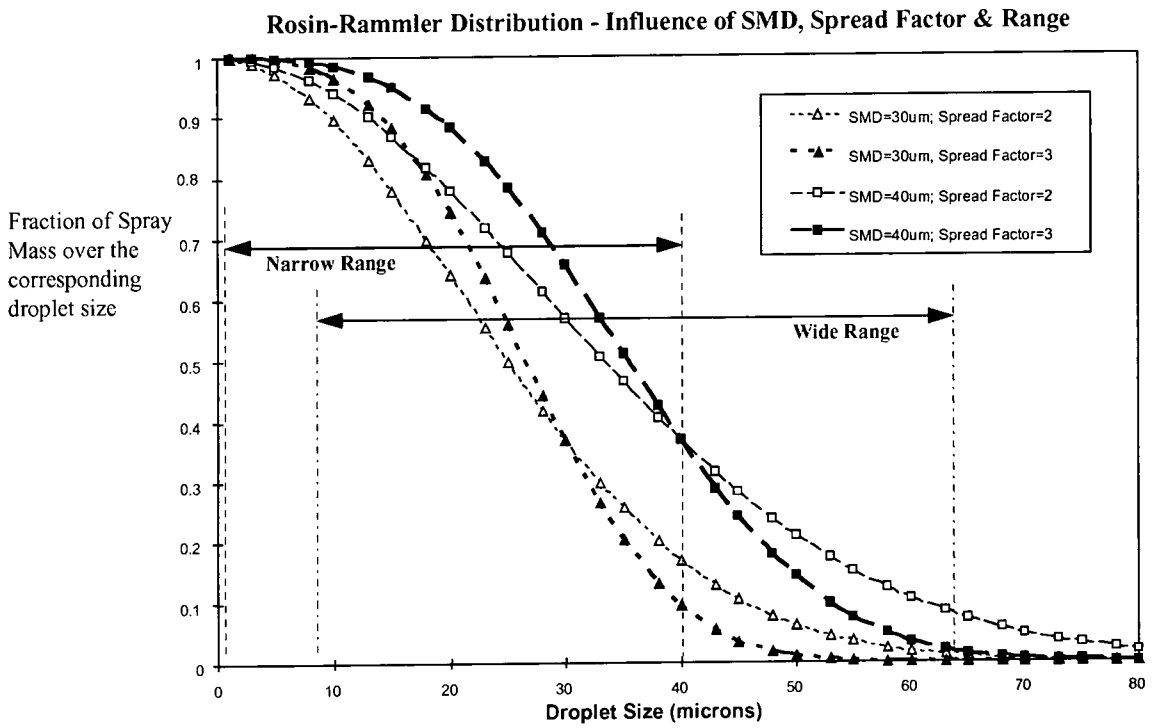

Figure 54

The spray from each hole has been modelled as a full cone each consisting of 25 groups of droplets. All are injected from the same point although with differing angles. The outer 16 groups make up the full spray angle, the middle 8 consist of the half angle, and one in the middle is in the line of injection. (see Fig. 53)

All groups have similar mass flow rates and also similar SMD's and spread factors. Each group follows the Rosin Rammler distribution.

In all cases the axial position of the injection points was 100mm upstream of the transition piece, and the radial position at 7mm radius from the burner centreline.

4-hole turbulent enhanced nozzles have also been experimentally tested for the AEV75, with results obtained from a nozzle of axial angle 30°, tangential angle 13°, and single spray angle of 20° (as shown in figures 52 and 53). This was used as the base case for the investigation.

5.5 Choice of Parameter Values.

5.5.1 Axial / Radial Angle

Three different angles were tested. The base case of 30° revealed that the outer region was still too lean, and therefore calculations on increased angle sizes of 45° and 60° were done.

5.5.2 Tangential Angle

The base angle of 13° and a further angle of 20° were investigated. It should be noted that the base case uses 13° in order to direct the spray along the wake of the shell of the burner. Therefore deviations from this angle could have secondary effects due the velocity and turbulence of the air into which the oil is injected.

5.5.3 Circumferential Positioning

The circumferential positioning of the nozzle was kept the same, in all calculations, due to the ease in which it can be experimentally investigated. The nozzle was positioned so that the sprays were directed towards the wake of the shells.

5.5.4 Single Spray Angle

Using a turbulent enhanced jet, single spray angles can only be relatively small. Two realistic spray angles of 10° and 20° were investigated. It was seen that this parameter can have a large influence on the lambda profile.

5.5.5 SMD and spread factor

Average droplet size values were taken from Malvern particle sizer tests undertaken using *water* for appropriate single hole nozzles. These results were then converted to an equivalent *oil* droplet size accounting for the surface tension and viscosity differences, the oil temperature and the higher air pressure, and could be used to make a direct comparison between experimental and numerical results. However, droplet sizes of 30 and 40 microns were studied for the AEV100, as smaller droplets would not have

penetrated far enough into the air field. The conversion can be worked backwards, to calculate what droplet sizes need to be obtained in the Malvern particle sizer tests for an appropriate nozzle for the burner at operating conditions. This was done to define the nozzle sizes. After manufacture they were tested with the Malvern particle sizer using water to confirm nozzle quality and correct design.

The spread factor (a relation of the distribution of droplet sizes within a spray - taken from the Rosin-Rammler equation) could also be measured and was between 1.5 and 2 for all turbulent enhanced nozzles tested. This is considerably wider spread than for the hollow cone model. As a result a spread factor of 2 was taken for the calculations.

5.5.6 Droplet size Range

The droplet size input range for the numerical calculations in order to obtain an accurate result depends mainly on the SMD and spread factor used. The initial range of 1 to 50 microns was good enough to define a spray of SMD 30um and a narrow bandwidth of spread factor 3. Here less than 1% of droplets were greater than 50um and therefore unaccounted. However as the SMD rises and spread factors fall giving a larger bandwidth, there is a need for a larger range to cover droplets upwards of 50um. This can be seen in Fig. 54, which shows the fraction of mass flow remaining for a spray over a certain droplet size. Two different SMD sizes and two different spread factors are plotted. When using an SMD of 40 microns, a narrow range of droplets would truncate the distribution, excluding more than 20% of the (important) larger droplets. For this reason a wider band was chosen. In most of the cases, two ranges were calculated: 1-50um, and 10-80um. However, the wider the range, the larger the interval between droplets sizes in each group, as the total number of droplets modelled is forced to be constant, i.e. =1000.

5.5.7 Oil Back Pressure

Two different back pressures were investigated: the usual 100bar and a 200 bar case. Computationally the oil pressure changes only the injection velocity, and does not have any influence on the droplet size (although in reality there is some influence).

5.5.8 Oil Pressure Loss in the Nozzle

The main value taken for the pressure loss in the nozzle was taken as 42%. This was calculated through experimental results. The pressure loss percentage, is the percentage of back pressure that is lost through the nozzle. The remaining pressure is taken to be directly converted into kinetic energy at the point of injection.

One other value of pressure was investigated, that was 0% pressure loss. This would correspond to a plain jet type of nozzle without any turbulent enhanced stage. As a plain jet has a slightly smaller angle than a turbulent enhanced jet, the single spray angle was modelled as only 10°.

Using this simplification, a variation of the nozzle type could be studied.

5.5.9 Cases Tested

The following table shows the cases calculated. It was produced in order to test the widest variety of parameters in the least computational effort.

Table 3

Case	Axial Angle (deg.)	Tang. Angle (deg.)	Single Jet Angle (deg.)	SMD size (μm)	Droplet Range Narrow 1-50 Wide 10-80	Pressure Loss	Back Pressure (bar)	See Figure
Case 1	30	13	20	30	Wide	42%	100	all
Case 2	45	13	20	30	Wide	42%	100	9
Case 3	60	13	20	30	Wide	42%	100	9
Case 4	30	13	20	30	Narrow	42%	100	10
Case 5	30	20	20	30	Narrow	42%	100	10
Case 6	45	13	20	30	Narrow	42%	100	10
Case 7	45	20	20	30	Narrow	42%	100	10
Case 8	30	13	10	30	Wide	42%	100	11, 13
Case 9	30	13	10	40	Wide	42%	100	12, 13
Case 10	30	13	10	30	Narrow	42%	100	13
Case 11	30	13	10	40	Narrow	42%	100	13
Case12	30	13	20	30	Wide	42%	200	14
Case 13	30	13	10	30	Wide	0%	100	15

5.6 Results

The results that give the most important information are the lambda plots at position 125mm along the mixing tube i.e. 13mm before the exit of a short AEV100. These are plotted against dimensionless radius and give an indication of the mixing of the oil vapour for a 4-hole nozzle, and therefore an idea of the quality of the NOx emissions. The results are shown in Figures 56 – 62.

5.6.1 Analysis of Results

The majority of the results show the same overall trend. A relatively fast evaporation, in terms of burner length, means that after the transition piece all the oil is in the vapour phase. Any unevaporated droplets, hit the walls of the burner in this region.
As a result of the relatively fast full evaporation of the oil, it would appear possible to work with a short mixing tube length, maybe 125mm.

Due to the initial radial position of the nozzle holes, the mixture is relatively weak at the axis of the burner. However in the most cases, this zone sharply turns rich by r/R of around 0.3. From then on, the vapour concentration weakens again with increasing radius. Due to the fast evaporation of droplets in the swirl generator, which in turn drastically reduces their mass conservation, centrifugal and coriolis forces, it is difficult to obtain a satisfactory richness in the outer zones. Attempts to do so, for example by increasing droplet size, generally result in too much oil liquid hitting the walls.

Another important result, is to look at the mixing effectiveness of the oil from the four holes. This can be seen clearly in Figure 55, which shows an iso-contour of oil vapour (corresponding to Lambda = 2). At the injection point there is naturally little or no vapour, as the majority of the oil is in the liquid phase. The four initial spikes that quickly disappear before the main section illustrate that the mixing and dissipation of oil vapour per unit volume at that point is faster than evaporation of the droplets. From

there on the profile grows. It is at around 125mm downstream of the transition piece that the surface becomes both rotationally symmetric and unchanging. This shows the full mixing of all four jets and that from this point on, minimal diffusion (i.e. slow mixing) of the oil vapour takes place. (The tube that appears in the middle of the burner is there because the lambda profile passes through lambda=2 twice across the radius - i.e. the profile across the radius is lean-rich-lean)

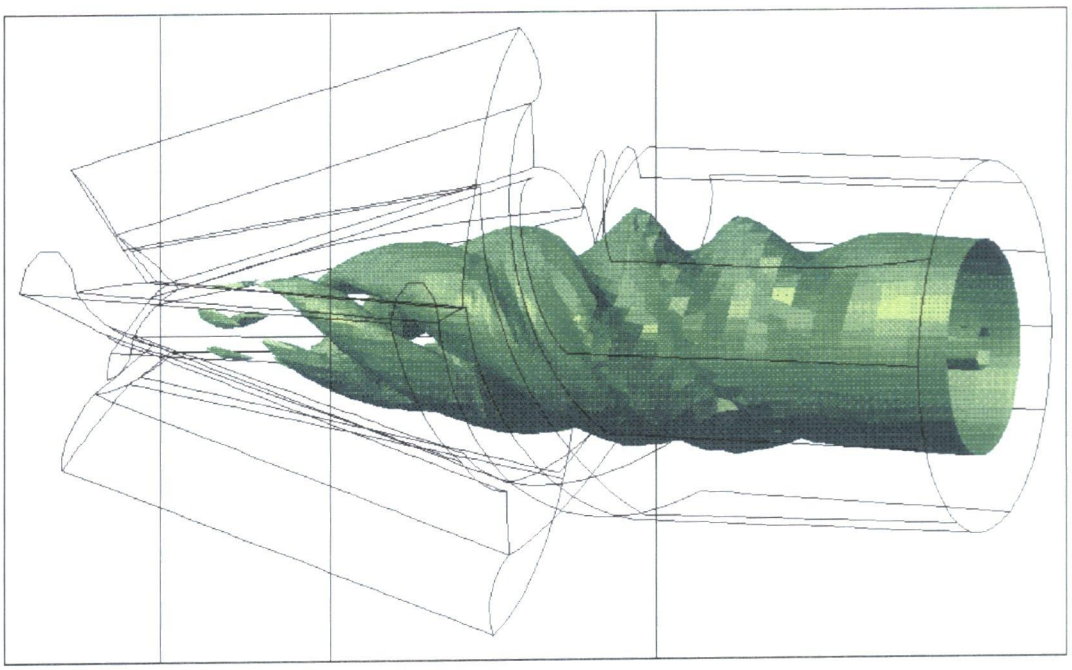

Figure 55

Nozzle Parameter Results

5.6.2 Radial / axial angle

Using a hollow cone spray in the AEV75, an increase in the axial angle causes a richer region to be formed in the near wall region and more droplets to hit the wall.

In the AEV100, it was found that lean regions occurred near the wall. It was assumed that for the 4 hole nozzle, a similar increase in axial injection angle of the sprays, may help make the outer regions richer. However, it was found that an increase in the axial angle of the spray injection for a 4-hole nozzle *decreases* the oil concentration in the outer regions. This is shown clearly in the Figure 56.

There are two main reasons for this phenomena to occur. Firstly, by increasing the angle of injection, the spray is directed further into the main flow of the slots instead of in the wake of the shells. This main flow has higher momentum and does not allow droplets to penetrate the air field so well. Droplets are carried by the air into the centre of the burner. The second reason for the less attractive profile is probably due to the higher relative velocity at which the oil is injected. The higher the angle the larger the relative velocity of the oil to air, and hence the faster the evaporation and reduction in mass of the oil droplet. This is likely to be a minor phenomena, if at all, else a similar theory would be applicable to the contradictory hollow cone case.

The characteristics that occurs here may well change for a different circumferential nozzle position.

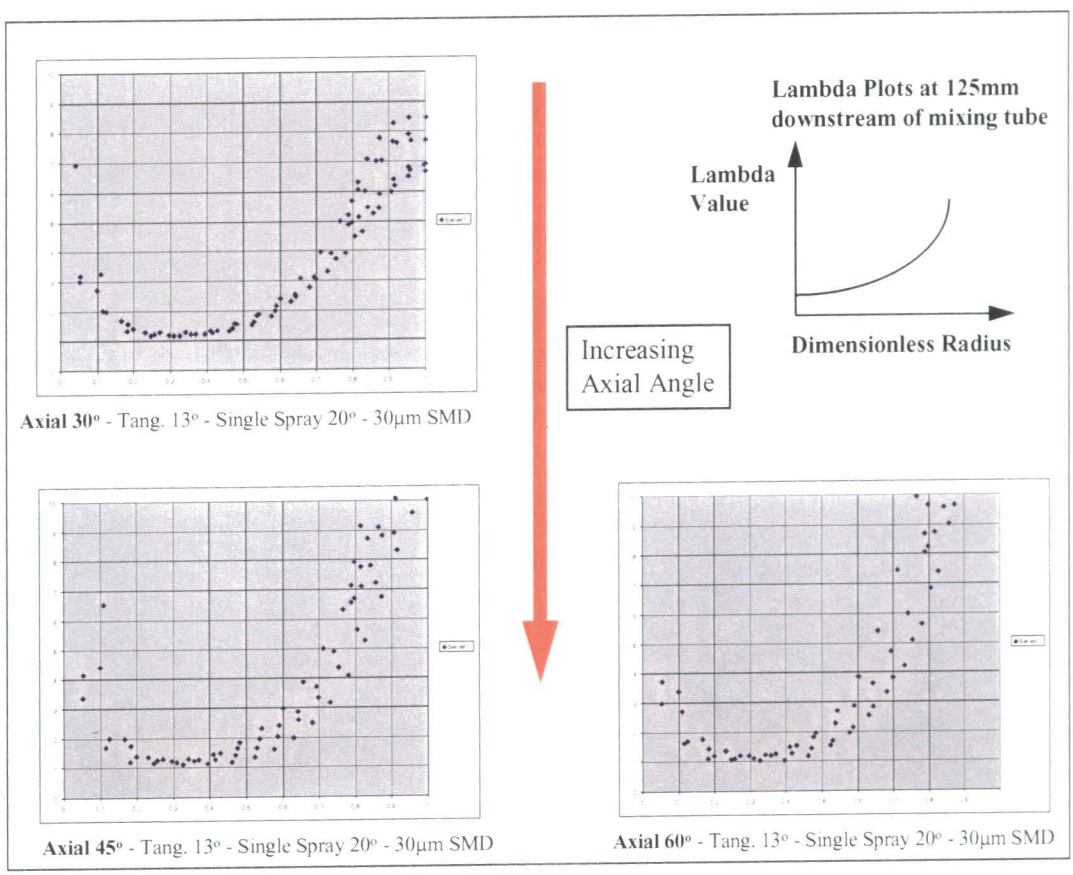

Figure 56

In the case of 4 hole nozzle, an increase in axial angle, does not necessarily mean a richer near wall region.

5.6.3 Tangential Angle

A change in the tangential angle can be seen to give a similar effect to increasing the axial angle. Figure 57 shows this for two different radial and tangential cases. The change is less marked than that of the axial angle change, and the influence on the lambda profile is more complicated to understand. At first glance, it may be suggested that an increase in tangential angle simply weakens the oil concentration in the outer region due to the fact that the spray is no longer injected in the direction of the wake of the burner shell.

However, a closer look at the 30° axial case would seem to contradict this theory. It would seem that both axial and tangential angle in combination have a role to play, along with the uninvestigated circumferential positioning of the nozzle. Nevertheless, the best lambda profile occurs when the line of injection is in the same direction as the trailing edge of the burner shell.

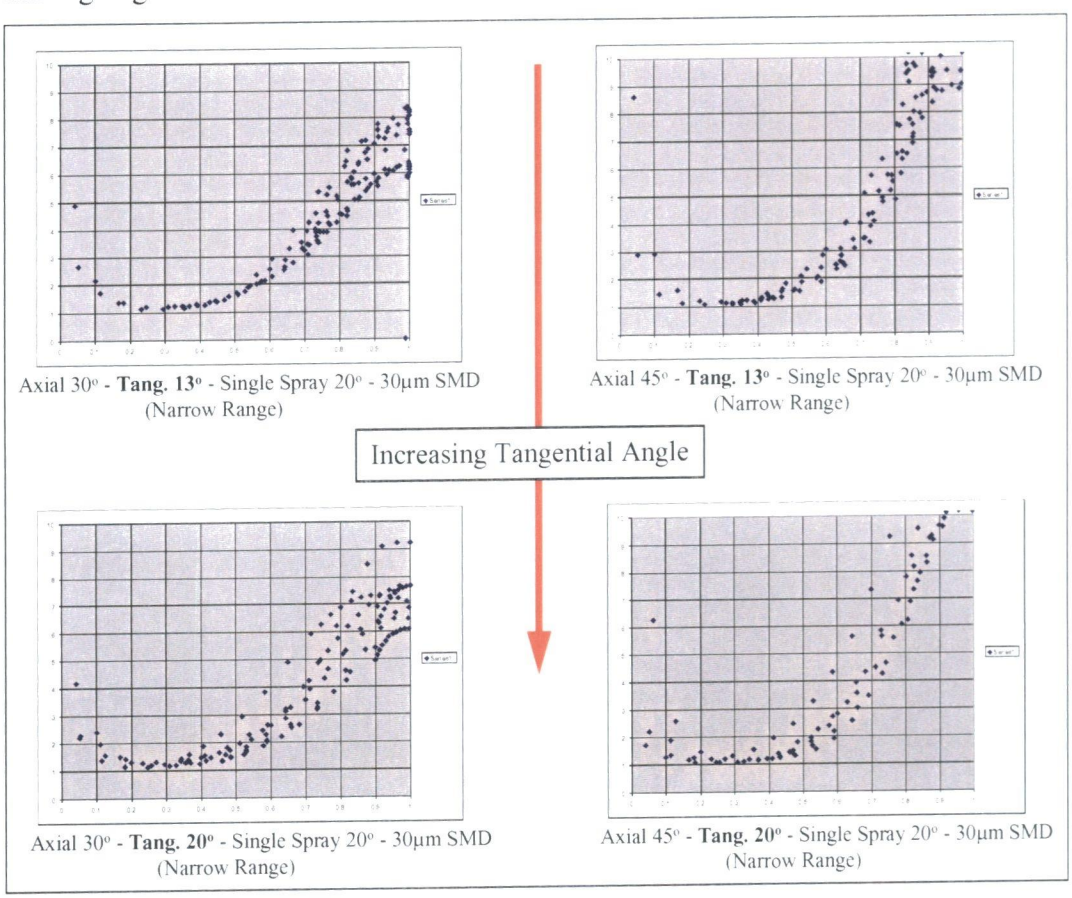

Figure 57

5.6.4 Single Spray Angle

- Figure 58 shows nozzles modelled with 10° jets and 20° jets.

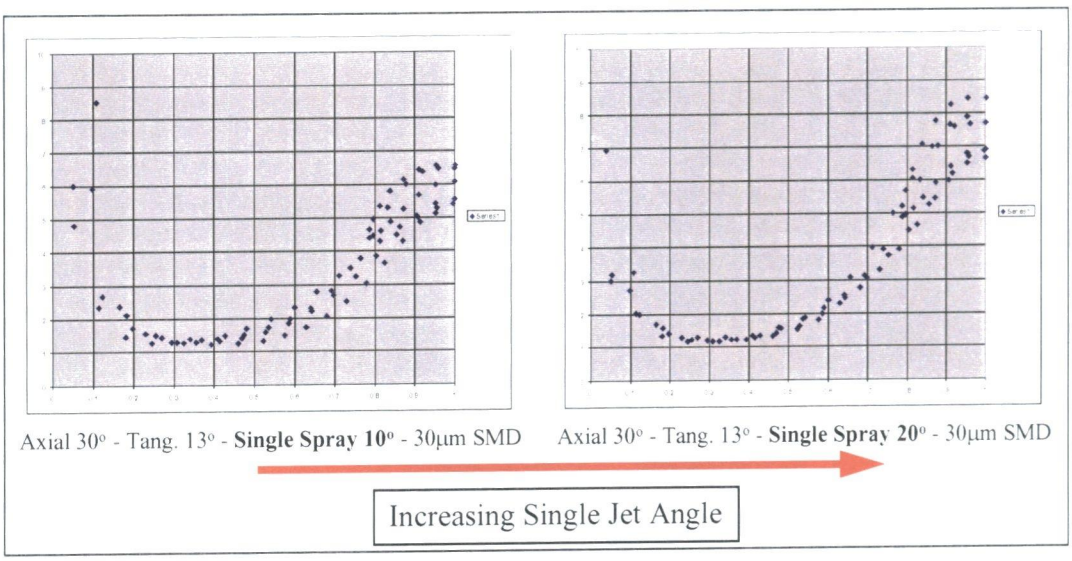

Figure 58

Due to the concentrated momentum of the narrower jets, a distinct improvement can be made in the outer regions of the lambda profile by penetrating further into the air field. Also, narrower jets mean that local oil concentrations are higher than with wider jets, and as a result, have less tendency to evaporate early on. This means that a large change in the lambda profile can be made in the 0.7 to 0.9 radius region. This is particularly advantageous as the near wall region is not considerably altered, i.e. there is no major increase in the number of droplets hitting the wall.

In short, the middle-outer region of the lambda profile can be flattened out by changing the spray angle of the single jets. This can be achieved by changing the internal design of the nozzle.

5.6.5 SMD or Droplet Size

As expected, droplet size is the one of the main parameters that affects the profile. The influence can be seen in Figure 59. One can clearly see that with a larger droplet size, more oil reaches the outer regions This is due to the larger momentum to carry them in this direction, and their reluctance to evaporate so quickly. Heat up times are much longer for larger droplets. A 40 micron droplet has more than double the volume of a 30 micron droplet. Once influenced by the air, larger droplets have higher centrifugal forces, and tend to reach the outer regions more easily.

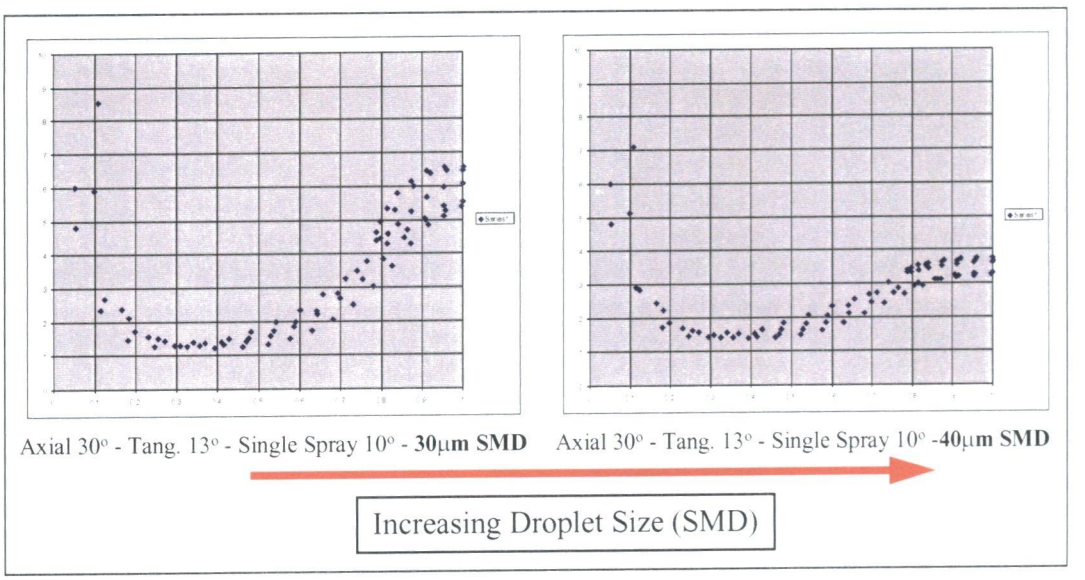

Figure 59

The centre region of the profile stays almost the same, even though the outer region changes so drastically. It is important to realise that changes in regions of low oil vapour concentrations have a large effect on the lambda value. Take the following example:

$\lambda = (1\text{-}C) / (14.6C)$

where C is oil vapour concentration (mass based) and λ is the lambda value,

at a value for C of 0.03, λ is 2.2.

for a change in concentration dC of 0.001, $d\lambda$ is only 0.07.

at a value for C of 0.01, λ is 6.7.

however for an equal concentration change dC of 0.001, $d\lambda$ is now 0.6.

This is the reason why large changes can be seen for different droplet sizes in the outer region where oil concentrations are relatively low, and less visible changes occur in the richer region. (This is also the reason why the accuracy of the lambda values decreases with lower concentrations - any rounding error means deviations which in turn means larger fluctuations)

Unfortunately, although the lambda profile improves with larger droplets, a much greater proportion of them hit the wall. With around 11.4 % of oil mass hitting the wall, the chance of flashback is too high to risk for an SMD of 40μm. With an SMD of 30μm, the percentage of droplets hitting the wall is between 2% and 4% for all cases calculated. This is acceptable, when one takes into account that no film air holes have been modelled.

To summarise, SMD size is important for the lambda profile.

5.6.6 Droplet Range

From a computational point of view, this is a very important parameter to consider, if one is to obtain accurate and reliable results. The droplet range considers the maximum and minimum droplet sizes used in the numerical calculation. It is dependent on both the SMD and spread factor used, as explained in the earlier chapter. The wider range considers droplet between 10 to 50 microns, while the narrow range considers droplets between 1 to 50 microns (see figure 54). Figure 60 shows the influence of using different ranges. For the 30μm SMD case, there are minor differences seen, as most droplets are covered between 1 to 50 or 10 to 80 microns. However, with an SMD of 40μm, a range of 1 to 50 microns was too small to cover the larger droplets in the group. Such a range acts as a truncated distribution and is not properly modelling an important part of the spray. Consequently it is necessary to model larger SMD sizes with higher ranges, in this case 10 to 80 microns. One should be aware of this disguised parameter, as it can results in considerable errors on the final lambda profile.

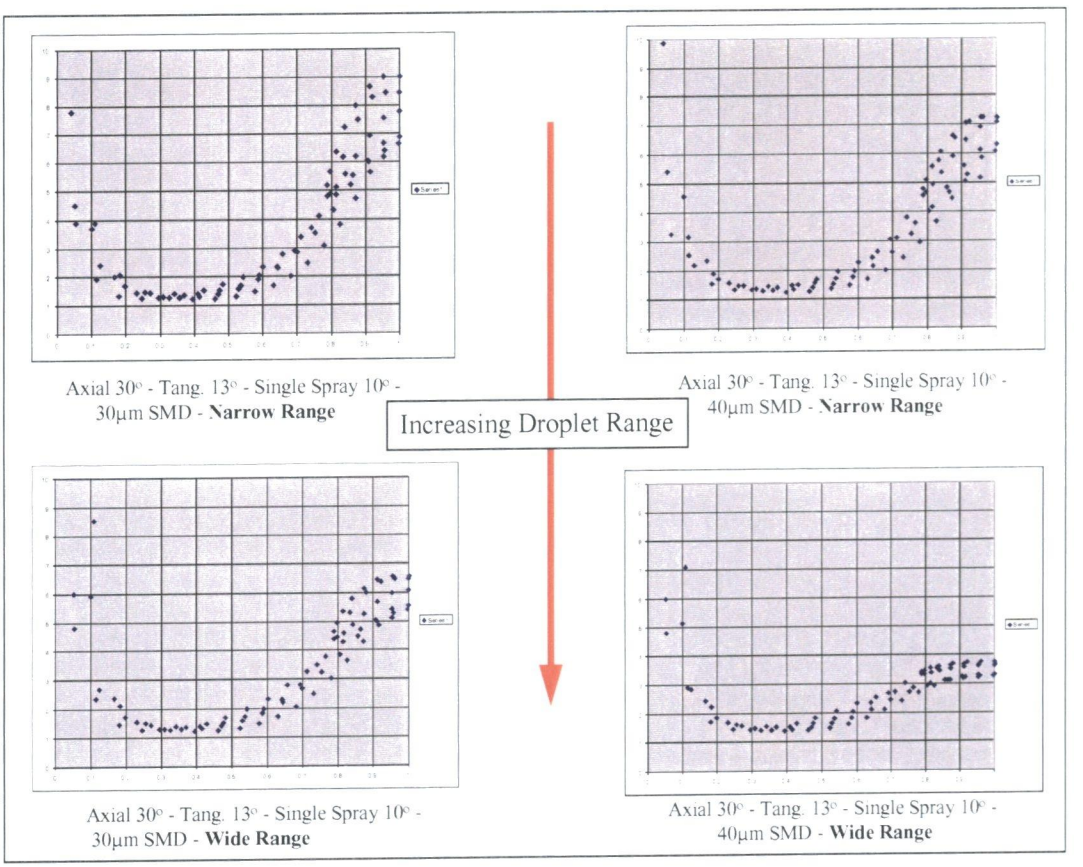

Figure 60

5.6.7 Oil Back Pressure

Computationally oil supply pressure leads to an increased injection velocity, but not a decreased droplet size. Doubling the supply pressure of oil from 100 to 200 bar, leads to an increase in injection velocity from 118m/s to 168m/s.

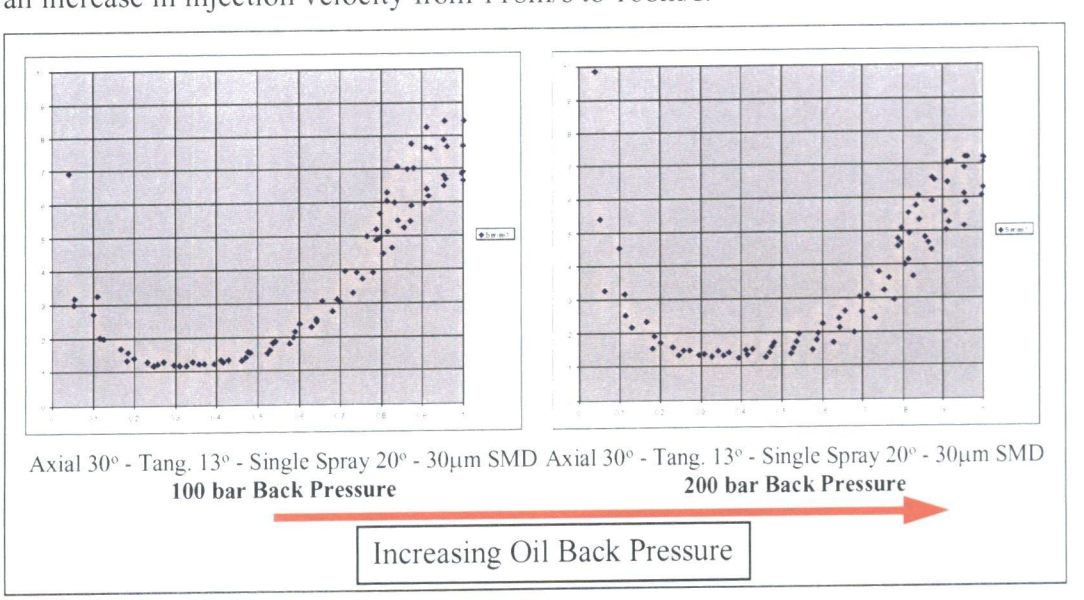

Figure 61

Correspondingly droplet momentum increases and penetration of the air field is much improved. As a result the outer regions become richer, and a flatter lambda profile is produced. (Figure 61). When altering the oil pressure, the counteracting effect of change in oil droplet size should also be considered. This decrease in droplet size with higher back pressures is not taken into account in the computations. In the case of the four hole nozzle in the AEV100 burner, the following rule can be used as a rough guide: computationally doubling the oil pressure can be counteracted with around a 20% decrease in SMD to give roughly the same lambda profile.

In reality, doubling the oil pressure increases velocity by 42% and reduces droplet size by around 25%. Droplet break up is related to droplet velocity squared, and droplet velocity is proportional to the root of the oil pressure. Therefore in practice, for higher oil pressures, a pressure change should not bring about major differences in lambda profiles.

5.6.8 Oil Pressure Loss in Nozzle

A decrease in oil pressure loss in the nozzle simply leads to an increase in the pressure available for conversion into kinetic energy at the point of injection. However, a major change in pressure loss coefficient occurs only with a change of atomiser. By modelling the difference between 0% loss and 42% loss, a simplification can be made for the comparison between a plain jet and turbulent enhanced type nozzle respectively. When using the plain jet correction (0%), the single jet angle was also reduced to provide a more accurate model. From Figure 62, it can be seen that a reduction of lambda values can be achieved in the outer regions for a plain jet. This is merely a combination of increase in injection velocity, and decrease in single jet angle. What has not been modelled here is the possibility of increased SMD size, due to the lack of turbulent enhancement. This would, of course, push the lambda value even further down, at larger radii, as more droplets would be expected to hit the wall.

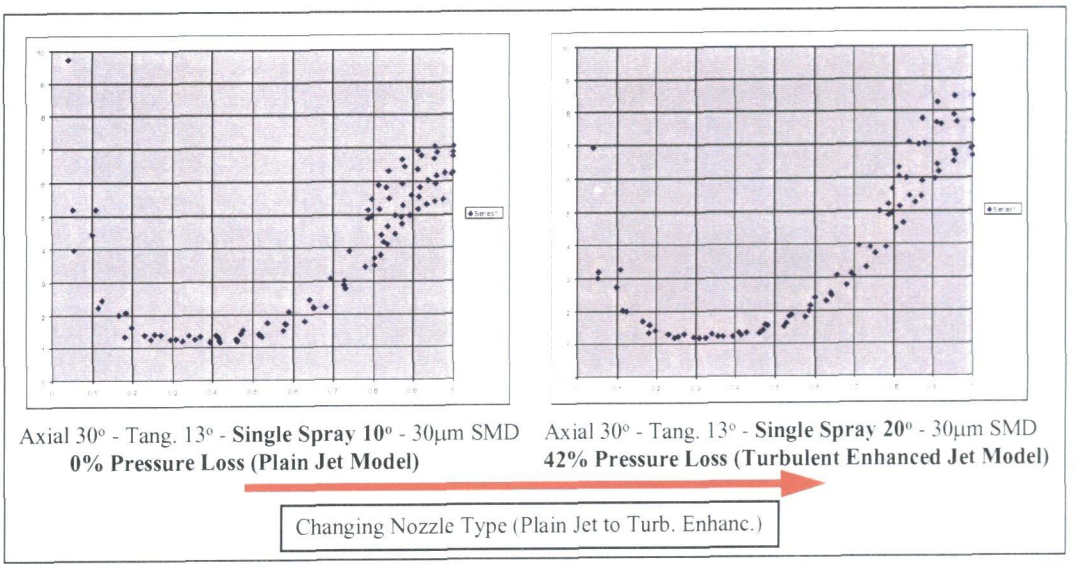
Axial 30° - Tang. 13° - **Single Spray 10°** - 30μm SMD
0% Pressure Loss (Plain Jet Model)
Axial 30° - Tang. 13° - **Single Spray 20°** - 30μm SMD
42% Pressure Loss (Turbulent Enhanced Jet Model)
Changing Nozzle Type (Plain Jet to Turb. Enhanc.)

Figure 62

5.7 Conclusion

The **AEV100** has been numerically simulated to assess the possibility of running under **Dry Low NOx oil operation**. The criterion used to assess this possibility was the lambda profile at the end of the mixing tube.

The continuous phase air field for the AEV100 was calculated. Results using the RNG K-ε turbulence model showed close agreement with water test LDA results.

In order to make a comparison between burners, **similar hollow cone nozzles** (with identical parameters except mass flow rate) were simulated in both the AEV75 and AEV100. While the AEV75 showed a near even profile at the end of the mixing tube, the AEV100 gave a profile that was far too lean in the outer regions for low NOx emissions.

As a result, the proposed solution of a **4-hole nozzle** was simulated in the AEV100. Changes in one of the many parameters can produce different lambda profiles.

Axial Angle - an increase in the angle decreases the oil concentration in the outer regions.

Tangential Angle - an increase in the angle decreases the oil vapour in outer regions.

Circumferential Position - this parameter was not simulated.

It was seen that the best lambda profile was obtained when the line of injection is in the same direction as the trailing edge of the burner shells.

Single Spray Angle - tighter jets cause oil to be penetrated further into the flow field.

SMD (Droplet Size) - larger droplets reach the outer regions more easily, with the danger of them hitting the walls. The SMD value should lie around 30 microns if wall wetting needs to be lower than 5%.

Radial Position of the Holes - this parameter has not been investigated. Only one value of 7mm was used.

Oil Back Pressure - this shows little influence on the profile, as the effect of any increase in injection velocity is cancelled by the decrease in droplet size.

Oil Pressure Loss in a Nozzle (change of atomizer type) - moving from a turbulent enhanced jet to a plain jet, slightly increases the oil vapour concentrations at larger radii.

Droplet Range - the correct droplet range should be modelled for accurate results.

For an initial test, a recommended nozzle would be a turbulent enhanced nozzle of axial angle 30°, tangential angle 13°, single jet 15°, SMD 30μm, and radial position 7mm. Circumferentially, it should be positioned so that the sprays are in the direction of the wakes of the burner shells. If outer regions are still too lean, a move towards larger droplets or plain jets might be considered.

5.8 Main References

1. Fluent User Manual, Version 4.3, January 1995

2. Lefebvre A., Atomization and Sprays, Hemisphere, pp.211-214, 1989

3. Lloyd J., Allen P., Numerical Modelling of Oil Evaporation in the AEV Burner, ABB Technical Report - CHCRC 96-45, 1996

4. Stefan M., Berechnung der Bewegung und Verdampfung von Brennstofftropfen in Heissgasströmungen hohen Druckes, ABB Corporate Research Report - CRBT 92-10., 1992

6. AEV125/135 - Larger Scaled Burners

6.1 Design Considerations

A noticeable difference in the droplet behaviour has been seen when scaling the burner from AEV75 to AEV100. A further scaling up to AEV125 or 135 requires more consideration. Not only the dimensional change, but also the operating conditions of the machine into which it is proposed to be implemented, should be accounted for.

Change in Dimensional scales: increase of diameter by up to 35%

Problems: longer penetration into the airfield is needed; velocity profile is stretched across the new diameter, although the mean velocity remains the same.

As the mass of oil is also increased proportionally to the air mass flow and subsequently the burner size, the following may be deduced: on injection the momentum ratio of oil to air remains constant. However as soon as the spray/jet starts to atomise, single droplets can be observed individually. The forces on these single droplets are different in a larger scaled burner, and penetration to a larger burner diameter is harder to achieve. Therefore larger initial droplet sizes are required.

Change in Machine dependent external variations: ambient pressure increase of upto 100% (30bar), a preheat temperature of 820K, a density of 13kg/m^3.

Problems: The main influence of the increased pressure ratio is the considerable rise in air density. This causes a larger air to fuel momentum ratio, in turn hindering deep penetration of the droplets into the burner even further. The drag force is closely related to the Reynolds number of the droplets, and therefore fast deceleration occurs.

However the major concern when scaling the burner for use at other machine conditions is the chance of droplet self-ignition.

Self-ignition is mainly a function of pressure and preheat temperature. There is also the effect of radiative heat transfer from the flame front, but this is generally considered negligible and is complex to calculate.

Spadaccini (Ref. 16) acquired data for the self-ignition time of various liquids, and found a good comparison with the classical Arrhenius equation

$$\tau = \frac{A}{p^n} e^{E/RT} \Phi^k \qquad \text{Eq. 68}$$

where p is air pressure, R is the universal gas constant, T is the temperature in Kelvin, and Φ is the fuel to air ratio. For oil number 2, constants n, A, m & E (the activation energy) are found to be 2.53, $1.28e^{-6}$, -0.35 and 34.31kcal/mol respectively.

Further work in the ABB laboratories by Döbbeling, Krieger, Pennell & al. (Ref. 6) showed similar results for up to 500°C, whereon the profile flattened out to a constant ignition delay time.

It is clear from the formula that the fuel to air ratio plays little role in the self-ignition time (proportional to the third root), while pressure and temperature have large effects.

Using the above information, estimates of the ignition delay time can be made for two contrasting machines:

I. a 14 bar machine, with a preheat temperature of 400°C gives a value of τ as around 50ms.

II a 30 bar machine, with a preheat temperature of 550°C gives a value of τ as around 1-2ms

The residence time of a droplet in the burner can also be estimated. Taking the injection velocity of a normal plain jet at 100 bar to be around 130m/s, the mean air velocity in the burner is 75m/s. Due to the relative fast deceleration of the drop the mean speed of the trajectory lies somewhere in between these two values; as an estimate 100m/s. The distance from the point of injection to the flame front in a scaled AEV135 is 250mm. This gives a residence time of 2.5ms.

6.2 Design Solutions

For machine I, there is no considerable concern about self-ignition in the burner. On the contrary, machine II, at a higher pressure and temperature has every chance of auto-ignition in the burner, leading to possible flashback, pulsations and bad NOx emissions. For this machine measures have to be taken to avoid the problem. There are several options.

The first possibility would be to operate with a small amount of water mixed in the oil (wet operation). As discussed in the introduction, this increases the thermal capacity and therefore lengthens auto-ignition times. It also reduces the flame temperature, which in turn reduces thermal NOx emissions. There are two possibilities of water injection. The first is to make an emulsion of water and oil before injection. Disadvantages of this are the change in droplet size that one achieves, and the lack of flexibility. Another way would be to inject the water at a separate injection point (see Fig63). By doing so, the amount of water fraction can easily be varied, depending on the conditions and loading. The disadvantage is that there is the need for a separate FDS (fuel distribution system) and that an even distribution of the water into the fuel mixture is not guaranteed. A final option would be to inject steam in the air in the pre-plenum before the burner.

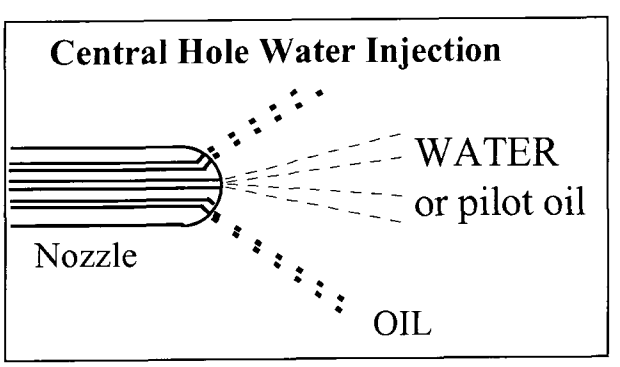

Figure 63

In general water injection is undesired, as it leads to extra costs through design and construction, is less efficient in power production and provides more chances for malfunction.

The second possibility to avoid self-ignition is to shorten the residence of the droplets in the burner. Methods of achieving this through increased velocities are unrealistic. Air velocities must remain the same for a similar mass flow rate, and an increase in initial droplet velocity is limited by the amount of back pressure available (100 bar). That aside, with higher back pressures, a similar mass flow rate of oil would produce smaller droplets which decreases penetration distances. The other option is to reduce the length of nozzle to flame front position. This can be achieved by either moving the nozzle tip further into the burner domain, or reducing the length of the burner mixing tube. Moving the tip is provisionally less viable, as the effects it has on the internal burner flow are unknown. Reducing the burner length is the most realistic option. The main disadvantage is the length available for full homogeneous mixing to occur, in both gas and oil operation is restricted. Additionally, reducing the length changes the Eigen-frequency of the burner and the corresponding pulsation behaviour. Therefore the optimisation of mixing capabilities and perfect oil vapour distribution should be approached.

In all cases with a large scaled burner, there is the problem of achieving high penetration without the impingement of oil on the burner walls. Three options are proposed in order to assist this:

i.) a new nozzle design - rather than use the central positioned nozzle (as seen in Fig. 64a), utilise the maximum available space in order to eject the oil at the largest available diameter. The limiting factor is the largest lance (nozzle) diameter. All nozzles must be retractable through the backside of the burner in the case of malfunction due to blocking or coking. A suggestion for this is shown in Figure 64b. Rather than having the head-air flowing convectionally around the outside of the nozzle (as described in the introduction), with the redesign of the nozzle it can exchange positions, allowing the head air to flow along the axis, at the same time bringing the injection points of the nozzle to an outermost diameter. If the injection point lies at a larger diameter, penetration to a larger diameter is automatically achieved. Additionally, due to entrainment from head-air, the conventional nozzle layout influences the droplets to take the path of the head-air (i.e. in an axial-direction). With the altered design, this influence is removed and a more radial trajectory can be obtained.

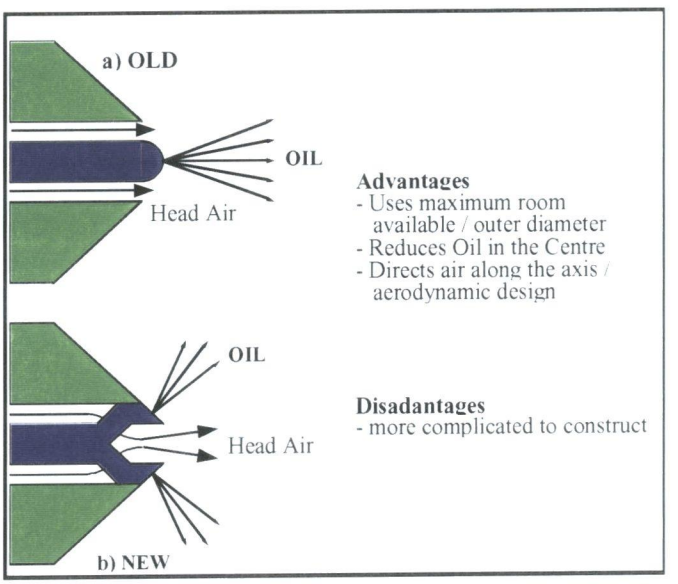

Figure 64

ii.) a new orifice design - presently all nozzles in ABB burners contain only circular orifices. However, Schetz and Padhye (Ref. 16) have shown that elliptical orifices can have the advantage of longer penetration lengths if positioned correctly in relation to the ambient flow field. The disadvantage is the cost of construction of such holes, which most likely would have to be bored by laser techniques. If elliptical holes increase the penetration length, other orifice shapes should also be considered, which could easily be bored if laser techniques have to be used anyway. Such ideas would include star shapes, crosses or long length to width ratios.

iii.) the decrease in inlet oil temperature - it has been shown in Chapter 4, that by increasing the oil preheat temperature, one obtains much shorter trajectory. It can be therefore assumed that a decrease in the oil preheat temperature would hinder early evaporation and droplet size reduction, resulting in longer trajectories to larger burner diameters.

Prevention of wall impingement needs to be achieved by the optimisation between penetration distance and droplet size, meaning any droplets that hit the wall should be small enough to bounce or result in immediate evaporation.

A final influence of the machine conditions on the vapour distribution inside the burner is the increase in the air preheat temperature. This causes a faster evaporation

of the droplets, leading to a fast size change, and a different trajectory path. In-house software was used to look at the influence in penetration distance between two different machine conditions at 400°C and 550°C. Using correlations for the drag function, the influence of density change (due to different machine pressure ratios) on penetration distance could also be considered.

Finally knowing which droplet size is optimal for the AEV100 under certain machine conditions, an optimal droplet size could be correlated for the AEV135 for machines I and II. From here a new nozzle layout could be designed. Experimental results are not yet available.

In summary, there are several points to consider when up-scaling the burner for different machines:

i.) the increased dimensions require larger penetration depth

ii.) changes in air preheat temperature cause quicker evaporation and consequently shorter penetration

iii.) higher pressures relate to higher density, resulting in larger drag forces and shorter penetration depths

iv.) high operating pressures and temperatures considerably reduce self-ignition times of oil that have to be compensated

Possible solutions to overcome these problems have been considered.

7. Advances in Nozzle Technology

The previous chapters have shown the optimization of a nozzle for a variety of burner sizes and machine conditions. However all these optimizations have only considered combustion at full load conditions.

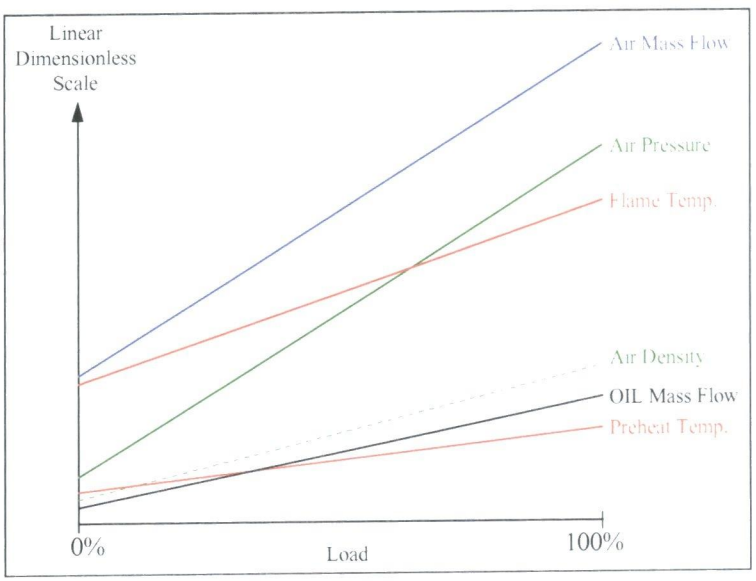

Figure 65

Figure 65 shows a simplified graph for different parameters across the full range of load conditions. The main characteristics that can be seen at part load are the reductions in air mass flow rate, along with a drop in ambient pressure, and a significant reduction in oil mass flow. This leads to several effects:

- reduction in air density (while oil density stays the same) causes a lower air-fuel momentum ratio
- reduction to the air temperature, reducing the evaporation rate
- lower flame temperatures
- higher chance of wall impingement
- the problem of piloting (initial start up)

Therefore at part load less penetration is required and droplets need to be smaller. This is unfortunately contradictory to the fact that a reduction in oil mass flow means a lower oil pressure, which translates into larger droplets being formed. (At higher pressure

smaller droplets are formed due to the earlier break-up of the more turbulent jets). Due to their momentum and lower drag force, these larger droplets penetrate too far into the field, evaporate slowly and hit the wall, creating the risk of flashback. This is undesired and needs to be avoided.

In order to design for a better extinction limit, and controlled combustion at the very lean pilot conditions, oil vapour should be distributed near the burner axis at such conditions. This creates flame stability by having a slightly richer region at the tip of the vortex breakdown (see Section 1.3). NOx emissions at pilot conditions are a minor problem due to the low adiabatic flame temperatures and correspondingly small thermal NOx production.

7.1 Nozzle Philosophy

Consequently it was required to develop a new concept for part load and pilot operation with the following criteria:

- small droplets and penetration at low mass flow rates
- flexibility in mass flow over a range of load conditions
- integration in the optimised full load nozzle design
- retractable and therefore serviceable
- continued requirement for low emissions across the full load range

The optimised full load nozzle contains 4 turbulent enhanced jets as described in Chapter 5 - AEV100 CFD, and Chapter 2 about nozzle design theory. This leads to the restriction of volume available for further design. It would be advantageous to use the four orifices and their chambers with some adaptation for part load conditions.

For identical orifice diameters and the same oil pressure, pressure swirl nozzles are known to produce smaller droplets than turbulent enhanced jets. This is due to the exiting oil film of a swirl nozzle being thinner than the diameter of a turbulent jet. It is also known that the mass flow rate of a swirl atomiser is smaller than that of a turbulent jet for identical orifice diameters and oil pressures, due to the blockage effect of the air core in a swirl nozzle. These two facts can be used advantageously, and hence the 2-stage multi-hole nozzle was born.

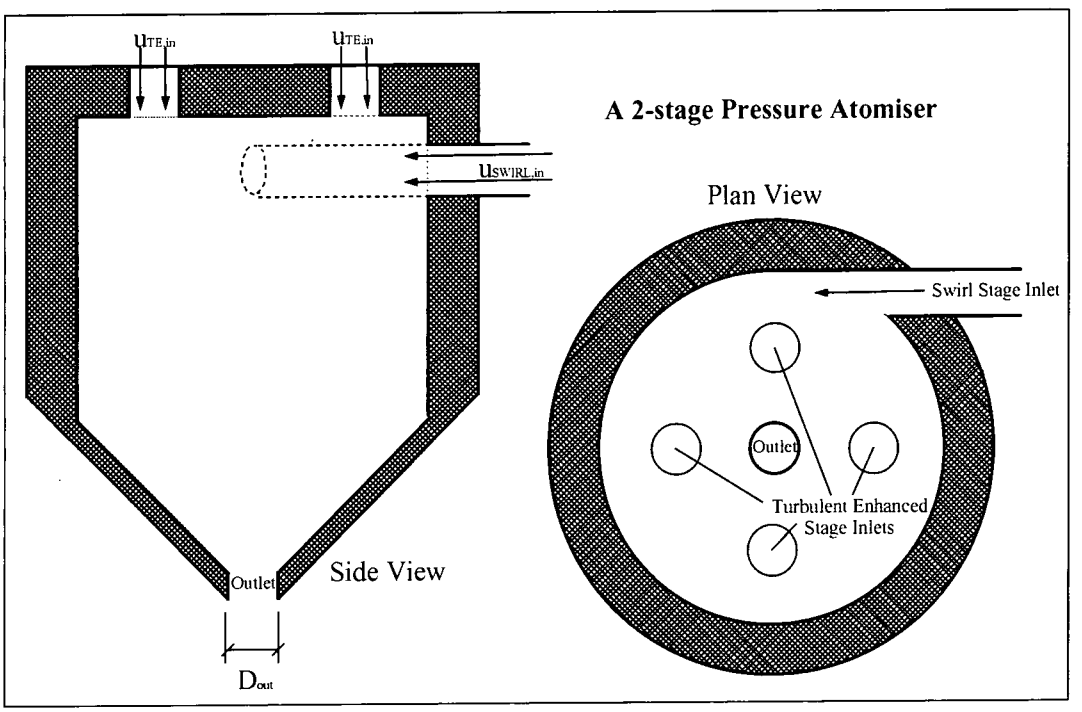

Figure 66

The 2-stage concept is an integration of a pressure swirl atomiser and a turbulent enhanced atomiser. A single orifice chamber is represented in figure 66.

At **full load** (shown in Figure 67), a 100% turbulence enhanced set-up shall be used. The oil enters the nozzle in the axial direction through two or four small holes in the top chamber which provide turbulence. The position of these holes has been optimised in scaled water tests, using LDA (Laser Doppler Anenometry) to inspect the turbulence levels (Ref. 13 / Hoferer & Steinbach 1997). The droplets should provide large momentum in small angled jets, directed towards the walls and therefore be able to penetrate the air field, many reaching the outer regions, and finally forming an even vapour profile at the burner exit.

When reducing to **part load**, the ratio between swirl and turbulent enhanced staging can be changed by increasing the mass flow through the tangential inlet (see Figure 67) and decreasing the flow through the turbulence orifices. In general at part load conditions, the mass flow of air, and hence the air momentum decreases, causing the need for smaller spray momentum (smaller droplets). If designed correctly, increasing swirl ratio

will gradually reduce mass flow rate of oil automatically. A near-constant oil pressure is required to avoid increase in droplet size. A mixture of swirl and turbulent staging is aimed to produce a wide-angle full-cone spray, giving less penetration and smaller droplets.

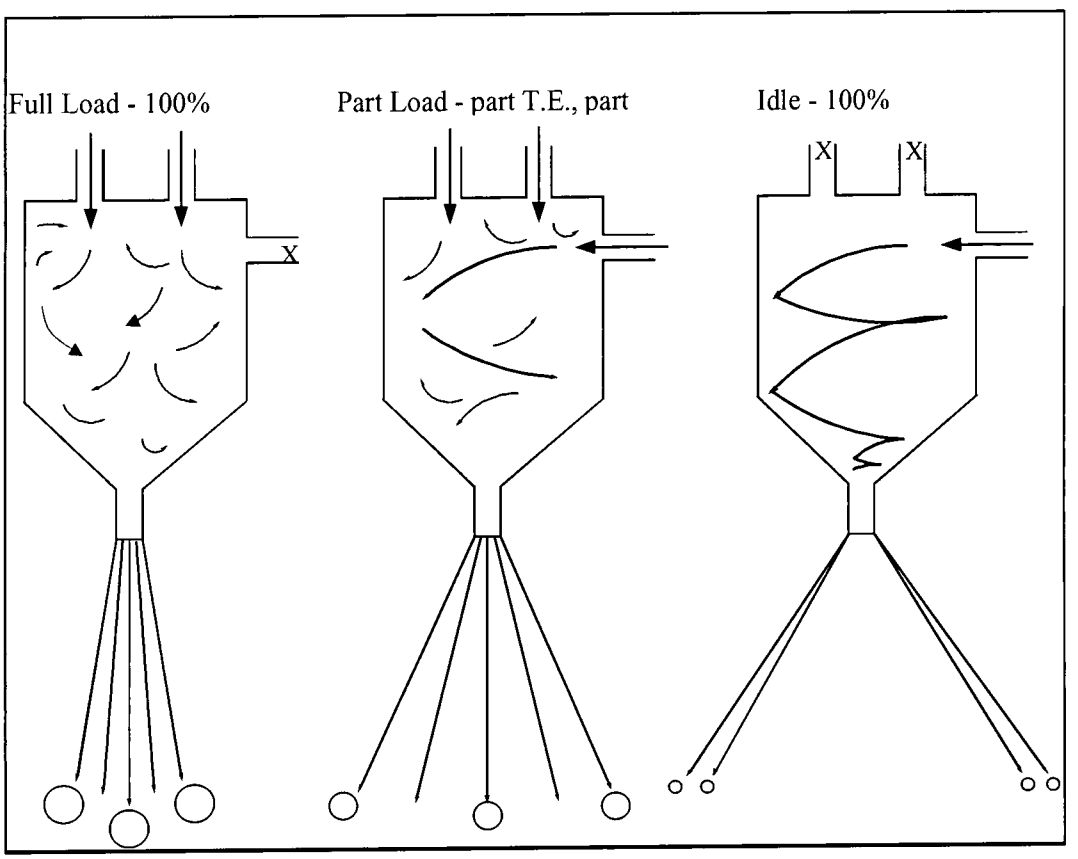

Figure 67

A further reduction in oil droplet size and mass flow necessary for **piloting (idle)** can be obtained by moving to 100% swirl operation (see Figure 67). This is required so that droplets do not hit the side walls, but stay in the centre zone creating flame stability at lean operation. Here a hollow cone spray is created with very small droplets. These are heavily influenced by the burner head air and carried straight along the burner axis, evaporating quickly.

Four such chambers can be integrated in a single nozzle design, to produce 4-sprays as optimised for the AEV100.

7.2 Design Methodology

The first design point is at 100% load using turbulence enhanced staging only. There is an available oil pressure, and a set oil mass flow rate that have to be met. The assumption made is that there is little or no contracta vena in the outlet orifice at full load conditions.

Firstly, experimental experience suggests that around 25% of the available pressure is transferred into turbulent energy in the nozzle chamber (Ref. 13 pp 19 / Hoferer & Steinbach 1997). The other 75% will be dissipated in the nozzle orifice and at the outlet. Assuming two axial injection holes into the nozzle chamber:

$$0.25\Delta P = \frac{\rho_{FLUID}}{2} u_{IN}^2 \qquad \text{Eq. 78}$$

and

$$0.75\Delta P = \frac{\rho_{FLUID}}{2} u_{OUT}^2 \qquad \text{Eq. 79}$$

Using continuity,

$$u = \frac{\dot{m}}{\rho_{FLUID} A} \qquad \text{Eq. 80}$$

Combining equations 69, 70 and 71 results in:

$$A_{IN}^2 = \frac{3}{4} A_{OUT}^2 \qquad \text{Eq.81}$$

where A_{IN} is one of the two inlet holes, and A_{OUT} is the outlet orifice.

Such a configuration (corresponding to equation 81) was built as a single chamber test model, and 100 bar of water gave a mass flow rate of 34kg/s for an outlet orifice diameter of 0.7mm. This enables the calculation of the pressure loss coefficient ($1/\zeta$) for such a nozzle:

$$\frac{\Delta P}{\zeta} = \left(\frac{\rho}{2} u^2\right) \qquad \text{Eq. 82}$$

and

$$u = \frac{\dot{m}}{\rho_{WATER} A_{OUT}} = \frac{0.034}{1000 \cdot 0.00035^2 \pi} = 88 \, m/s \qquad \text{Eq. 83}$$

Pressure across the outlet orifice is 75% of the oil back pressure

$$\Delta P = 0.75 \cdot 10^7 = 7{,}500{,}000 Pa \qquad \text{Eq. 84}$$

Using these values in equation 82, ζ can calculated to be 1.94, the pressure loss coefficient therefore being 0.52.

The full load conditions for oil can now be laid out. Knowing that finally there will be four such configurations in each nozzle, the outlet orifice must be calculated for a quarter of the mass flow of oil per burner. The maximum available oil pressure required for machine conditions is 100bar.

Equation 82 can be now used in reverse in order to calculate u (with ζ as 1.94, and the density of oil instead of water), and a further reverse calculation with equation 80 to find A_{OUT}. Finally equation 81 can be used to determine the diameter of the axial inlet holes to the nozzle chamber.

As a consequence the outlet diameter is fixed. Now using extended equations mentioned in the theory chapter, it is possible to design a pressure swirl nozzle with a similar outlet diameter. As there is no unique solution for a swirl atomiser, it allowed a certain amount of flexibility. However certain restrictions and limitations remained:

- due to the compactness of the nozzle, only one swirl inlet channel could be allowed
- the angle of the hollow cone spray should be as large as possible by changing the internal nozzle design parameters. The danger was the theoretical creation of a small cone angle, that in reality would collapse.
- the design point considered a lower mass flow rate at 100bar to allows for the blockage effect of the air core in the outlet orifice.
- a certain restriction was set for the nozzle chamber diameter, also for reasons of space.

This optimisation provided the design with the nozzle chamber diameter, and the swirl inlet hole dimensions, along with a forecast spray angle and mass flow rate.

7.3 Prototype testing

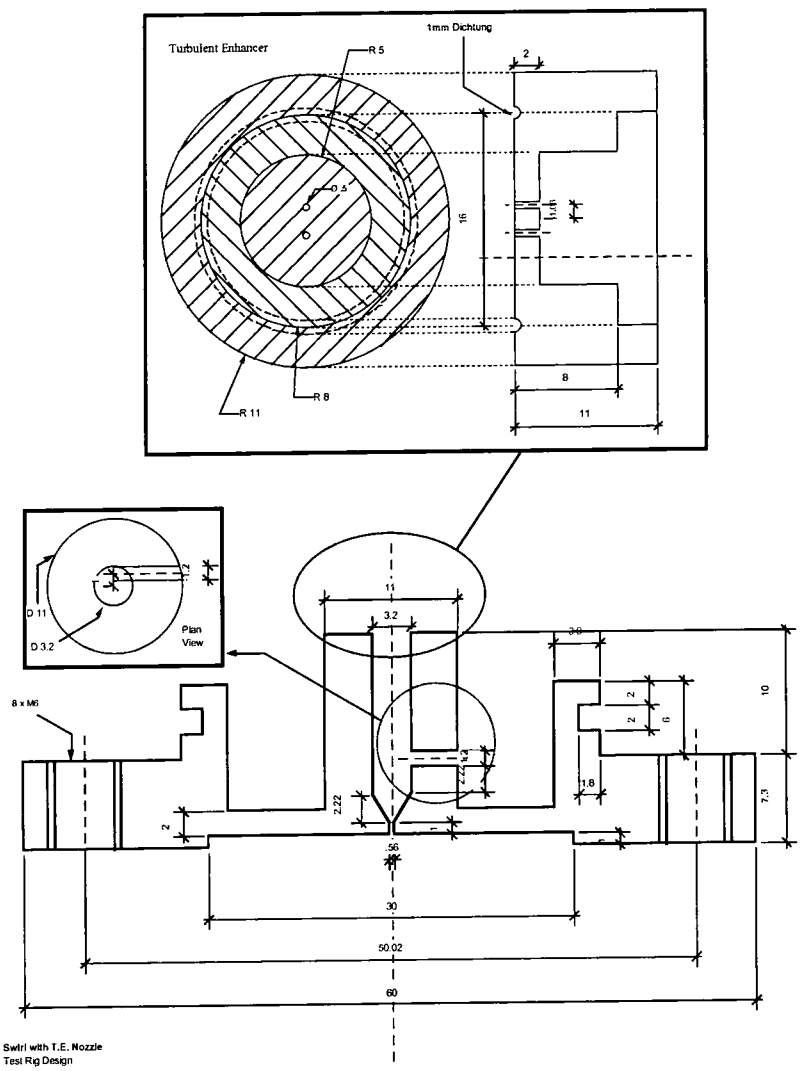

Figure 68

Using the above dimensions, a single chamber 2-stage nozzle test rig was designed and tested. A diagram of the test piece is shown in figure 68. It was possible to independently vary the pressure to both the axial and swirl inlets, and to accurately calculate the mass flow rate of each inlet.

Testing was undertaken at three different oil pressures: 20, 50 and 100 bar. For each pressure condition, values at different fractions of turbulent enhanced:swirl staging were measured, ranging from pure turbulent enhanced operation to swirl-only staging.

Several phenomena were observed.

The full spray angle was measured (as seen in Figure 69). Results at 0% turbulent enhanced fraction (i.e. 100% swirl) showed values varying between 33° and 43°, compared to a design value of 37° at 100bar. As the turbulent enhanced staging is increased (and swirl staging respectively decreased), a constant angle value is seen until the point where the hollow cone spray starts to collapse. At this point a solid cone spray is formed that then gradually reduces in angle size with increased turbulence staging. This spray characteristic was expected.

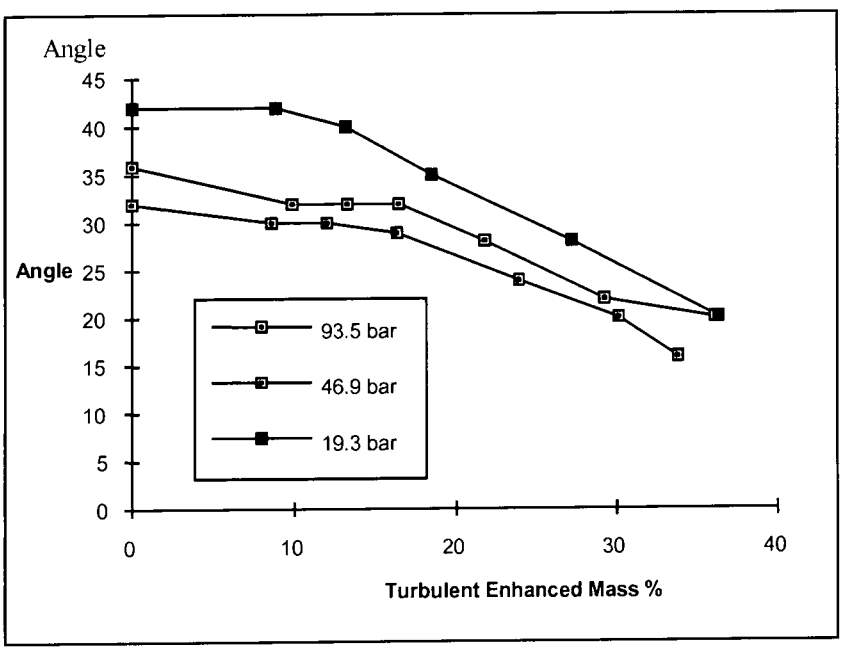

Figure 69

1. Mass flow rate were measured at different staging fractions across ranges of constant pressure (see Figure 70). As expected mass flow rates gradually rose as the influence of the air core diminished. As soon as the spray changed from a hollow cone to a full cone, no more change was seen in mass flow rate. The mass flow rate at 100% turbulence enhanced staging and 100bar pressure, corresponded well to the design value.

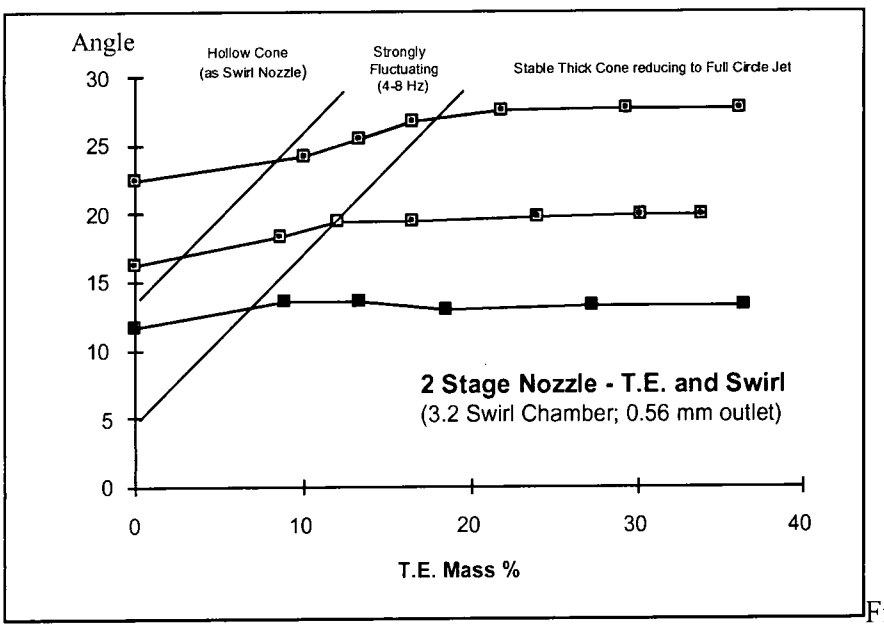

Figure 70

2. Another unexpected phenomena seen, was that of pulsations. As the turbulence staging was increased, a transition zone was recognised between hollow cone and full cone, where the spray pulsated at estimated frequencies of 4-8Hz. This resulted in pulsating spray angles of magnitude around 10°. An initial postulation for this phenomena was the conflict in the internal nozzle chamber between the axial inlets and the swirl inlet. It was hypothesised that vortices formed on entering the chamber from one type of inlet blocked the other respective inlet, until the vortex shed away when roles would reverse.

Finally average droplet diameters (SMD) were measured (see Figure 71).

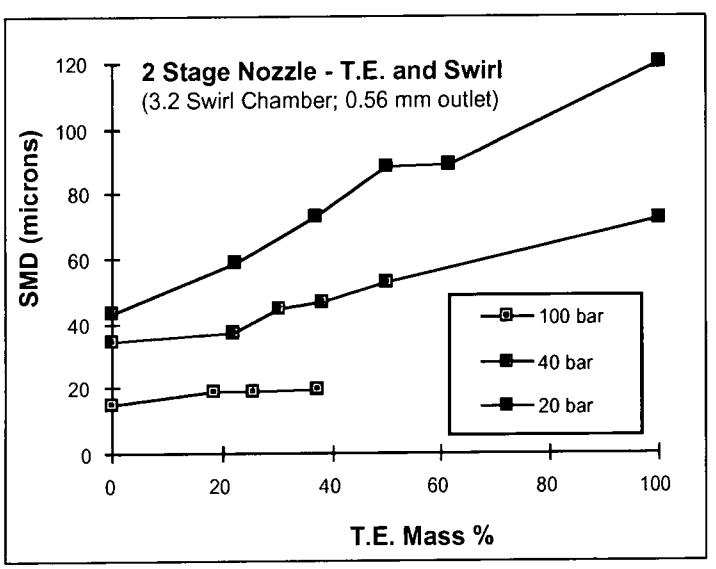

Figure 71

It was seen that at low pressures, pure swirl staging produced droplet sizes less than half of those at pure turbulence enhanced staging. This was expected and desired. However as pressures increased, not only did droplet sizes decrease, but also the gradient of droplet sizes across the staging spectrum, so that at 100bar almost no change in droplet size was seen between swirl and turbulence enhanced. This can be explained as follows: in the turbulence enhanced staging, droplet size is a function of exit velocity and turbulence in the jet. As pressure rises these are both increased and therefore smaller droplets are produced. In the case of swirl staging, droplet size is proportional to exit velocity and proportional to liquid film size. While exit velocity increase with pressure, film thickness stays the same or even increases. This means the reduction in droplet size with pressure is not so strong as with turbulence enhanced staging, and explains Figure 71.

It was also noted that there is a strong correlation between the quality of the orifice manufacture and the quality of the pressure swirl spray. By orifice quality one means the roundness of the hole, and the sharpness of the exit edge. One test case was bored to +/- 2 microns. The quality of the spray is defined by rotational symmetry and the lack of unwanted 'streaks' (weak and strong regions) in the spray cone. It was noticeable that high quality holes produce higher quality sprays. However it is known that after long periods of operation in a machine, the spray characteristics change due to the gradual erosion of the sharp edge. Such nozzles are quality controlled and differences can be accounted for in new designs.

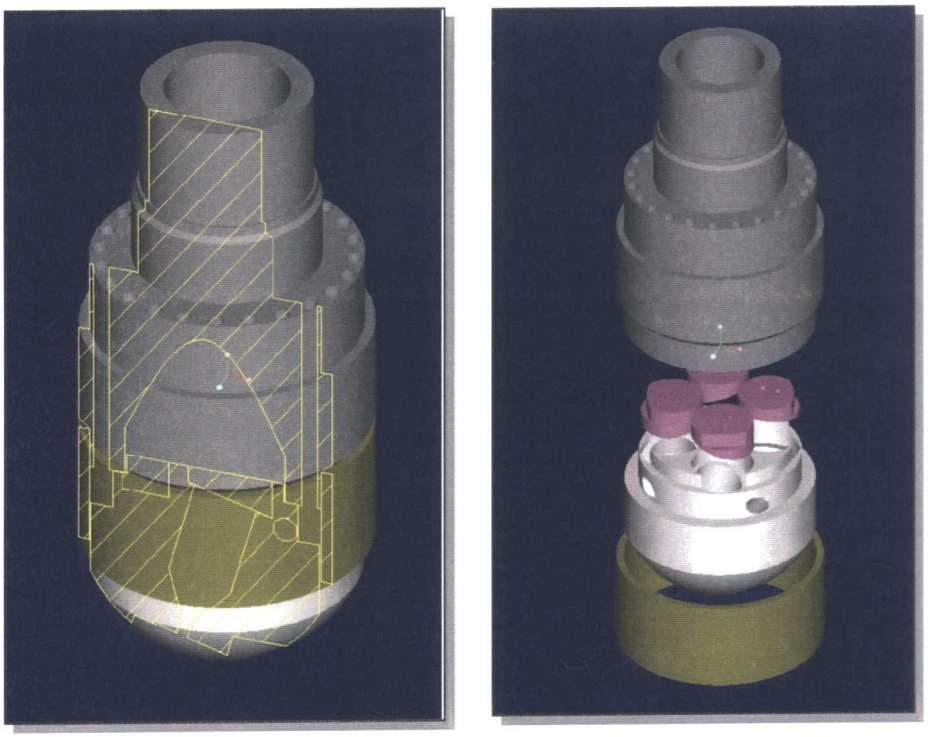

Figure 72

Having produced a single chamber nozzle that achieved the characteristics desired, this needs to be integrated into a nozzle with four outlet orifices.

Such a design has been created, as in shown in Figure 72. It is important to note the single distribution line for all four chambers of the turbulence enhanced staging, and similarly an outer concentric tube for the swirl staging.

A prototype was produced (see figure 73) and tested.

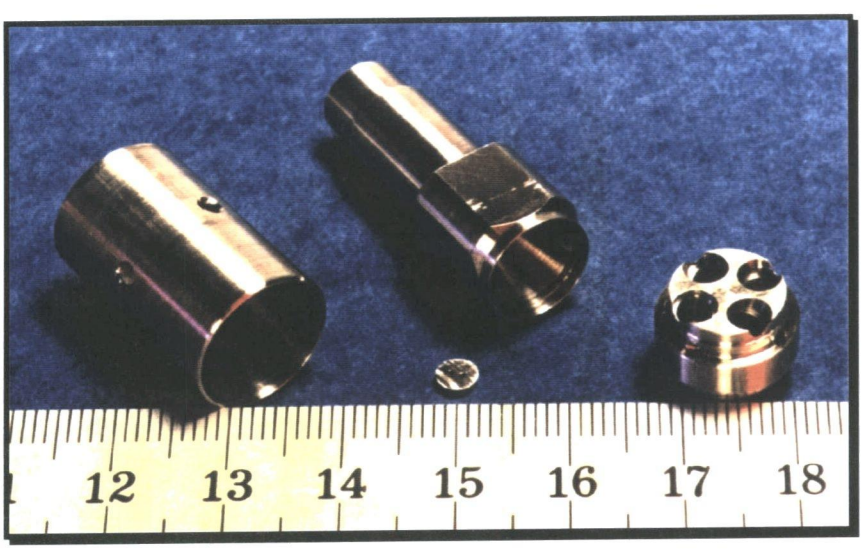

Figure 73

Spray photos of swirl only staging and turbulent enhanced only staging for pressures of 20 bar and 100 bar are shown in Figure 74. A laser light sheet is projected across the axis of the nozzle illuminating two of the four jets. The other two jets can be seen weakly in the background. Clearly shown is the fineness of the swirl spray in contrast to the turbulent enhanced spray, and also the shape of the hollow cone produced.

Further investigations and optimisation of the nozzle has been undertaken on the single nozzle chamber by student K-D Wassmer under the supervision of the author and Dr. C. Steinbach at ABB (Ref. 33). His results strengthened those described above, and offered an additional explanation to the cause of spray instability in particular operating ranges, namely that of an unstable precessing air core. This could be solved by including an insert along the nozzle chamber axis, to which the air core can attach and stabilise.

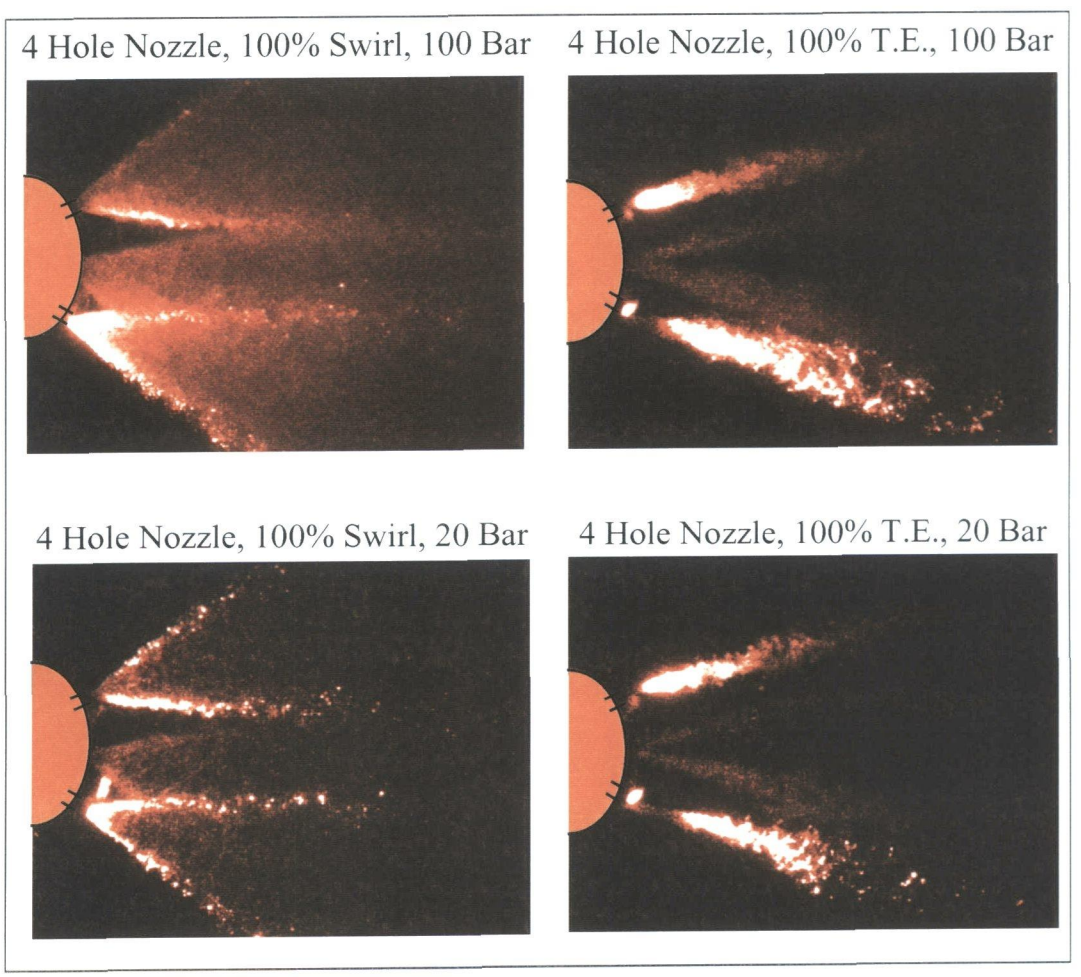

Figure 74

This nozzle has now been implemented during high pressure testing of the burner and produces NOx values below 25ppm for full load conditions. It has yet to be fully tested at part load conditions.

A patent application has been made for the described design. This is shown in Appx B.

8. Conclusion

The optimization technique for oil combustion in a Dry Low NOx Gas Turbine has been presented. This consisted of four main stages:

i. the understanding of the influence of certain parametric changes of a pressure swirl nozzle in the AEV75 burner. This was attained through an independent parameter study using a CFD code to model both the continuous air flow field and the droplet trajectories, including momentum and heat exchange, and also an evaporation model. Conclusions drawn were that air pressure and droplet size are the most influential factors affecting vapour distribution shortly before combustion. Other parameters that can be used to optimise the distribution are spray angle and preheat temperatures.

ii. the optimization of the mixture for oil combustion in the slightly larger AEV100 burner. Initially this involved the comparison of a pressure swirl nozzle and a four orifice nozzle. The investigation was completed with an independent numerical study of the four hole nozzle in the AEV burner. This showed the importance of average droplet size and individual spray angle on the mixture distribution exiting the burner.

iii. the problems of burners larger than the AEV100 were discussed, especially with respect to their implementation in machines with different operating conditions. The major hurdles were recognised. There is the need for large penetration distances under high pressures coupled with the risk of short self-ignition delay times. Suggested solutions to the problem were the shortening of the residence time of the oil in the burner and an increase in penetration depth. This could be achieved through a new nozzle design and the possible addition of water to reduce emissions.

iv. finally the development program was completed with the design of a 4-hole nozzle capable of running across the whole load range. This requires low mass flow rates and small droplets at idle conditions, and larger droplets and higher mass flow rates at full load. It has been solved by using an integrated '2-stage' nozzle that runs as a pressure swirl atomiser at idle conditions and a full turbulent enhanced jet nozzle a full load. Appropriate staging of the two can achieve ideal mixture distribution

at part load conditions. Prototype testing has been completed and a Patent application submitted.

As a result, a competitive dual-fuel Low NOx Gas Turbine burner has been developed that was available for commercial production in 1998. When in full operation, it will have the lowest emissions for dry oil combustion of any burner in that power range on the market.

With this technology, the limit of this burner system, concerning low emissions, have been achieved. Future work would need to concentrate on a whole new burner generation.

9. References

1. Abramzon B, Sirignano W, , Droplet Vaporization Model for Spray Combustion Calculations, Int. Journal of Heat & Mass Transfer, Vol. 32, No.9, pp1605-1618, 1989

2. Andrews, Course Notes on Ultra Low NOx Gas Turbine Combustion, Univ. of Leeds, 1998

3. Bayvel L., Orzechowski Z., Liquid Atomisation, Taylor & Francis 1993

4. Benjamin B., Theory of Vortex Breakdown Phenomenon, Journal of Fluid Mechanics, Vol 14, pp593, 1962

5. Chin J., Lefebvre A., Steady State Evaporation Characteristics of Hydrocarbon Fuel Drops, AIAA Journal Vol 21, No.10, Oct 1983

6. Döbbeling, Krieger, Pennell et al., Grundlagen zur Verbrennung flüssiger Brennstoffe unter gasturbinentypischen Bedingungen, ABB CHCRC 96-75, October 1996

7. Dorfner, Domnick, Durst & Köhler, Viscosity and Surface Tension Effects in Pressure Swirl Atomization, Journal of Atomization and Sprays, vol.5, pp.261-285, 1995

8. Faeth G.M., Current Status of Droplet and Liquid Combustion, Prog. Energy Combustion Science, Vol. 3, pp 191-224, 1977

9. Faeth G.M., Evaporation and Combustion of Sprays, Prog. Energy Combustion Science, Vol. 9, pp 1-76, 1983

10. Fluent Manual, Version 4.4, Fluent Inc., 1996

11. Grubb M., Energy Policies and the Greenhouse Effect, Dartmouth Publishing Company, pp443-450, 1990

12. Hidy G., Atmospheric Sulphur and Nitrogen Oxides, Academic Press, San Diego, 1994

13. Hoferer U, Steinbach C., Auslegung, Konstruktion und Aufbau einer modularen Modell-Zerstäuberdüse, ABB Student Report, February 1997

14. Kaer S., Nielsen K., Numerical Modelling of Turbulent Reacting Sprays, ABB STAL and Aalborg Univ., June 1996

15. Kneer R., Grundlegende Untersuchungen zur Sprühstrahlausbreitung in hochbelasteten Brennräumen: Tropfenverdunstung und Sprühstrahlcharakterisierung, Univ. Karlsruhe, 1993

16. Krämer M., Untersuchungen zum Bewegungsverhalten von Tropfen in turbulenter Strömung im Hinblick auf Verbrennungsvorgänge, Univ. Karlsruhe 1988

17. Kreutzer R., Dreidimensionale Berechnug von tropfenbeladenen Brennerströmungen, Diplomarbeit, Univ. Karlsruhe, Oct 1992

18. Law C., Recent Advances in Droplet Vaporization and Combustion, Prog. Energy Combustion Science, Vol. 8, pp171-201, 1982

19. Lefebvre A., Atomisation and Sprays, Hemisphere Publishing, 1989

20. Massey B.S., Mechanics of Fluids, Chapman and Hall, 1990

21. Matlosz R., Leipziger, Torda T, Investigation of Liquid Drop Evaporation in a High Temperature and High Pressure Environment, Int. Journal of Heat and Mass Transfer, Vol. 15, pp831-852, 1972

22. McCartney E., Absorption and Emission by Atmospheric Gases, Wiley & Sons, pp259-261, New York, 1983

23. Morsi S. & Alexander A., An Investigation of Particle Trajectories in Two Phase Flow Systems, Journal of Fluid Mechanics, Vol 55, pp193-208, 1972

24. Pilch M., Erdman C., Use of Breakup Time Data and Velocity History Data to Predict the Maximium Size of Stable Fragments for Acceleration-induced Breakup of a Liquid Drop, Int. Journal Multiphase Flow, Vol. 13, No. 6, pp741-757, 1987

25. Prandtl L., Oswatitsch K., Wieghardt K., Führer durch die Strömungslehre, Vieweg Verlag 1990

26. Prommesberger K., Willmann M., Wittig S., Modellierung des Verdunstungsvorganges von Gasturbinenbrennstoffen auf Grundlage ihrer Siedekurve und variabler tropofeninterner Diffusion, Univ. of Karlsruhe, 1997

27. Schetz J., Padhye A., Penetration and Breakup of Liquid in Subsonic Airstreams, AIAA Journal Vol 15, No. 10, October 1977

28. Sirignano W., Fuel Droplet Vaporization and Spray Combustion Theory, Prog. Energy Combustion Science, Vol 9, pp 291-322, 1983

29. Soo S. L., Fluid Dynamics of Multiphase Systems, Blaisdell Publishing Company, Massachusetts 1967

30. Spadaccini, TeVelde, NASA-CR-159886, 1980

31. TascFlow3D, Version 2.4, Advanced Scientific Computing, Ontario, Canada, March 1995

32. Warnatz J, Maas U., Technische Verbrennung, Springer-Lehrbuch, pp201-212, 1993

33. Wassmer K-D, Untersuchung und Optimierung des Zerstäubungsverhaltens an Dralldruckdüsen, Diplomarbeit, FH Offenburg, Nov 1997

10. Appendices

10.1 Appendix A - Paper Abstracts

1. Ilass Conference, Florence 1997, The Effect of Nozzle and Operating Parameters on the Mixture Preparation for Dry Low NOx Combustion. Written solely by the author
2. ASME Conference, Stockholm 1998, ABB's Advanced EV Burner - A Dual Fuel Dry Low NOx Burner for Stationary Gas Turbines. Written by Dr.C.Steinbach, ABB; contributions from the author

10.2 Appendix B - Patent Applications

1. A 2-stage Multi-hole Nozzle

10.3 Appendix C - The GTX100 machine

10.4 Appendix D – Derivation of formula for setting CFD spray conditions

Appendix A1: Abstract for ILASS Conference in Florence 1997
(European Conference on Liquid Atomization and Spray Systems)

The Effect of Influencing Spray Parameters in a Confined Swirling Flow Environment on the Mixture Preparation for Dry Low NOx Oil Combustion

Jonathan Lloyd, Christian Steinbach, Klaus Döbbeling, Peter Jansohn,
ABB Corporate Research Centre Ltd, Baden-Dättwil, Switzerland.

Abstract:

Numerical and experimental investigations have been undertaken to determine the most important influencing parameters controlling the oil-air mixture shortly before combustion in a Dry Low NOx burner system.

In modern fuel premix burners the dominating swirling flow has a specific length from the point of injection to the exit of the burner, where the flame stabilizes. In this length the most homogeneous mixture should be produced, in order to help obtain the lowest NOx emissions possible.

Parameters controlling the quality of the mixing derive mainly from the initial conditions of the spray. In this study a simplex swirl nozzle has been investigated, changing the spray angle, droplet size and injection velocity. Alongside this two ambient conditions were investigated: operating pressure and air temperature.

Numerical simulations showed a close comparison to experimental results, and trends were seen to agree in both cases.

Most influencing parameters were seen to be operating pressure and droplet size. Operating pressure, directly proportional to air density, controls the momentum ratio between air and oil. Larger droplets also increase the oil to air momentum ratio. It is this relationship that controls the destination of the droplets.

The preheat temperature of the air also has a large influence on the mixture quality, in determining the rate of evaporation of the droplet.

Other parameters such as velocity injection and angle, have a less significant effect within the framework of this investigation.

Lambda profiles show the qualitative trends associated with each parameter. Using these projections, the iterative process of obtaining the optimal nozzle is considerably shortened.

Several short-comings of the numerical method are recognised. These are also discussed.

Appendix A2: Abstract for ASME Conference in Stockholm 1998

ABB's Advanced EV Burner - A dual Fuel Dry Low NOx Burner for stationary Gas Turbines

Christian Steinbach, Thomas Ruck, Jonathan Lloyd, Peter Jansohn, Klaus Döbbeling, Thomas Sattelmayer
ABB Corporate Research Ltd, Baden-Dättwil, Switzerland

Torsten Strand, ABB STAL AB, Finspång, Sweden

Abstract:

A dual fuel burner has been developed to meet stringent NO_x goals without the use of water or steam injection. This combustion system is based on the proven ABB EV burner dry low NO_x technology and uses the same type of aerodynamic vortex breakdown flame stabilisation. A more advanced aerodynamic design improves the quality of the fuel air mixture for both gaseous and liquid fuels. The design of liquid fuel injection and fuel-air-mixture preparation is described in this paper. Fuel air mixture homogeneity was improved with the help of experimental and numerical tools. This way an optimisation in fuel atomiser design was possible. Distinct differences in fuel distribution were observed for different designs of pressure atomisers.

Combustion tests of the burner were performed at pressures up to 20 bars. The NO_x levels measured under gas turbine full load conditions are <25 vppm using oil no. 2 and <10 vppm using natural gas. These results highlight the potential of achieving similar combustion performance for gaseous and liquid fuels for perfect lean premix conditions.

Operating parameters and test results at part load conditions are discussed as well in this paper. Wide operating range of the burner in the full premix mode restricts the need for pilot application or burner staging to low load (<50 %) conditions. This allows for low emissions on NO_x, CO and UHC in entire load range.

Appendix B: Patent Application for a 2-Stage Multi-hole Nozzle

Due to confidentiality, this can not yet be printed.

Appendix C: The GTX100 machine

Who says good money and a clean conscience don't go together?

Concern for the environment has been part of ABB corporate strategy for many years, a fact which has put us at the forefront of environmental technology. The GTX100 will serve to reinforce ABB's leading position in the emission field.

We have taken the environmental impact of the GTX100 into account at every stage of its development, from R&D and design, through manufacturing and supply to operation, service and maintenance.

The new AEV combustor system cuts NOx and CO emissions from gas fuel to an impressive 15 ppm (15% O_2) and to 25 ppm (15% O_2) for liquid fuel when operating at loads in the 100 - 50% range. This gives the operator enormous flexibility.

The new AEV burner is based on the proven EV technology introduced in 1988. Today, over 140 EV-based units are in operation worldwide. Delivering a dry NOx capability of 25 ppm in ABB gas turbines, these units have clocked up a total of over 1,600,000 operating hours.

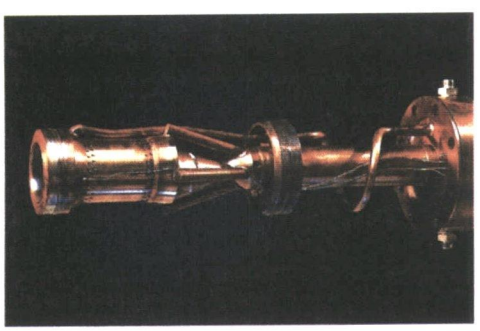

Dry low-NOx and CO emissions of 15 ppm (15% O_2) for gas fuel and 25 ppm (15% O_2) for liquid fuel are now possible with the GTX100 AEV dual-fuel burner.

Now installed in more than 30 units, the GTX10 dry low-NOx system has been in operation since 1991. Of simple, robust design, it still enjoys a leading position in the field of proven dry low-emission technology.

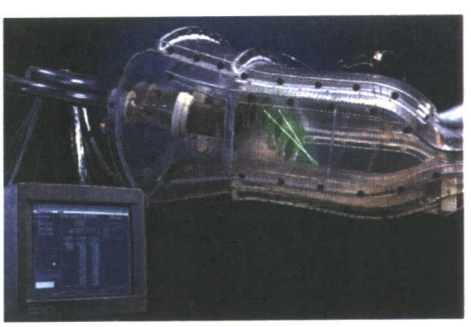

A laser-based combustor flow test – one of several advanced modelling techniques used to validate the GTX100 combustor design.

Appendix D: Derivation of formula for setting CFD spray conditions

Describing the droplets at the nozzle exit, both in size and quantity, in order to set the initial conditions of the spray for the CFD modelling was also completed within the scope of this thesis work. This was done by utilising theoretical, empirical and experimental results as set out on pages 21 and 22.

Initial investigations included commercial nozzles, before developing onto in-house designed nozzles. Commercial nozzles were chosen for testing, which from the manufacturers definitions along with the knowledge of the burner, were concluded could be a possible fit for the AEV burner. In order to gain more exact knowledge of the spray characteristics, the nozzles was firstly physically tested and evaluated using water as a medium. These tests (undertaken as part of this work) used PDPA measurement systems and gave the spray angles, and droplet distribution for water under atmospheric conditions.

To be able to utilise this data in the CFD model, these results then had to be converted into appropriate spray characteristics for an identical nozzle, but using oil under higher ambient pressures. As testing these nozzle *characteristics* under such conditions was not possible in the laboratories available, an empirical conversion was derived (by the author) using a mixture of correlations from other literature.

The main dependencies of SMD were identified to be surface tension, viscosity and air pressure.
Literature provided independent studies and empirical correlations for each of these variables. These were then accumulated and derived the final conversion formula from the laboratory tests at atmospheric conditions, to a droplet distribution that corresponds to oil at machine operating conditions.

The independent correlations and empirical formulae were obtained from the following sources:

Surface tension	-	Dorfner	Reference 6
Viscosity	-	Dorfner	Reference 6

Air pressure - Lefevbre Reference 9

Further dependences, such as temperature are taken account for in the calculations for viscosity and air pressure.

Using the derived conversion formula (eq. 25), the spray characteristics measured at atmospheric testing (PDPA) using water, could then converted to oil spray characteristics (SMD) and used for the input and initial spray conditions for the CFD model. In this way, the nozzle being tested for the AEV burner could be modelled in CFD.